PEOPLE'S DEMOCRATIC REPUBLIC OF ALGERIA
MINISTRY OF HIGHER EDUCATION AND SCIENTIFIC RESEARCH

ÉCOLE NATIONALE POLYTECHNIQUE

Department of Mechanical Engineering

End of Study Project Thesis

For the attainment of the State Engineer degree in Mechanical Engineering

---

Design and Development of an Autonomous Delivery Drone: A Comprehensive Study

---

BOUSSOUSSOU Nacer Eddine

Under the supervision of **Pr. RECHAK Said** ENP

Presented publicly on July 18th 2024

Members of the jury:

President:	Mr. GUERGUEB Brahim	ENP (MAA)
Supervisor:	Mr. RECHAK Said	ENP (Professor)
Examiner:	Mr. BELKACEMI Yacine	ENP (MCA)
Invited:	Mr. ZEHANA Halim	USIPRECIS (Manager)

ENP 2024

Department of Mechanical Engineering/ ENP, 10 Rue des Frères OUDEK, El Harrach 16200 Algiers Algeria.

PEOPLE'S DEMOCRATIC REPUBLIC OF ALGERIA
MINISTRY OF HIGHER EDUCATION AND SCIENTIFIC RESEARCH

ÉCOLE NATIONALE POLYTECHNIQUE

Department of Mechanical Engineering

End of Study Project Thesis

For the attainment of the State Engineer degree in Mechanical Engineering

---

Design and Development of an Autonomous Delivery Drone: A Comprehensive Study

---

BOUSSOUSSOU Nacer Eddine

Under the supervision of **Pr. RECHAK Said** ENP

Presented publicly on July 18th 2024

Members of the jury:

President:	Mr. GUERGUEB Brahim	ENP (MAA)
Supervisor:	Mr. RECHAK Said	ENP (Professor)
Examiner:	Mr. BELKACEMI Yacine	ENP (MCA)
Invited:	Mr. ZEHANA Halim	USIPRECIS (Manager)

ENP 2024

Department of Mechanical Engineering/ ENP, 10 Rue des Frères OUDEK, El Harrach 16200 Algiers Algeria.

RÉPUBLIQUE ALGÉRIENNE DÉMOCRATIQUE ET POPULAIRE
MINISTÈRE DE L'ENSEIGNEMENT SUPÉRIEUR ET DE LA RECHERCHE SCIENTIFIQUE

ÉCOLE NATIONALE POLYTECHNIQUE

Département de Génie Mécanique

Mémoire de projet de fin d'études

Pour l'obtention du diplôme d'ingénieur d'état en Génie Mécanique

---

Conception et Développement d'un Drone de Livraison Autonome : Une Étude Approfondie

---

BOUSSOUSSOU Nacer Eddine

Sous la direction de **Pr. RECHAK Said** ENP

Présenté publiquement le 18 Juillet 2024

Composition du jury:

Président:	M.GUERGUEB Brahim	ENP (MAA)
Encadrant:	M.RECHAK Said	ENP (Professeur)
Examinateur:	M.BELKACEMI Yacine	ENP (MCA)
Invité:	M.ZEHANA Halim	USIPRECIS (Gérant)

ENP 2024

Département de Génie Mécanique / ENP, 10 Rue des Frères OUDEK, El Harrach 16200 Alger Algérie.

ملخص

تمثل الطائرات بدون طيار للتسليم تقنية تحوّلية متمثلة في ثوره في صناعات الخدمات واللوجستيات على الصعيد العالمي. قام هذا المشروع التخرج بإجراء استكشاف شامل لتصميم وتحسين وتصنيع طائره تسليم متعدده الاستخدامات (كواد كوبتر) مصممة للعمليات الفعالة والمستدامة. بدأ المشروع بمراحل تصميم دقيقة تشمل اختيار محرك الدوار والتحسين الديناميكي للإطار للحد من السحب. تم إجراء تحليلات هيكلية متقدمة، بما في ذلك الأمثلة التبولوجية واختبارات الاهتزاز والساكنة الصارمة، لضمان أداء قوي تحت ظروف تشغيل متنوعة.

يسهم هذا المشروع ليس فقط في تقدم الطائرات بدون طيار المصنعة محلياً، ولكنه يضع أيضاً أسساً للتعاونات بين التخصصات والشراكات التعليمية التي تهدف إلى تعزيز الابتكار التكنولوجي في مجال الطائرات بدون طيار في الجزائر. من خلال متابعة هذه الطرق، يهدف المشروع إلى مواجهة التحديات المجتمعية والصناعية المتنوعة بينما يعزز التنمية المستدامة والابتكار في مركبات الطيران غير المأهولة.

الكلمات الرئيسية :

طائرات التسليم، كواد كوبتر، تحسين ديناميكي، تحليل هيكلي، أمثلة تبولوجية، هياكل خفيفة الوزن، مواد مركبة، تطبيقات الطائرات

Abstract

Delivery drones represent a transformative technology poised to revolutionize logistics and service industries globally. This graduation project comprehensively explored the design, optimization, and fabrication of a versatile delivery drone (quad-copter) tailored for efficient and sustainable operations. The project began with meticulous design phases encompassing propeller motor selection and aerodynamic optimization of the frame to minimize drag. Advanced structural analyses, including topology optimization and rigorous static and vibrational testing, were conducted to ensure robust performance under varying operational conditions. This project not only contributes to the advancement of locally manufactured drones but also lays the foundation for interdisciplinary collaborations and educational partnerships aimed at fostering drone technology innovation in Algeria. By pursuing these avenues, the project aims to address diverse societal and industrial challenges while promoting sustainable development and innovation in unmanned aerial vehicles.

Keywords : Delivery drones, Quad-copter, Aerodynamic optimization, Structural analysis, Topology optimization, Lightweight structures, Composite materials, Drone applications

Résumé

Les drones de livraison représentent une technologie transformative destinée à révolutionner les industries de la logistique et des services à l'échelle mondiale. Ce projet de fin d'études a entrepris une exploration approfondie de la conception, de l'optimisation et de la fabrication d'un drone de livraison polyvalent (quad-copter) conçu pour des opérations efficaces et durables. Le projet a débuté par des phases de conception méticuleuses comprenant la sélection du moteur

de l'hélice et l'optimisation aérodynamique du châssis pour minimiser la traînée. Des analyses structurales avancées, incluant l'optimisation topologique et des tests rigoureux de statique et de vibration, ont été menées pour garantir des performances robustes dans diverses conditions opérationnelles.

Ce projet contribue non seulement à l'avancement des drones fabriqués localement, mais pose également les bases de collaborations interdisciplinaires et de partenariats éducatifs visant à promouvoir l'innovation technologique des drones en Algérie. En poursuivant ces voies, le projet vise à répondre à divers défis sociétaux et industriels tout en favorisant le développement durable et l'innovation dans les véhicules aériens sans pilote.

Mots-clés: Drones de livraison, Quad-copter, Optimisation aérodynamique, Analyse structurelle, Optimisation topologique, Structures légères, Matériaux composites, Applications des drones

Dedications

To the memory of my father, who bravely fought cancer, I am confident that you would be proud of the man I have become, just as you always were.

Thanks

First and foremost, I extend my heartfelt gratitude to the esteemed jury members who have dedicated their time and effort to evaluate this work, providing valuable feedback and guidance on the day of the presentation.

I am deeply grateful to each and every member of my family for their unwavering support and boundless love throughout my life's journey.

Special thanks to Nessrine for her invaluable assistance and unwavering support.

I express my sincere appreciation to Professor Rechak for his exceptional supervision and insightful guidance throughout this project.

I extend my thanks to Dr. Belkacemi, Professor Smaili, Mr. Bousbai, Mr. Lahlah, Tayeb, and Mohammed for their invaluable contributions and assistance in this project.

I would also like to acknowledge and appreciate Mr. Zouaghi, Mr. Mekhaldi, and the school's general secretary for fostering an excellent educational environment.

My heartfelt thanks go to my colleagues, friends, and everyone who supported me, even with a simple smile.

Nacer Eddine

Contents

List of Tables

List of Figures

Chapter 1

Introduction

"**The sky is not the limit, it's just the beginning**"

In recent years, the rapid advancement of drone technology has revolutionized various industries, offering innovative solutions and applications that were once considered science fiction. Among these, the development of delivery drones stands out as a transformative technology with the potential to significantly enhance logistics and supply chain efficiency. Drones, or Unmanned Aerial Vehicles (UAVs), are being increasingly employed for tasks ranging from aerial photography and surveillance to environmental monitoring and agricultural management. However, their application in the delivery sector promises to redefine the way goods are transported, particularly in regions where traditional logistics face significant challenges.

The necessity to develop and adopt drone technology in Algeria is particularly pressing. Algeria, with its vast and diverse terrain, poses unique logistical challenges that can be effectively addressed by deploying delivery drones. These drones can navigate remote and inaccessible areas, ensuring timely delivery of essential supplies, medical aid, and consumer goods. Furthermore, the integration of drone technology in Algeria's logistics sector can spur economic growth, create new job opportunities, and position the country as a leader in technological innovation within the region.

Figure 1.1: Illustration of a delivery drone: [4]

This project focuses on the design and development of a quadcopter delivery drone, tailored to meet the specific needs of the Algerian context. The study encompasses a comprehensive examination of the various aspects critical to successfully implementing such a drone, including design considerations, aerodynamic efficiency, structural integrity, and control systems. By leveraging advanced design tools and simulation techniques, the project aims to optimize the drone's performance, ensuring it is both efficient and reliable.

The primary objectives of this study are to design a lightweight and aerodynamically efficient delivery drone, develop a robust structural framework capable of withstanding operational stresses, and implement advanced control systems for stable and autonomous flight. The project also involves extensive testing and validation through simulations and experimental prototypes to ensure the drone meets the required performance standards.

By addressing these goals, the project not only contributes to the academic field of UAV design and engineering but also provides practical insights and solutions that can be applied in real-world scenarios. The successful development of this delivery drone has the potential to improve the logistics infrastructure in Algeria significantly, enhancing delivery efficiency and accessibility across the country.

This dissertation is organized into 14 chapters, each dedicated to a specific aspect of the design, development, and analysis of a delivery drone. The chapters are structured to provide a comprehensive understanding of the project from theoretical foundations to practical implementations.

Chapter 1 Introduction:

This chapter introduces the concept of drones, exploring their various applications across different industries. It emphasizes the importance of developing drone technology in Algeria and provides a brief history of drones.

Chapter 2 Literature Review & Objectives: - A review of existing technologies and innovations in the field of drones, particularly focusing on delivery drones. This chapter also covers theoretical background relevant to drone design and operation, drawing from recent academic and industry research. Then define the goals and objectives of the study. This chapter outlines the project's specific aims, detailing the scope and expected outcomes. It sets the stage for the detailed design and development process that follows.

Chapter 3 Design & Calculations:

Discusses the selection of critical components such as propellers, motors, and electronic speed controllers (ESCs). It also covers mechanical considerations including the center of mass, symmetry, and motor configuration to ensure dynamic balance and vibration prevention.

Chapter 4 Aerodynamic Analysis:

Focuses on the aerodynamic aspects of the drone. This chapter describes the methods used to minimize drag, including computational fluid dynamics (CFD) simulations and aerodynamic profiling, to optimize the drone's efficiency.

Chapter 5 Structural Design and Analysis:

Details the design optimization process using topology optimization and generative design techniques. It includes considerations for 3D printing materials and processes and presents experimental testing methods to validate structural integrity.

Chapter 6 Vibration Analysis:

Examines the vibration characteristics of the drone, including motor speed interval analysis and the impact of vibrations on different structural prototypes. This chapter includes both simulation studies and experimental observations.

Chapter 7 Designing Auxiliary Mechanisms & Assembly: - Explores the design and 3D printing of the gripping mechanism, landing legs, and protective shell for waterproofing and weatherproofing the drone to ensure reliable performance in various environmental conditions

Chapter 8 Conclusion and Future Perspectives:

Summarizes the key findings and achievements of the project. This chapter also discusses potential improvements and future research directions, highlighting the impact of the project on the development of drone technology in Algeria.

References :

A comprehensive list of all sources and references used throughout the dissertation, providing the academic and technical foundation for the study.

Chapter 2

Literature Review & Objectives

2.1 What is a Drone (UAV) ?

An unmanned aerial vehicle (UAV), commonly known as a drone, is an aircraft that operates without a human pilot, crew, or passengers on board. Initially developed in the twentieth century for military missions deemed too dull, dirty, or dangerous for humans, UAVs became crucial assets for most militaries by the twenty-first century. With advancements in control technologies and cost reductions, drones have increasingly been utilized in a wide range of non-military applications [21].

Figure 2.1: DJI Phantom 4 Pro V2.0: [5]

These applications include:

- Aerial photography: Capturing images from the air.
- Area coverage: Surveying and mapping large areas.
- Precision agriculture: Optimizing crop management and monitoring.
- Forest fire monitoring: Detecting and tracking wildfires.
- Environmental monitoring: Tracking environmental changes and conditions.
- Policing and surveillance: Enhancing law enforcement and security.

- Infrastructure inspections: Inspecting bridges, buildings, and other structures.
- Smuggling: Illicit transportation of goods.
- Product deliveries: Transporting goods to customers.
- Entertainment: Providing aerial views for events and filmmaking.
- Drone racing: Competitive racing of drones.

2.2 History

2.2.1 Early Developments

The development of unmanned aerial vehicles (UAVs) dates back to the 19th century. The earliest recorded use of a UAV for warfighting occurred in July 1849, when Austrian forces besieging Venice attempted to launch incendiary balloons at the city. These balloons were precursors to aircraft carriers and represented the first offensive use of air power in naval aviation. However, due to changing winds, many balloons missed their target and drifted back over Austrian lines.

In 1903, Spanish engineer Leonardo Torres Quevedo introduced a radio-based control system called the *Telekino* at the Paris Academy of Science. This system was designed to test an airship without risking human lives.

Significant UAV development began in the early 20th century, initially focusing on providing practice targets for military personnel. The first powered UAV attempt was A. M. Low's "Aerial Target" in 1916. By 1917, successful demonstrations of UAV control were conducted, leading to further development for military applications.[22]

2.2.2 World War I and Interwar Period

During World War I, various UAV prototypes were developed, such as the Kettering Bug by Charles Kettering and the Hewitt-Sperry Automatic Airplane. These early UAVs were designed to carry explosive payloads to predetermined targets.

Figure 2.2: The Aerial Target, a British radio-controlled aircraft from the First World War.[6]

In the 1930s, a film star and model airplane enthusiast, Reginald Denny developed the first scaled remote-piloted vehicle. Soviet researchers also experimented with controlling Tupolev TB-1 bombers remotely.[23]

2.2.3 World War II

In 1940, Reginald Denny founded the Radioplane Company, which produced UAVs for training anti-aircraft gunners and flying attack missions during World War II. Nazi Germany developed and used various UAVs, such as the Argus As 292 and the V-1 flying bomb. Fascist Italy developed a specialized drone version of the Savoia-Marchetti SM.79, although it was never deployed operationally due to the truce.[24]

Figure 2.3: Prime Minister Winston Churchill and Captain David Margesson, Secretary of State for War, watching preparations being made to launch a De Havilland Queen Bee seaplane L5984 from its ramp.[6]

2.2.4 Postwar Period

Post-World War II UAV development continued with vehicles like the American JB-4, the Australian GAF Jindivik, and the Teledyne Ryan Firebee I of 1951. The U.S. Air Force began planning for UAV use over hostile territory in 1959, leading to the highly classified "Red Wagon" program after the 1960 U-2 incident.[25]

Figure 2.4: A remote-controlled drone prototype based on a B-17 Flying Fortress airframe takes off from Hilo Naval Air Station in Hawaii on 6 August 1946.[6]

2.2.5 Vietnam War and Tactical UAVs

During the Vietnam War, UAVs like the Ryan Model 147 were used for reconnaissance missions. Israeli intelligence also tested the first tactical UAVs equipped with reconnaissance cameras during the War of Attrition (1967–1970).[26]

Figure 2.5: IAI Scout, a reconnaissance UAV used during the War of Attrition.[7]

2.2.6 Modern UAVs

With the miniaturization of technologies in the 1980s and 1990s, interest in UAVs grew within the U.S. military. The U.S. Navy adopted the AAI Pioneer UAV, jointly developed by AAI Corporation and Israeli company Malat. UAVs saw extensive service during the 1991 Gulf War, demonstrating their potential as cheaper and more capable fighting machines.

Superior UAV technology, such as the Bayraktar TB2, played a significant role in Azerbaijan's successes in the 2020 Nagorno-Karabakh war against Armenia.[27]

Figure 2.6: Bayraktar TB2: [8]

The advancement of smart technologies and enhanced electrical power systems has resulted in a significant rise in the use of drones for consumer and general aviation activities. As of 2021, quadcopter drones have become particularly popular as hobbyist radio-controlled aircraft and toys. The 2010s witnessed a remarkable surge in the popularity of consumer drones, primarily fueled by companies like DJI. These drones became more affordable, compact, and user-friendly, resulting in widespread adoption for various applications, including aerial photography, videography, and even delivery services.[28]

Figure 2.7: DJI Mini 2 SE: [9]

2.2.7 NASA Missions

UAVs are also used in NASA missions. The *Ingenuity* helicopter, an autonomous UAV, operated on Mars from 2021 to 2024. The *Dragonfly* spacecraft, set to launch in 2027, aims to explore Saturn's moon Titan by examining diverse soil types.[29]

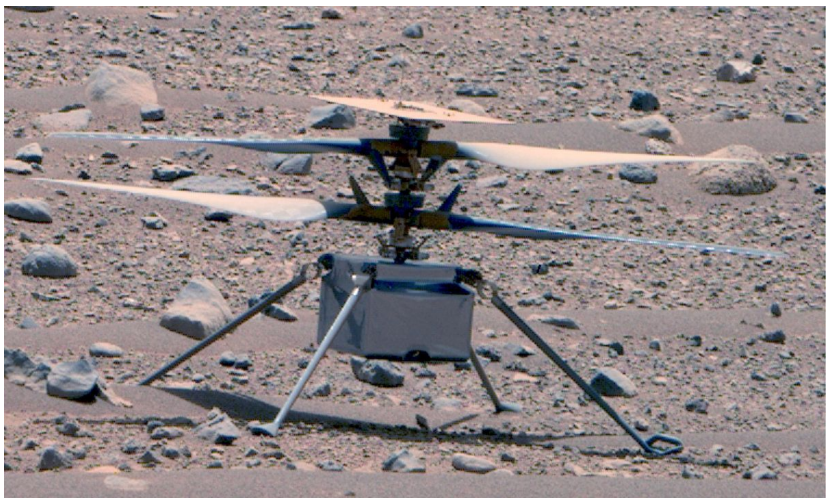

Figure 2.8: The Ingenuity helicopter: [10]

2.2.8 Future Projections

Miniaturization supports the development of small UAVs, which can survey large areas quickly. The global military uncrewed aerial systems (UAS) market is projected to grow from $12.5 billion in 2024 to an estimated $20 billion by 2034, representing a compound annual growth rate of 4.8%.[30]

2.3 Delivery Drones: A Detailed Review

Delivery drones are designed to transport packages, medical supplies, and other goods to various locations, enhancing efficiency and reducing delivery times. This review provides an overview of delivery drones, their statistics, companies utilizing them, specific models, and the technology involved.

2.3.1 Companies and Delivery Drones

Several major corporations have invested in the development and deployment of delivery drones. Here are some notable companies and their respective drone models:

Company	Drone Model	Key Features
Amazon	Amazon Prime Air	Autonomous navigation, vertical takeoff and landing (VTOL), range of up to 15 miles
Google	Wing	VTOL, lightweight design, precision delivery, automated flight paths
UPS	UPS Flight Forward	Partnership with Matternet, VTOL, designed for medical supply delivery
DHL	Parcelcopter	VTOL, capable of delivering in rural and urban areas, autonomous operations
Zipline	Zipline Zips	Fixed-wing design, long-range capability, primarily for medical supplies in remote areas
Walmart	Flytrex	Partnership with Flytrex, automated delivery, VTOL, focus on residential deliveries

Table 2.1: Companies and their Delivery Drones [1]

Figure 2.9: Prime Air: Amazon's proposed delivery service by drone: [11]

2.3.2 Technology

The technology behind delivery drones involves several key components and systems, including:

- **Autonomous Navigation**: Using GPS, sensors, and machine learning algorithms to navigate and avoid obstacles.
- **VTOL (Vertical Takeoff and Landing)**: Allows drones to operate in confined spaces and deliver packages directly to doorsteps.
- **Payload Capacity**: Varies by drone model, typically ranging from a few pounds to over 10 pounds.

- **Battery Life and Range**: Advanced battery technology extends flight time and delivery range, with some drones capable of flying over 15 miles on a single charge.
- **Communication Systems**: Ensure real-time tracking and control, often involving 4G/5G networks or dedicated communication links.
- **Safety Mechanisms**: Redundant systems, emergency landing protocols, and collision avoidance technology to ensure safe operations.

2.3.3 Statistics and Adoption

2.3.3.1 Global Delivery Drone Market

Year	Market Size (USD Billion)	Growth Rate (%)
2020	1.2	20
2021	1.5	25
2022	1.9	26.7
2023	2.4	27.3
2024 (est.)	3.1	29.2

Table 2.2: Global Delivery Drone Market Growth [2]

2.3.3.2 Drone Deliveries by Company

Company	Number of Deliveries (2022)
Amazon	500,000
Google Wing	150,000
UPS	100,000
DHL	75,000
Zipline	200,000
Walmart	50,000

Table 2.3: Drone Deliveries by Company [3]

2.3.4 Key Advantages

- **Speed**: Drones can significantly reduce delivery times, particularly in urban areas with heavy traffic.
- **Cost Efficiency**: Lower operational costs compared to traditional delivery methods.
- **Accessibility**: Ability to reach remote or hard-to-access areas, crucial for medical deliveries in rural regions.
- **Environmental Impact**: Reduced carbon footprint compared to delivery trucks.

2.3.5 Challenges and Considerations

- **Regulatory Hurdles**: Different countries have varying regulations regarding drone usage, which can impact deployment.
- **Safety and Security**: Ensuring the safety of operations and preventing potential misuse or hacking.
- **Weather Dependency**: Adverse weather conditions can affect drone performance and reliability.
- **Public Acceptance**: Gaining public trust and acceptance for widespread drone deliveries.

2.4 Project Scope and Objectives

For our project, we will be using a quad-copter (four motors copter) for many considerations:

Stability and Control

- **Enhanced Stability**: Quadcopters are inherently more stable due to their four motor and propeller configurations. This design allows for balanced lift and thrust distribution, making it easier to maintain steady flight even in windy conditions.
- **Precise Control**: The four motors enable precise control over the drone's movement, including vertical takeoff and landing (VTOL) capabilities, which are crucial for delivering packages to specific locations without needing a runway.

Reliability

- **Simplified Mechanics**: Compared to hexacopters or octocopters, quadcopters have fewer mechanical components, simplifying maintenance and reducing the likelihood of mechanical failures.

Efficiency and Cost-Effectiveness

- **Power Efficiency**: Quadcopters typically have a favorable power-to-weight ratio. They can achieve sufficient lift and flight time with a relatively simple and lightweight design, making them energy-efficient for short to medium-range deliveries.
- **Cost-Effective**: The simplicity of the quadcopter design, with fewer motors and less complex construction compared to other multi-rotor drones, translates to lower manufacturing and maintenance costs. This makes them a cost-effective solution for delivery services.

Scalability

- **Scalable Operations**: Due to their cost-effectiveness and ease of use, quadcopter delivery drones can be scaled up in numbers to handle increased delivery demands without significant incremental costs.

Considering the key advantages and challenges faced by delivery drones, this project aims to design, develop, and analyze a quadcopter delivery drone tailored to the specific logistical and environmental challenges in Algeria. The primary focus is creating a cost-effective, efficient, and reliable drone that can autonomously deliver packages, leveraging the resources and fabrication capabilities available at L'École Nationale Polytechnique.

Objective	**Description**
Autonomous Operation	The drone must be capable of fully autonomous operation, including takeoff, navigation, delivery, and landing without human intervention.
Package Delivery	The drone must be able to deliver a package weighing at least 500 grams.
Fabrication Constraints	The drone must be fabricated using the machines available at L'École Nationale Polytechnique, specifically 3D printers and laser cutting machines, to minimize fabrication costs.
Structural and Mechanical Design	The structure of the drone must be as lightweight as possible while maintaining durability and resistance to vibrations. The design should be streamlined to minimize aerodynamic drag and improve flight efficiency. The drone must incorporate a robust latching and release mechanism for secure and efficient package delivery.
Stability and Control	The drone must exhibit stable flight characteristics under various load and environmental conditions. Advanced control systems, including different PID control algorithms, must be implemented to ensure precise and stable flight.
Weather Resistance	The drone must be weather resistant, specifically able to operate in rainy conditions and resistant to water exposure.
Environmental and Economic Impact	The project should consider the environmental impact of drone operations and strive for sustainable design choices. The economic feasibility of the drone's production and deployment in Algeria will be assessed to ensure cost-effectiveness.

Table 2.4: Summary of Project Objectives

Chapter 3

Design & Calculations

3.1 Main Components of a Quadcopter

First, we need to understand the components of a drone, their functions, and how to integrate them. This knowledge is essential for performing the necessary calculations to select the appropriate components. A quadcopter, in particular, consists of several key parts that work together to facilitate flight and control. Here are the main components:

3.1.1 Frame

- **Material Selection**: The frame is typically made from lightweight and durable materials such as carbon fiber, aluminum, or high-strength plastic.
- **Design**: The frame design must balance strength, weight, and aerodynamics. It typically consists of a central hub with four arms extending outward, where the motors are mounted. The frame must provide mounting points for all other components and ensure even weight distribution for stability.

Figure 3.1: F450 frame

3.1.2 Propellers

- **Material**: Propellers are typically made from plastic, carbon fiber, or composite materials. Carbon fiber propellers are more rigid and lightweight, providing better performance and durability.

- **Size and Pitch**: Propeller size (diameter) and pitch (angle of the blades) are critical factors affecting thrust, efficiency, and responsiveness. Larger propellers with higher pitch generate more thrust but may require more power.

- **Balance**: Properly balanced propellers are essential to minimize vibrations and ensure smooth flight. Unbalanced propellers can cause instability and stress on the motors and frame.

Figure 3.2: 1045 Propellers, one clockwise (CW) and one counterclockwise (CCW) to balance the rotational forces.

3.1.3 Motors

- **Type**: Brushless DC motors are commonly used due to their high efficiency, reliability, and power-to-weight ratio compared to brushed motors.

- **Function**: Each of the four motors is mounted at the end of one of the frame's arms. The motors generate thrust by spinning the propellers. Two motors spin clockwise (CW) and two counterclockwise (CCW) to balance the torque and stabilize the quadcopter.

- **Specifications**: Important specifications include KV rating (RPM per volt), thrust output, and power consumption. The motors must be chosen based on the desired performance characteristics and the total weight of the quadcopter.

Figure 3.3: 1000 kv BLDC Brushless Motor

3.1.4 Electronic Speed Controllers (ESCs)

- **Function**: ESCs regulate the speed of the motors by converting the DC power from the battery into the appropriate three-phase AC power. They receive control signals from the flight controller to adjust motor speeds dynamically.
- **Specifications**: Key specifications include current rating, voltage rating, and firmware compatibility. The ESCs must be matched to the motor specifications and the overall power system.
- **Features**: Modern ESCs may include features such as regenerative braking, active braking, and programmable settings for optimizing performance.

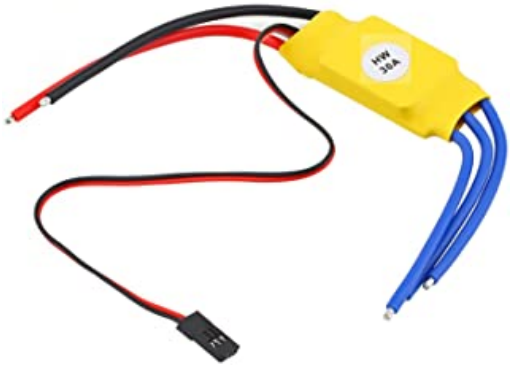

Figure 3.4: 30A ESC

3.1.5 How The Brushless Motor and the ESC Work Together

The brushless motor and ESC work together to convert electrical energy into mechanical motion, enabling precise control over the drone's propellers and overall flight dynamics. The ESC's role in switching the semiconductor switches in the correct sequence is crucial for generating the rotating magnetic field necessary for the motor's operation.

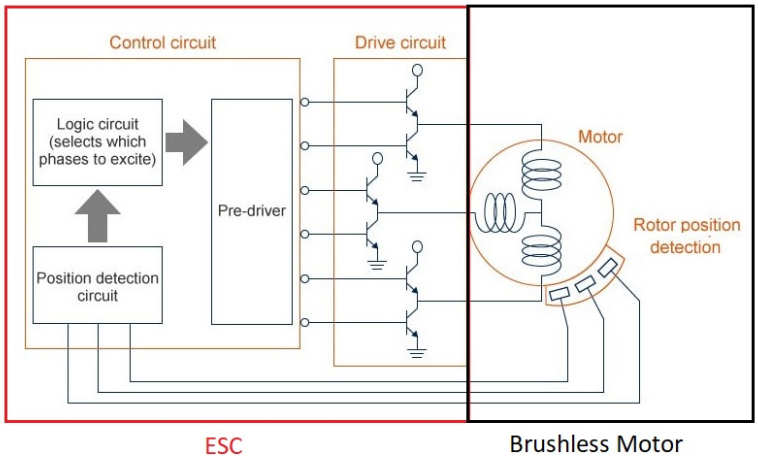

Figure 3.5: Bloc Diagram of the ESC-BLDC ensemble

- **Control Signal**: The flight controller sends a control signal to the ESC, specifying the desired speed of the motor.
- **Power Adjustment**: The ESC adjusts the electrical power sent to the motor based on the control signal.
- **Magnetic Field Creation**: The ESC energizes the windings in the stator in a specific sequence to create a rotating magnetic field.
- **Rotor Movement**: The rotating magnetic field interacts with the permanent magnets in the rotor, causing it to spin.
- **Continuous Operation**: The ESC continuously adjusts the power and commutation timing to maintain the desired motor speed and direction, based on real-time feedback from the rotor's position, often detected by a Hall sensor.

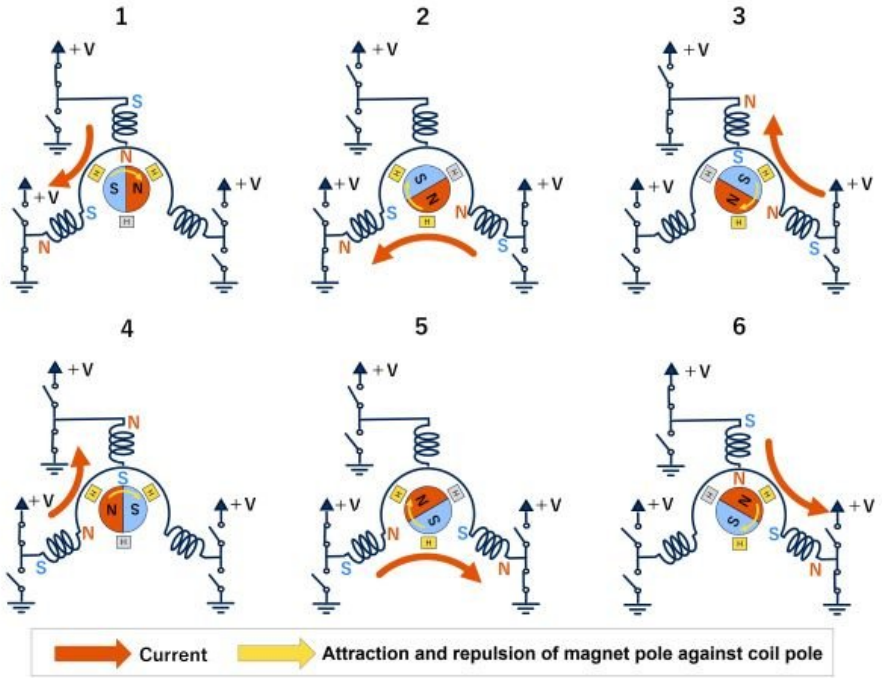

Figure 3.6: Steps executed by the ESC to rotate the motor

3.1.6 Flight Controller

- **Function**: The flight controller is the brain of the quadcopter, responsible for stabilizing and controlling the aircraft. It processes input from sensors and the remote controller to adjust the motor speeds and maintain desired flight behavior.

- **Sensors**: Integrated sensors typically include gyroscopes and accelerometers for measuring angular velocity and acceleration. Additional sensors like magnetometers, barometers, and GPS modules can be included for enhanced capabilities.

- **Firmware**: The flight controller runs firmware that implements flight stabilization algorithms, control loops, and additional functionalities such as autonomous flight modes and failsafe procedures.

Figure 3.7: Pixhawk PX4 PIX 2.4.8 32 Bit Flight Controller Autopilot with its accessories

3.1.7 Battery

- **Type**: Lithium-polymer (LiPo) batteries are commonly used due to their high energy density, lightweight, and ability to deliver high current.

- **Specifications**: Important specifications include voltage (measured in cells, e.g., 3S for 11.1V), capacity (mAh), and discharge rate (C rating). The battery must be chosen based on the power requirements of the quadcopter and desired flight time.

- **Safety**: Proper handling and charging are critical to prevent overcharging, over-discharging, and potential hazards such as fires.

Figure 3.8: 5000 mAh Li-Po Battery

3.1.8 Radio Receiver

- **Function**: The radio receiver receives control signals from the remote controller (transmitter) and passes them to the flight controller.
- **Specifications**: Key specifications include the number of channels (corresponding to the number of control inputs), frequency band (e.g., 2.4 GHz), and communication protocol (e.g., PWM, PPM, SBUS).
- **Antenna**: Proper placement and orientation of the antenna are crucial for maintaining a strong and reliable connection.

3.1.9 Remote Controller (Transmitter)

- **Function**: The handheld device used by the pilot to control the quadcopter. It sends control inputs to the radio receiver.
- **Features**: Modern transmitters offer programmable channels, telemetry feedback, customizable switches and sticks, and sometimes integrated screens for real-time data display.
- **Range and Frequency**: Important factors include operating range, frequency band, and signal strength to ensure reliable control over the quadcopter.

Figure 3.9: FlySky FS-i6x 2.4G Transmitter on the left, with its receiver on the right. It has a range of 1 km

3.1.10 GPS Module

- **Function**: Provides positional data to the flight controller for navigation and autonomous flight capabilities such as waypoint missions and return-to-home (RTH) functionality.
- **Integration**: The GPS module typically includes a GPS receiver and antenna, and may also include additional sensors like a compass for improved navigation accuracy.
- **Accuracy**: Factors affecting GPS accuracy include satellite signal strength, the number of satellites in view, and interference from the environment.

Figure 3.10: Pixhawk GPS Module

3.1.11 Telemetry Module

- **Function**: Transmits real-time flight data (e.g., battery voltage, GPS location, altitude) from the quadcopter to the pilot or ground station.
- **Benefits**: Provides valuable information for monitoring the quadcopter's status during flight, ensuring safe and efficient operation.

- **Communication**: Typically operates on frequencies such as 433 MHz or 915 MHz and can include data such as flight logs and the health status of the quadcopter.

Figure 3.11: Pixhawk Telemetry Module

3.2 Propeller Selection

One of the most critical components influencing our drone's performance is the propeller. The key parameter we need to focus on is the lift generated by the propeller and its efficiency. High-quality propellers are typically manufactured using plastic injection molding, which ensures minimal surface roughness and equal mass distribution. These factors are crucial for reducing drag caused by fluid-surface friction and minimizing vibration.

During my preparations for the Eurobot 2023 competition, I attempted to 3D print a propeller for an electric ducted fan using the finest resolution possible. However, the 3D-printed propeller only delivered about half the performance of a commercially produced, injection-molded propeller. The primary issue was the surface roughness of the 3D-printed blades, which caused significant power loss due to friction, resulting in insufficient lift.

Hence, for our project, utilizing high-quality, injection-molded propellers to maximize drone performance is crucial. Upon researching propeller options available for purchase in Algeria, which are relatively scarce, possibly due to restrictions, we found only one model that appeared compatible with our project: the 1045 propeller. Therefore, let's conduct a detailed study on this propeller to determine if it meets our requirements effectively.

Parameter	Specification
Weight	14 gm
Shaft Diameter	6 mm
Total length	10 inch / 254 mm
Material	ABS
Color	Black
Number of Blades	2
Plastic Reducers	2.75, 3, 3.17, 4, 4.70, 5, 6, 6.25"

Table 3.1: 1045 Propeller Specifications

3.2.1 1045 Propeller Specifications

3.2.2 Thrust vs Rotational Speed

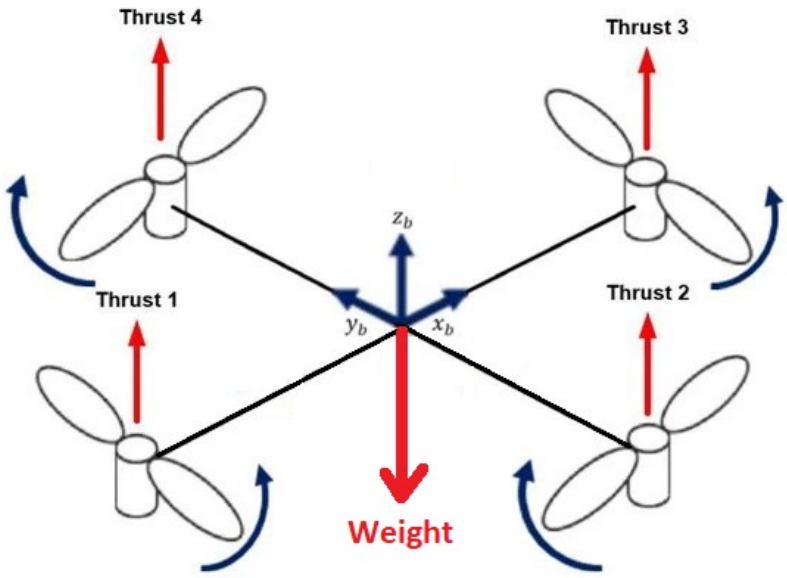

Figure 3.12: Forces Equilibrium in Quad-Copter

Based on the experimental data available on **database.tytorobotics.com** [31] for the 1045 propeller, we observe the following thrust versus rotational speed graph:

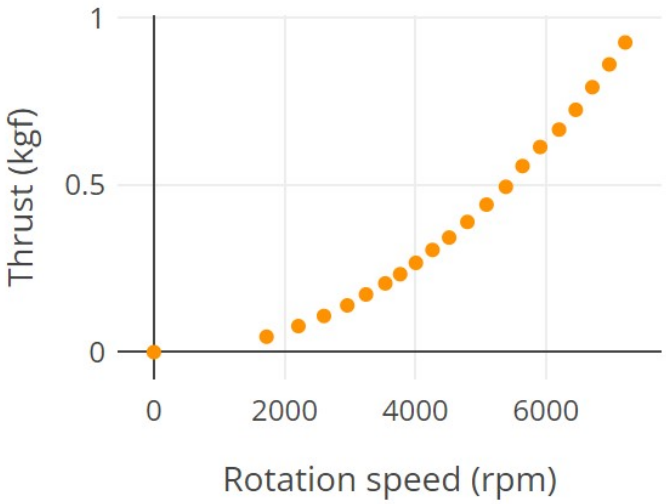

Figure 3.13: 1045 Propeller Thrust vs Rotational Speed graph

Initially, this graph indicates that the propeller can achieve a maximum thrust of **0.927 kgf** at an **rpm of 7214**. Therefore, with four propellers, the combined thrust could lift up to $4 \times 0.927 =$ **3.708 kg** (quad-copter weight + payload). However, achieving maximum thrust does not necessarily mean the propeller operates within its peak efficiency range. Thus, it's essential to examine the efficiency graph to understand its performance across different operational conditions.

3.2.3 Propulsion System Efficiency vs Rotational Speed

Upon analyzing the Efficiency of the Propulsion System versus the Rotational Speed graph, we observe that the peak efficiency occurs around a rotational speed of $N = 3542$ rpm. To optimize our drone's autonomy with the available energy, our propulsion system should operate close to this rotational speed to achieve maximum efficiency. This approach ensures we get the most out of our energy resources, enhancing the drone's overall flight time and performance.

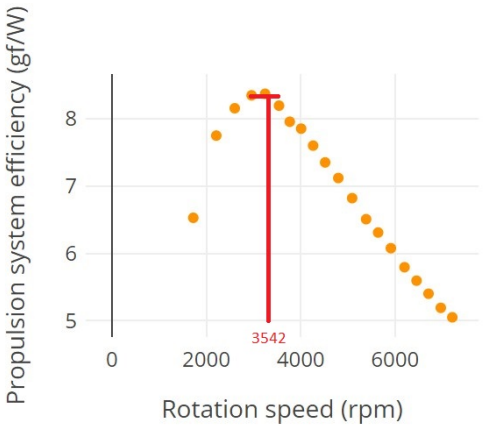

Figure 3.14: 1045 Propulsion System Efficiency vs Rotational Speed graph

The next step is to determine the optimal thrust corresponding to the rotational speed of$N =$

3542 rpm, which is identified from the Thrust vs Rotational Speed graph. At this specific speed, the thrust is:

$$T_{optimal} = T_{(N=3542rpm)} = 0.206\ kgf$$

This value represents the thrust at which the propulsion system operates most efficiently, allowing us to maximize the drone's performance and energy utilization.

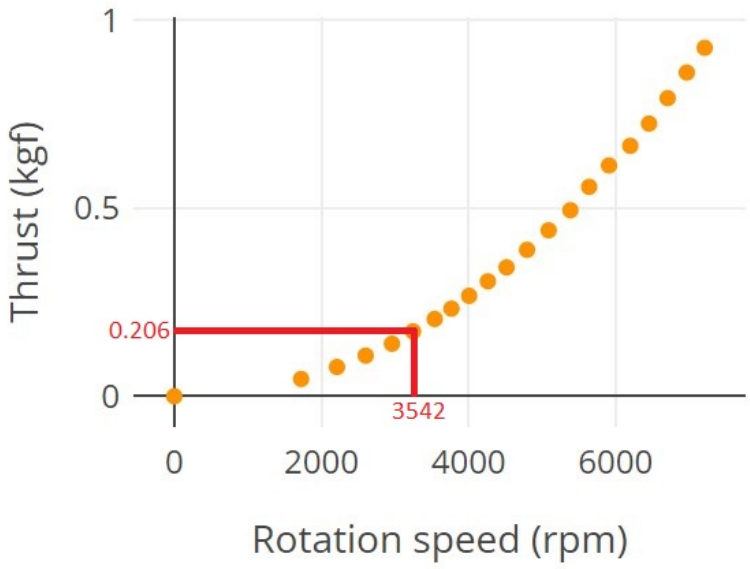

Figure 3.15: 1045 Propulsion System Optimal Thrust

Therefore, the total weight of our drone should be approximately four times this thrust value, as it is a quad-copter with four propellers.

$$W_{optimal} = 4 \times T_{optimal} = 0.824\ kg$$

To determine if the actual weight of the drone aligns with this optimal value, we need to select motors and a frame that is compatible with these propellers.

3.3 Motor Selection

After examining multiple data sheets for various BLDC (brushless DC) motors, we have determined that the A2212/13T model is well-suited for our selected propellers. The datasheet indicates that this motor has been tested with the APC E 10x5 propeller, which closely resembles our 1045 propeller model.[32] This motor weights **52.7 g**

A2212/13T TECHNICAL DATA

Propeller	Gear Ratio	Volts	Amps	Watts	RPM
GWS HD 8x4	1	7	3.35	23	6630
GWS HD 8x4	1	7.9	4.1	32	7410
GWS HD 8x4	1	8.9	4.85	43	8220
GWS HD 8x4	1	9.9	5.65	55	8940
GWS HD 8x4	1	10.9	6.5	70	9660
GWS HD 9x5	1	6.9	5.5	37	6000
GWS HD 9x5	1	7.9	6.7	52	6660
GWS HD 9x5	1	8.9	7.85	69	7290
GWS HD 9x5	1	9.9	9.25	91	7920
APC E 10x5	1	6.9	7	48	5610

Figure 3.16: Snipet from the A2212/13T data-sheet

3.4 ESC Selection

Upon reviewing the datasheet for the 30A BLDC ESC [33], which is both affordable and readily available in Algeria, we confirmed that its voltage and current ratings are compatible with our A2212/13T motor. This makes it a suitable choice for our project, ensuring reliable performance within the required specifications.

30A BLDC ESC

Specifications

- Output: 30A continuous; 40Amps for 10 seconds
- Input voltage: 2-4 cells Lithium Polymer / Lithium Ion battery or 5-12 cells NiMH / NiCd
- BEC: 5V, 3Amp for external receiver and servos
- Max Speed: 2 Pole: 210,000rpm; 6 Pole: 70,000rpm; 12 Pole: 35,000rpm
- Weight: 32gms
- Size: 55mm x 26mm x 13mm

Figure 3.17: Snipet from the 30A BLDC ESC data-sheet

3.5 Frame Selection

3.5.1 Frame Shape

There are multiple shapes for quadcopters. However, the X frame is the most common and popular choice for DIY quadcopters due to its balance of stability, durability, and versatility. In an X frame, the electronics are mounted at the junction, and the motors are placed at the tips of the arms. This configuration means that motors work in pairs to control the drone's movement in different directions, providing consistent and balanced control. **True X**: Completely symmetrical, offering equal stability on all axes. The key advantage of the X frame is its durability [12]. In the event of a crash, the impact is absorbed by two arms instead of one,

reducing the likelihood of damage. This makes the X frame a robust and reliable option for various applications, including stunts, FPV racing, and general use.

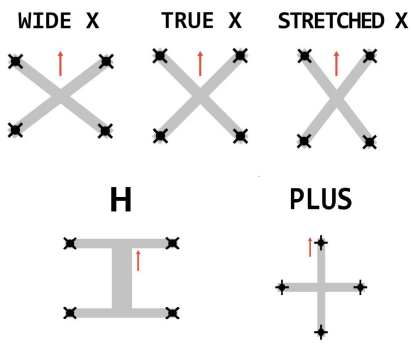

Figure 3.18: Different Frame Shapes: [12]

3.5.2 Frame Dimensions

According to the table extracted from **genstattu.com**[34] that outlines frame compatibility with various propeller sizes, a 450mm frame (450 mm is the distance between two motors on the same diagonal) is well-suited for 10-inch propellers. This compatibility ensures that the propellers have sufficient clearance and optimal performance, making the 450mm frame a reliable choice for our project when using 10-inch propellers.

Frame Size	**Prop Size (inches)**	**KV**
150mm or smaller	3 or smaller	3000KV and higher
180mm	4	2600KV – 3000KV
210mm	5	2300KV-2600KV
250mm	6	2000KV-2300KV
350mm	7	1200KV-1600KV
450mm	8, 9, 10 or larger	1200KV and lower

Table 3.2: Frame compatibility with various propeller sizes and motors

We will design our frame from scratch in the upcoming chapters. However, to estimate and calculate the drone's weight, we will use the weight of the F450 frame as a reference, which is **282 g**.

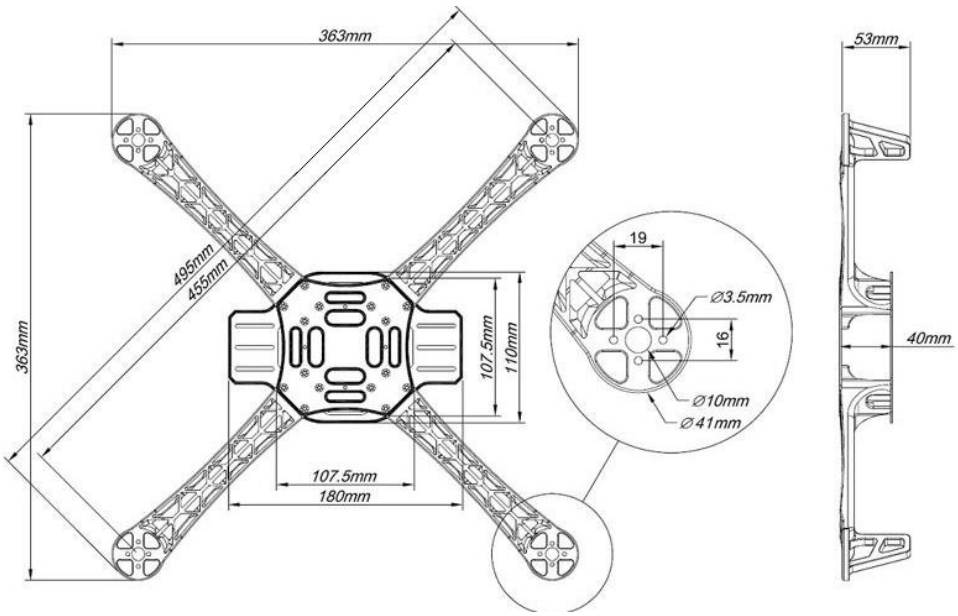

Figure 3.19: F450 Frame Dimensions: [13]

3.6 Battery

LiPo (Lithium Polymer) batteries are used in drones for several advantages:

1. **High Energy Density:** LiPo batteries have a high energy density, meaning they can store a large amount of energy relative to their size and weight. This is crucial for drones where minimizing weight while maximizing flight time is essential.
2. **High Discharge Rates:** LiPo batteries can discharge at high rates, providing the necessary power for motors and other components during flight maneuvers, take-offs, and landings.
3. **Compact and Lightweight:** LiPo batteries are relatively compact and lightweight compared to other battery chemistries like NiMH (Nickel Metal Hydride) or Li-ion (Lithium-Ion). This helps in reducing the overall weight of the drone, which is critical for maximizing flight efficiency and maneuverability.
4. **Availability of Different Configurations:** LiPo batteries are available in various configurations (voltage, capacity, and discharge rates), allowing drone builders to choose batteries that best suit their specific requirements for flight time, power, and size constraints.
5. **Fast Charge and Recharge Times:** LiPo batteries generally have faster charge and recharge times compared to other types of batteries, which is beneficial for minimizing downtime between flights.
6. **Suitability for High Power Applications:** LiPo batteries are well-suited for high-power applications like drones, where bursts of power are needed for quick accelerations and maneuvers.

3S (3-cell) batteries with a capacity of 4200 mAh and a 25C discharge rate are readily available at the FabLab in l'École Nationale Polytechnique. These batteries are compatible and suitable for our needs. Their weight is **305 g** per battery.

3.7 Flight Controller Selection

We will use the Pixhawk PIX4 as a flight controller, because it offers several advantages:

1. **Advanced Autopilot Features:** The Pixhawk PIX4 is equipped with advanced autopilot features, including GPS navigation, waypoint navigation, and autonomous flight modes. These capabilities are essential for various drone applications, from aerial photography to autonomous missions.
2. **Reliability and Stability:** Pixhawk flight controllers are known for their reliability and stability in controlling drones, even in challenging environments and weather conditions. This ensures precise and stable flight performance, critical for professional and hobbyist drone operations.
3. **Open-Source Software:** The Pixhawk PIX4 runs on open-source software, providing flexibility for customization and integration with third-party software and hardware. This allows developers and enthusiasts to modify and enhance its functionalities according to specific project requirements.
4. **Compatibility with Various Platforms:** It supports a wide range of platforms and configurations, accommodating different types of drones and payloads. This versatility makes it suitable for both fixed-wing and multirotor drones, as well as hybrid designs.
5. **Community Support and Development:** Being part of the Pixhawk ecosystem, the PIX4 benefits from a large and active community of developers, enthusiasts, and researchers. This community support contributes to ongoing software updates, troubleshooting resources, and collaborative development of new features.
6. **Sensor Integration:** The Pixhawk PIX4 supports integration with a variety of sensors, such as IMUs (Inertial Measurement Units), barometers, and magnetometers. This enables precise attitude estimation and navigation capabilities essential for accurate drone control.
7. **Available to buy in Algeria**

Its weight is **15.8 g**

Figure 3.20: Pixhawk PIX4 Flight Controller (Auto-Pilot)

3.8 Component Weights and Efficiency Analysis

The following table summarizes the weight of each component of our drone, along with the total weight both with and without payload:

Component	Unit Weight (g)	Quantity	Weight (g)
1045 Propeller	7	4	28
2212/13T Motor	52,7	4	210,8
30A BLDC ESC	32	4	128
f450 Frame	282	1	282
Battery	214	1	214
FlySky FS-i6 receiver	6,4	1	6,4
Pixhawk PIX4	15,8	1	15,8
Mechanism	9	1	9
Payload	500	1	500
Total Weight without payload			894
Total Weight with payload			1394
Thrust per Propeller without payload			223,5
Thrust per Propeller with payload			348,5

Table 3.3: Components and Total Weight of the Drone

Given that any delivery mission our drone undertakes is divided into two distinct phases—one with the payload during the outbound journey, and the other without the payload during the return to the home position—we will analyze both scenarios to ensure optimal performance and efficiency.

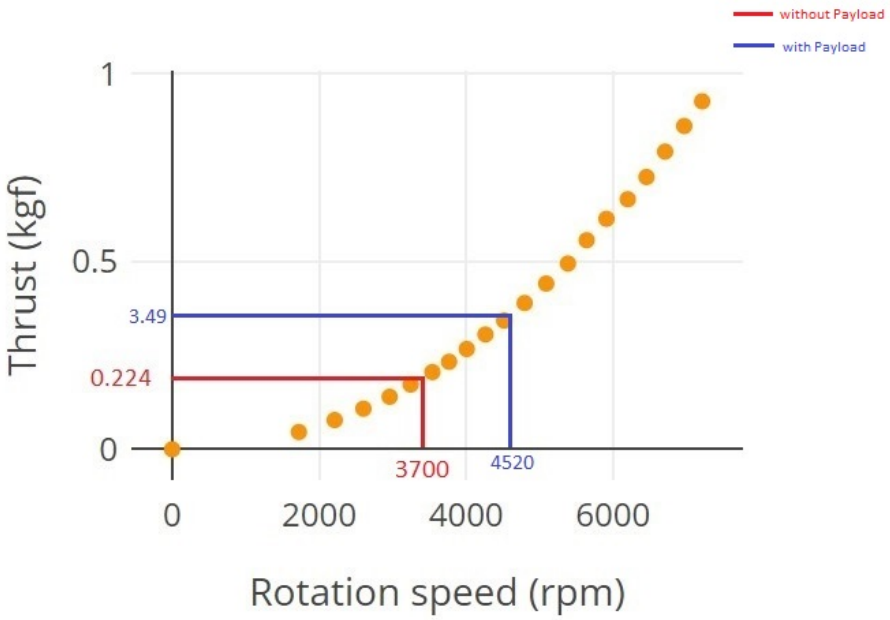

Figure 3.21: Thrust Analysis

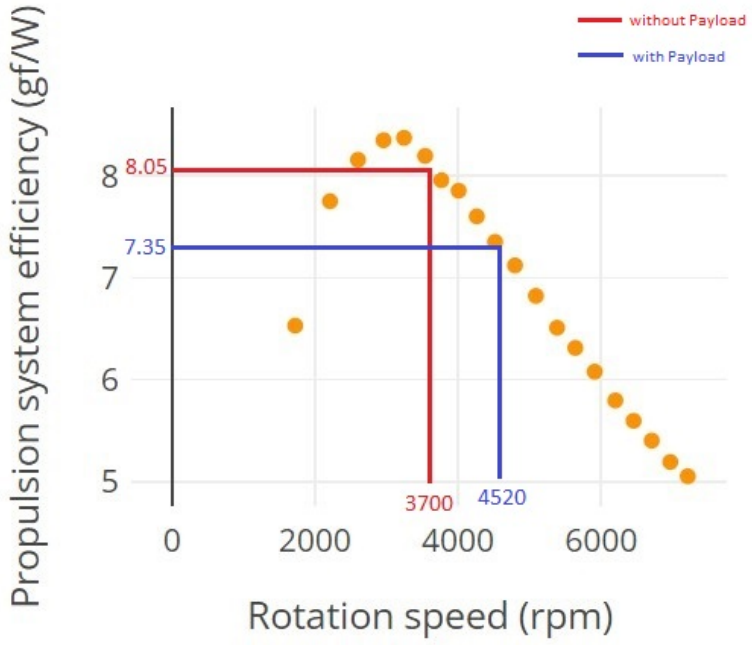

Figure 3.22: Efficiency Analysis

3.8.1 Without Payload

From the data, we observe that without a payload, each propeller needs to generate a thrust of

$$T_{\text{without payload}} = 0.2235 \text{ kgf}.$$

This is close to the optimal thrust value of

$$T_{\text{optimal}} = 0.206 \text{ kgf}.$$

By plotting $T_{\text{without payload}}$ on the Thrust vs. Rotational Speed graph, we find it corresponds to a rotational speed of

$$N_{T_{\text{without payload}}} = 3700 \text{ rpm}.$$

At this speed, the efficiency is

$$\eta_{\text{without payload}} = 8.05 \text{ gf/W}.$$

This efficiency is only

$$\Delta_{\eta_{\text{without payload}}}\% = \frac{8.37 - 8.05}{8.37} \times 100 = \boxed{4.82\%}$$

lower than the maximum efficiency.

3.8.2 With Payload

From the data, we observe that without a payload, each propeller needs to generate a thrust of

$$T_{\text{with payload}} = 0.3485 \text{ kgf}.$$

By plotting $T_{\text{with payload}}$ on the Thrust vs. Rotational Speed graph, we find it corresponds to a rotational speed of

$$N_{T_{\text{with payload}}} = 4520 \text{ rpm}.$$

At this speed, the efficiency is

$$\eta_{\text{with payload}} = 7.35 \text{ gf/W}.$$

This efficiency is only

$$\Delta_{\eta_{\text{with payload}}}\% = \frac{8.37 - 7.35}{8.37} \times 100 = \boxed{12.1\%}$$

lower than the maximum efficiency.

3.9 Conclusion

The efficiency values indicate that the 1045 propeller, even under varying load conditions, remains within a reasonable efficiency range. The minor deviations from optimal efficiency suggest that the 1045 propeller, along with the other selected components, is a well-suited and efficient choice for our drone.

Overall, the combination of the 1045 propeller, A2212/13T motors, 30A BLDC ESCs, and the 450mm frame provides a balanced and efficient system, ensuring that our drone performs effectively in both payload and no-payload phases of the mission.

Chapter 4

Aerodynamic Analysis

One significant issue that adversely affects the efficiency and autonomy of drones is the drag force acting on the arms. This drag force, resulting from air resistance, opposes the forward motion of the drone. The resistance increases with the square of the air stream velocity, making it a critical factor in high-speed or long-duration flights.

$$D = C_d \frac{\rho V^2}{2} A$$
$$\text{Drag force} = \text{drag coefficient} \times \text{density} \times \frac{\text{velocity}^2}{2} \times \text{reference area} \tag{4.1}$$

This aerodynamic drag leads to increased power consumption. To overcome the drag force, the motors must work harder, consuming more power from the battery. This increased power demand reduces the flight time and the distance the drone can cover on a single charge.

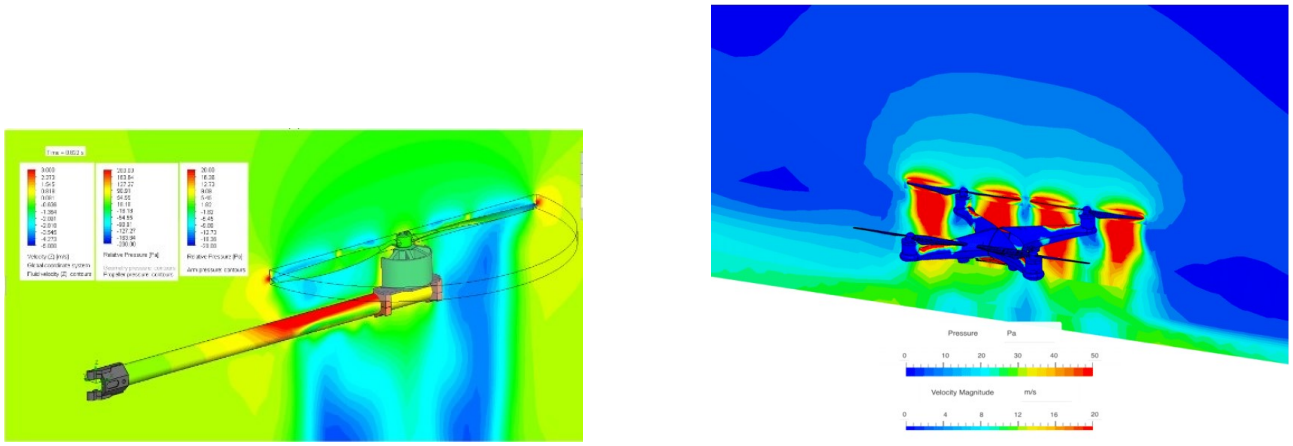

Figure 4.1: Quadcopter in hover mode, showing velocity and pressure contours on the drone arms [14] [15]

As shown in the figures above, there is high pressure in the region below the propeller on the arm. This high pressure is the source of drag force that pulls the quadcopter down and opposes the motors' lift force. To achieve a more efficient system, it is essential to minimize this parasitic force by optimizing the arm geometry and using an appropriate airfoil.

4.1 Shape Effects on Drag

The majority of quadcopter arms have circular or rectangular cross-sections, similar to the F450 frame. While these shapes provide structural stability, they do not minimize drag.

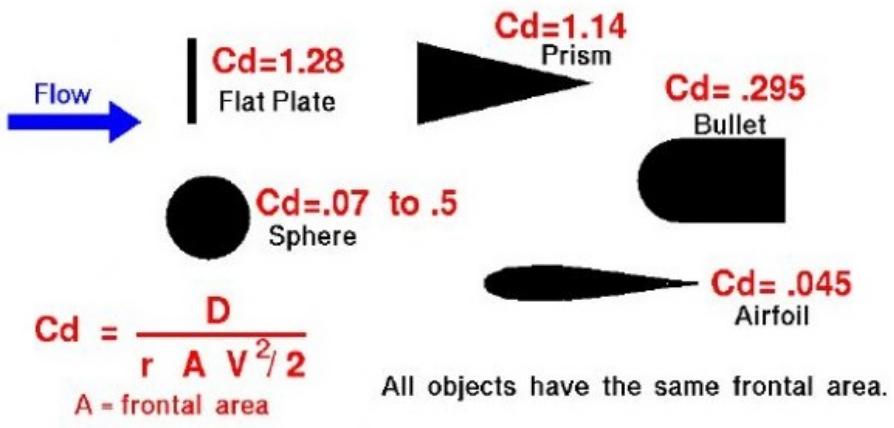

Figure 4.2: The effect of shape on the amount of drag [16]

As observed in the figure above, the shape that minimizes drag is the streamlined shape. However, there are numerous streamlined shapes to consider. To narrow down the options, we will focus on symmetrical airfoils. Symmetrical airfoils are preferred because they do not generate unnecessary lift forces that could cause the quadcopter to yaw.

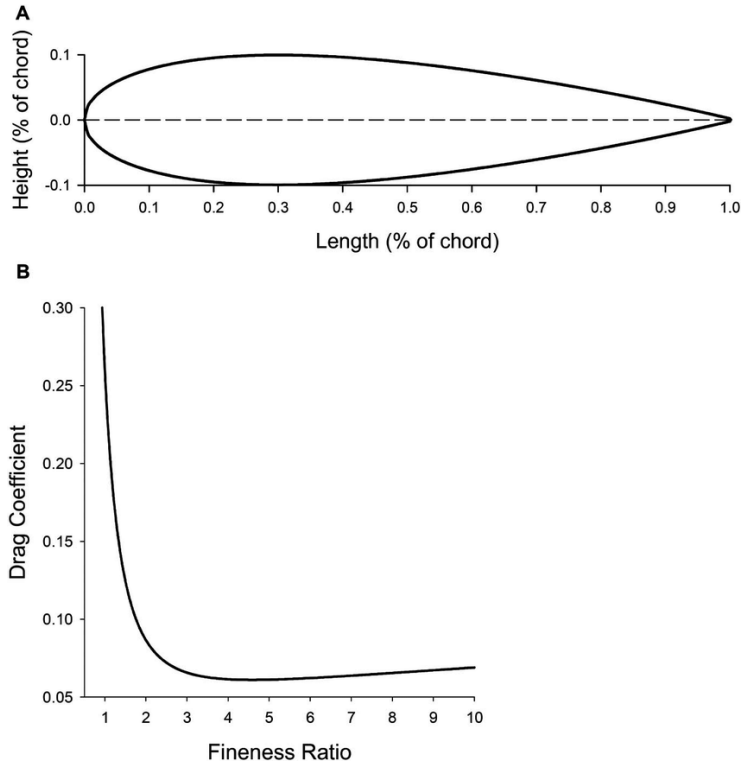

Figure 4.3: A streamlined shape illustrated using a foil without camber [17]

Another important factor to consider is the **Fineness Ratio**, which is the ratio of the chord length to the maximum thickness of an airfoil, expressed as a percentage. According to the National Advisory Committee for Aeronautics (NACA), the relationship between fineness ratio

and drag coefficient indicates that a streamlined body with minimal resistance typically has a fineness ratio around 4.5 (Jacobs et al., 1933; Hoerner, 1965) [17].

4.2 Selecting the appropriate airfoil

4.2.1 Measuring the Air Stream Velocity

Before selecting an appropriate airfoil, we need to determine the velocity of the air below the propellers. This information is crucial for calculating the **Reynolds number**, which will allow us to compare different airfoils and simulate various shapes effectively.

To measure the air stream velocity, an experiment was conducted using the 1045 propeller with its brushless motors. These components were isolated and mounted on an old drone arm. The rotational speed was varied to its maximum, and the free air velocity was measured using a Pitot tube. The experiment yielded a maximum air velocity of

$$V_{\max} = 18 \text{ m/s}.$$

Figure 4.4: The experiment was conducted in FABLAB using the LGMD's Pitot Tube

4.2.2 Using Airfoiltools.com Database Search

Airfoiltools.com is a comprehensive online resource providing detailed information on a wide range of airfoils. It offers tools for airfoil selection, comparison, and analysis, including coordinate data, performance graphs, and aerodynamic characteristics. This platform is extensively used by engineers and designers in the aerospace field to optimize airfoil designs for various applications.

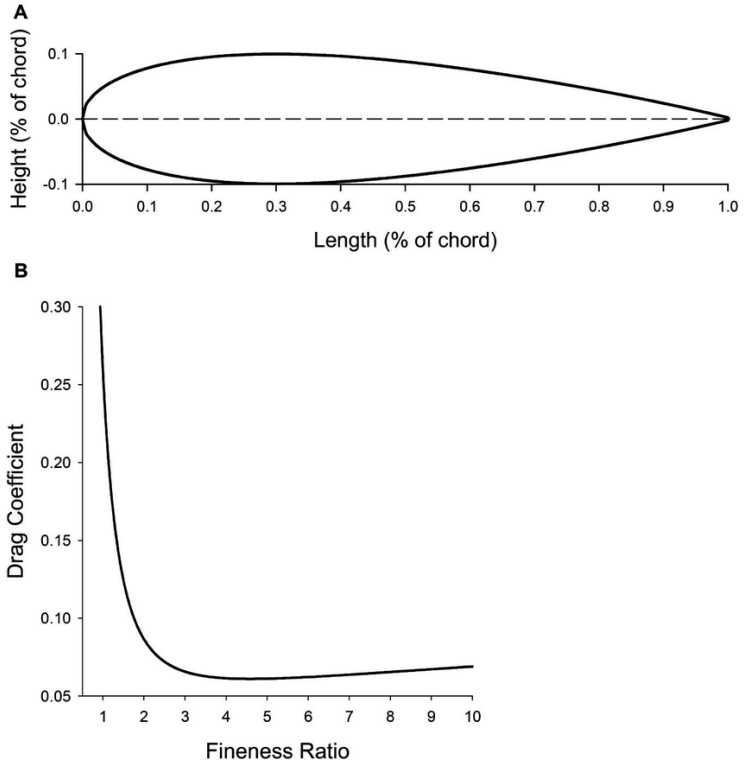

Figure 4.5: Airfoiltools.com search tool interface

In the search tool, a camber of 0 was specified to include only symmetrical airfoils. Additionally, a minimum thickness of 20% and a maximum of 25% were set to find airfoils with a fineness ratio around 4.5 ($\frac{1}{4} \times 100 = 22.22\%$). The following airfoils were identified:

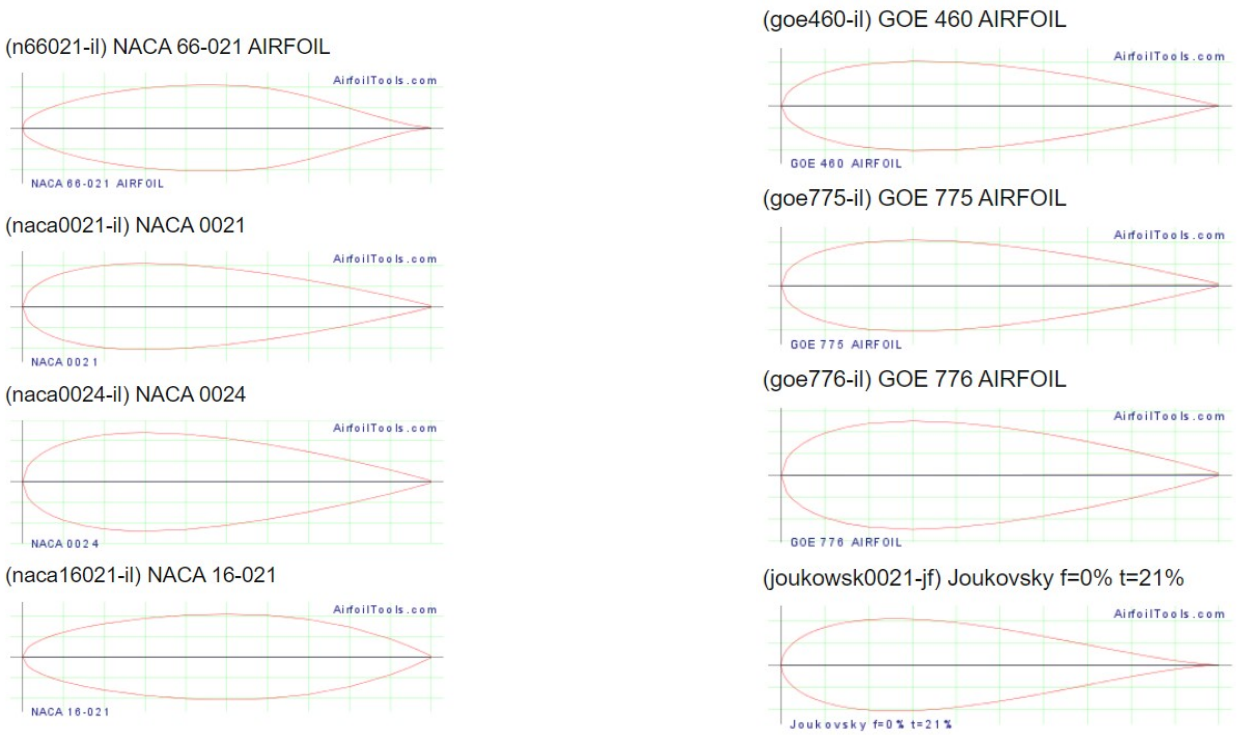

Figure 4.6: Search results from Airfoiltools.com

4.2.3 Airfoil Comparison

The next step is to compare the selected airfoils to determine which has the minimum drag coefficient at a 0° angle of attack. First, we need to calculate the Reynolds number to select the appropriate range for comparison. The Reynolds number is calculated using the following formula:

$$\mathrm{Re} = \frac{\rho v l}{\mu} = \frac{v l}{\nu}$$

where:

- v = Velocity of the fluid
- l = Characteristic length (chord width of the airfoil)
- ρ = Density of the fluid
- μ = Dynamic viscosity of the fluid
- ν = Kinematic viscosity of the fluid

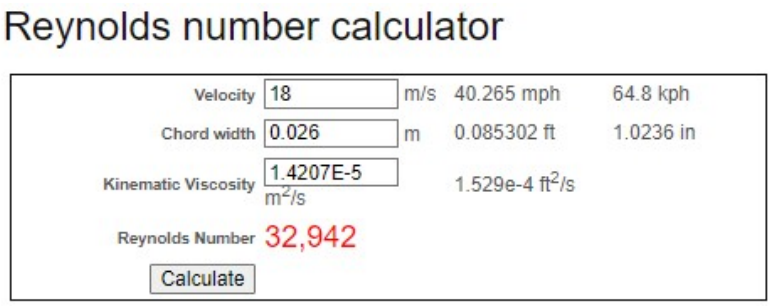

Figure 4.7: Calculating the Reynolds number

We calculated a Reynolds number value of:

$$\mathrm{Re} = 32942$$

We will select a value of 50000 in the comparison filters as it is the closest available option. Next, we compare the C_d (drag coefficient) graphs.

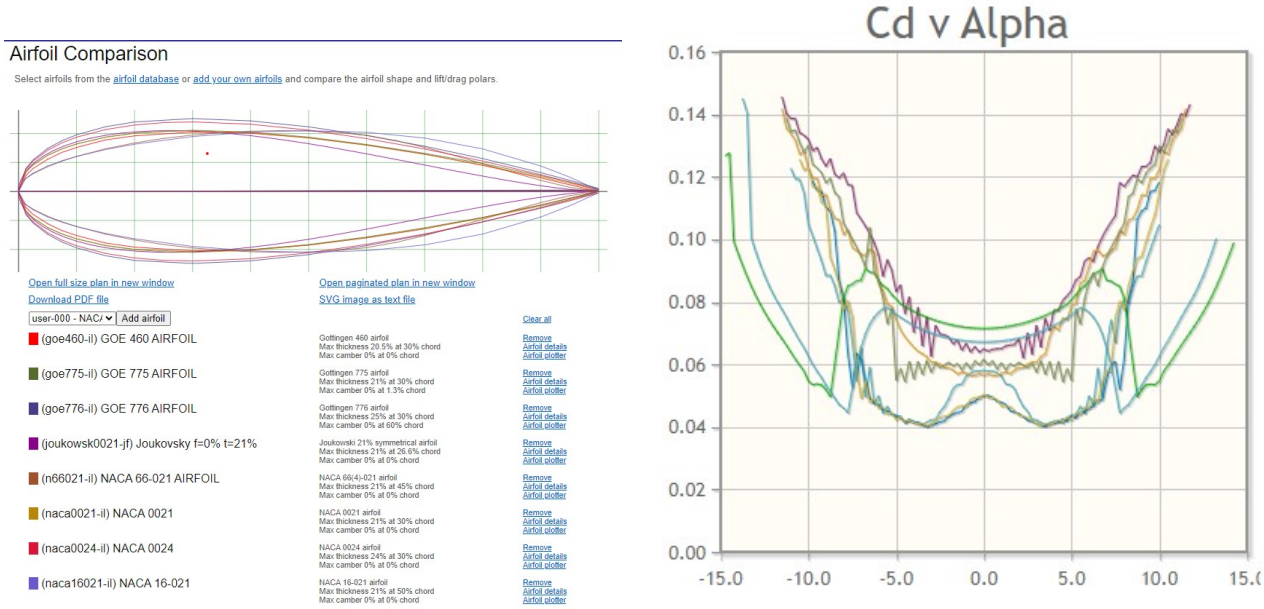

(a) Comparison of different airfoil geometries (b) Comparison of drag coefficients (C_d)

Figure 4.8: Airfoils Comparison

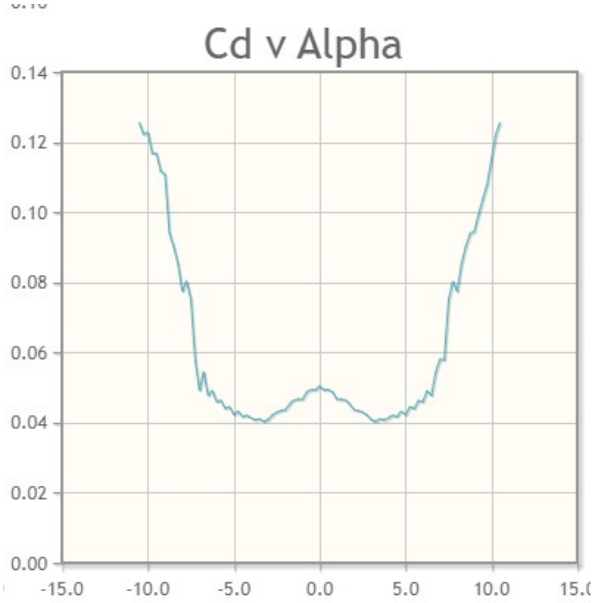

Figure 4.9: Drag coefficient (C_d) graph for NACA0021

As observed, the NACA0021 airfoil outperformed the others at a 0° angle of attack and a Reynolds number less than 50000. Thus, we will use the NACA0021 airfoil as the cross-sectional geometry for our quadcopter arms.

4.3 Comparative Study of Drag Coefficient (C_d) for Different Cross-Sections

To accurately assess the drag coefficient reduction when selecting a streamlined airfoil, we will conduct comparative simulations in ANSYS Fluent. We will compare the NACA0021 airfoil against a cylindrical cross-section and the approximate rectangular cross-section of the F450 frame, at an airspeed of $V = 18\,\mathrm{m/s}$.

4.3.1 Assigning Dimensions Based on Moment of Inertia

Since the purpose of these arms is to serve as structural members that support the drone's weight and the thrust force generated by the motors, they primarily function under bending loads. Therefore, we will use the moment of inertia as the main factor for comparing C_d coefficients. We will calculate the radius of the cylinder and the chord length of the NACA0021 airfoil.

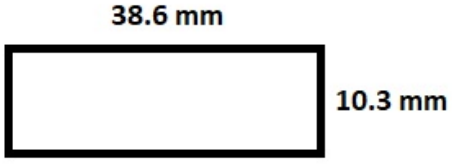

Figure 4.10: Approximate Dimensions of the F450's Arm Cross-Section

The moment of inertia for a rectangle is:

$$I_x = \frac{bh^3}{12}$$

We found that:

$$I_x = \frac{38.36 \times 10.31^3}{12} = 3525.18\,\text{mm}^4$$

The moment of inertia for a circular shape is:

$$I_x = \frac{\pi d^4}{64}$$

Solving for $I_x = 3525.18\,\text{mm}^4$, we find:

$$d = 16.4\,\text{mm}$$

For the airfoil, we do not have a direct formula to calculate its moment of inertia. Therefore, we used the SolidWorks tool to calculate the moment of inertia of the cross-section and an iterative method to adjust the chord length in SolidWorks to match $I_x = 3525.18\,\text{mm}^4$. We found a chord length of:

$$ch = 26\,\text{mm}$$

4.3.2 ANSYS Fluent Simulation

ANSYS Fluent is a powerful computational fluid dynamics (CFD) software used for modeling fluid flow, heat and mass transfer, and chemical reactions. It is widely utilized in engineering simulations to predict and optimize the performance of products and processes involving fluid dynamics.

Main Steps to Execute a Simulation

1. **Pre-Processing:**
   - **Geometry Creation:** Define the physical shape of the domain where the fluid flow will be analyzed, using DesignModeler.
   - **Mesh Generation:** Divide the geometry into smaller, discrete cells to create a computational grid (mesh). The accuracy of the simulation depends on the quality and resolution of this mesh.
2. **Setup:**
   - **Physics Definition:** Specify the physical models representing the fluid flow, including turbulence, heat transfer, and multiphase flow models.
   - **Boundary Conditions:** Define how the fluid interacts with the domain boundaries (inlets, outlets, walls, etc.).
   - **Material Properties:** Assign properties to the fluids and solids involved in the simulation, such as density, viscosity, and thermal conductivity.
3. **Solution:**
   - **Solver Settings:** Choose the numerical methods and algorithms to solve the governing equations of fluid dynamics.

- **Simulation Run:** ANSYS Fluent iteratively solves these equations on the computational grid, adjusting the values until convergence criteria are met.

4. **Post-Processing:**

   - **Results Visualization:** Analyze and visualize the results using various tools to interpret the flow patterns, pressure distribution, drag coefficient, and the y^+ value.
   - **Data Export:** Extract quantitative data for further analysis or validation with experimental results.

We will illustrate this process with one simulation (for the NACA0021 airfoil) and finally compare the results.

4.3.2.1 Geometry Creation

First, we plot the NACA0021 Airfoil with a chord length of 26 mm using the airfoiltools.com plotter.

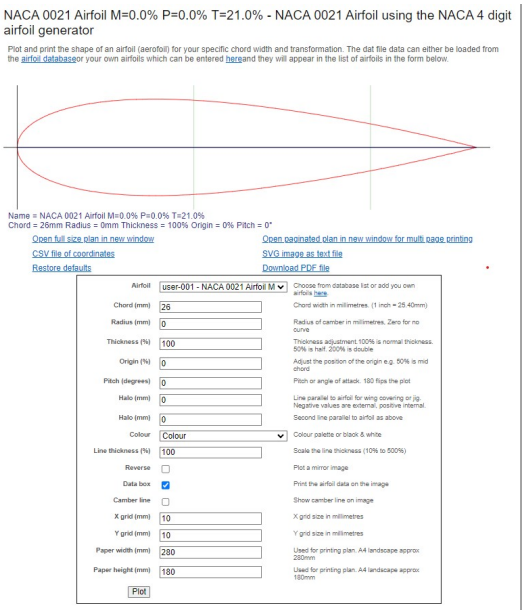

Figure 4.11: NACA0021 Plot

Then, a CSV file is downloaded, processed in Excel, and saved as a .txt file so that DesignModeler can read it.

naca0021-il_CH26.txt - Notepad

File Edit Format View Help

#group	#points	#x	#y	#z
1	1	26.000000	0.000000	0
1	2	25.993578	0.001638	0
1	3	25.974338	0.006526	0
1	4	25.942306	0.014664	0
1	5	25.897482	0.026000	0
1	6	25.839944	0.040560	0
1	7	25.769744	0.058240	0
1	8	25.686908	0.079014	0
1	9	25.591592	0.102830	0
1	10	25.483822	0.129636	0
1	11	25.363728	0.159302	0
1	12	25.231440	0.191802	0
1	13	25.087088	0.227032	0
1	14	24.930802	0.264888	0
1	15	24.762764	0.305292	0
1	16	24.583078	0.348114	0
1	17	24.391978	0.393250	0
1	18	24.189646	0.440596	0

Figure 4.12: Processed Text File

We create the geometry in DesignModeler and the C-shaped domain with a radius of 7.5 × chord and a length of 15 × chord.

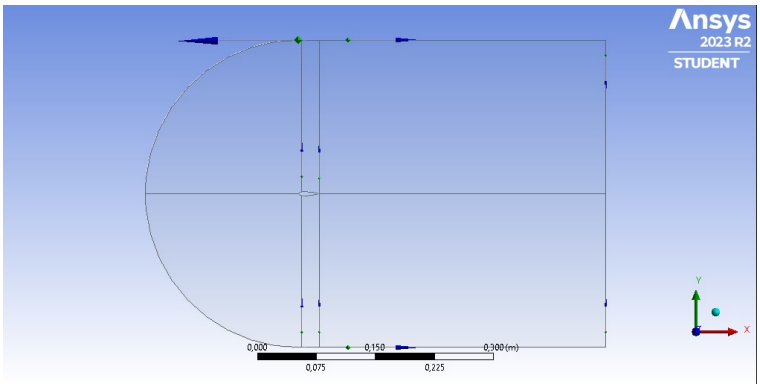

Figure 4.13: C-Shaped Domain with Airfoil in the Middle

After that, we divide the domain into subdomains to introduce sizings in the mesher.

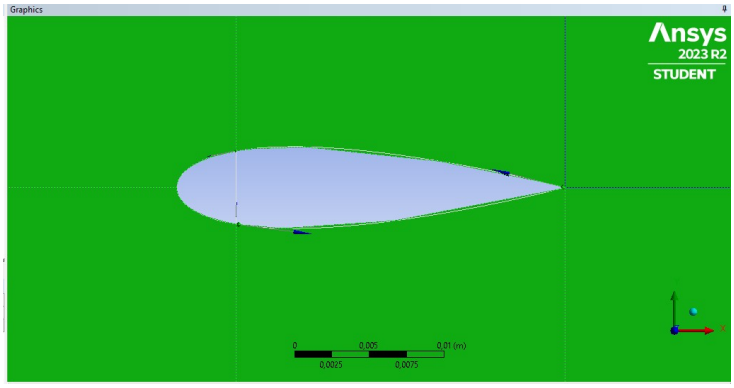

Figure 4.14: Subdomains

4.3.2.2 Mesh Generation

After defining the domain, we introduce sizings to refine the mesh in regions where we need more information about the fluid, especially near the walls, to ensure y^+ values under 1. We also define the contours of the inlet, outlet, and wall (airfoil).

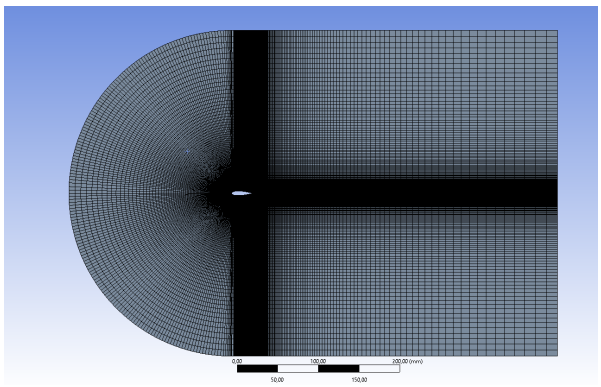

Figure 4.15: C-Shaped Domain After Sizing and Meshing

4.3.2.3 Physics Definition

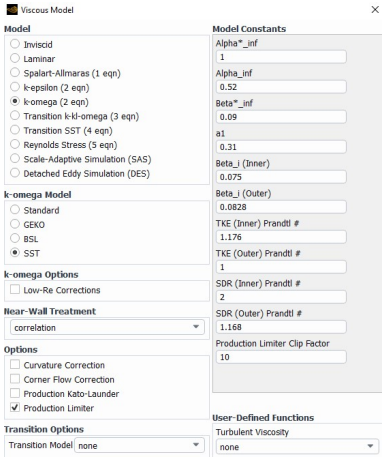

Figure 4.16: Defining the Viscous Model (K-Omega SST)

4.3.2.4 Boundary Conditions

We set the boundary conditions as a no-slip condition on the wall, an inlet speed of $V = 18\,\mathrm{m/s}$, and an outlet gauge pressure of $P_0 = 0\,\mathrm{Pa}$.

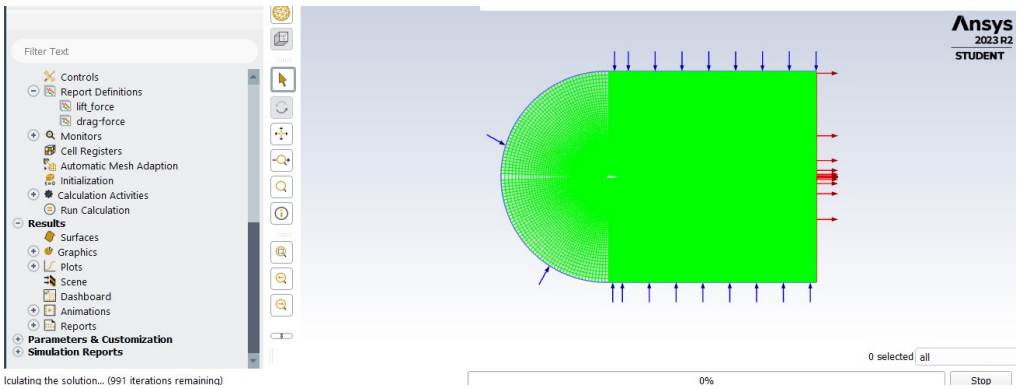

Figure 4.17: Domain with Boundary Conditions

4.3.2.5 Material Properties

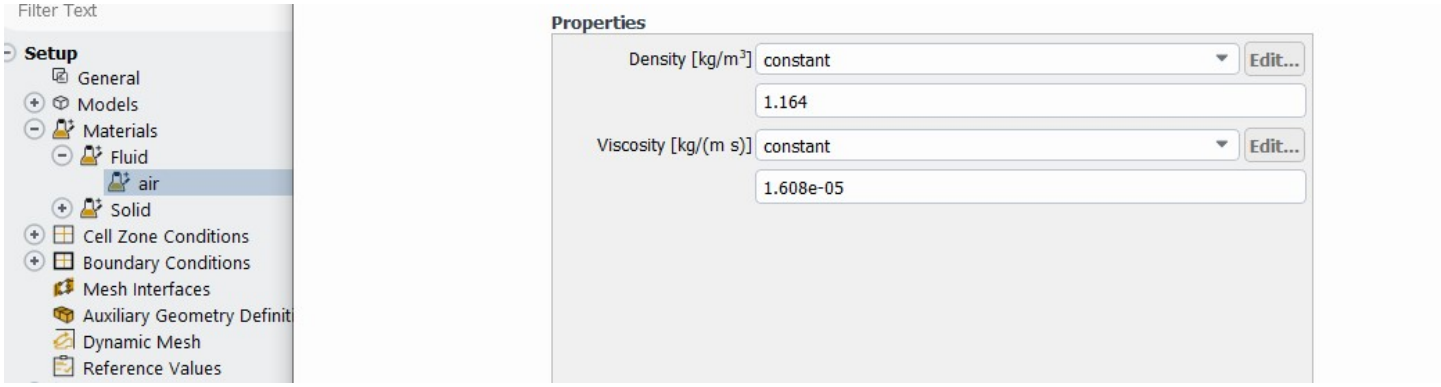

Figure 4.18: Defining Air Properties

4.3.2.6 Solver Settings

We set up the solver to report definitions for the drag coefficient and lift coefficient. If the lift coefficient is close to zero, it indicates that the simulation is well-conducted. We also set the residual monitors criteria.

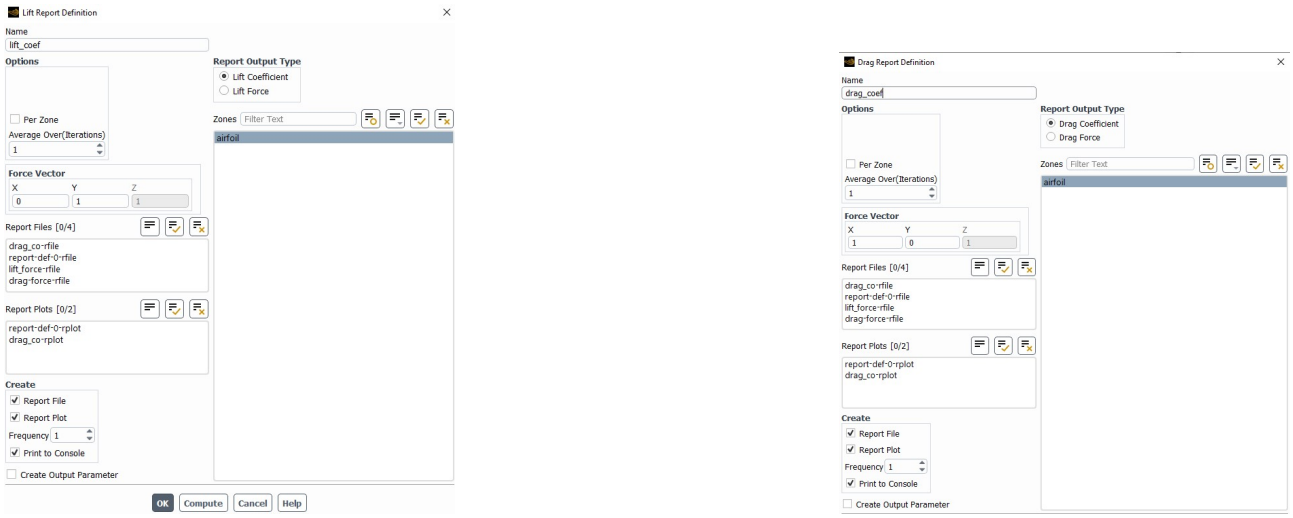

(a) Setting Report Definitions (b) Residual Monitors Criteria

Figure 4.19: Solver Settings

4.3.2.7 Simulation Run

We initialize the model and run the simulation, observing the following convergence graphs:

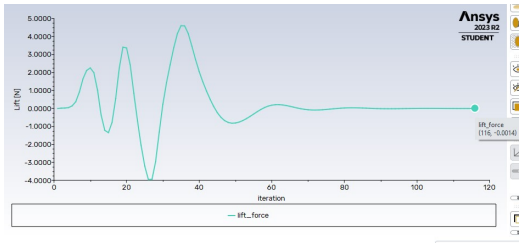

(a) Lift Graph

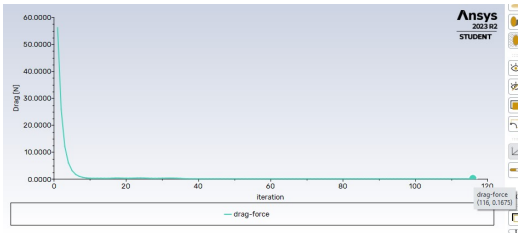

(b) Drag Graph

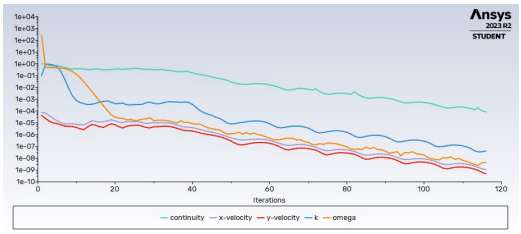

(c) Residuals Graph

Figure 4.20: Convergence Graphs

4.3.2.8 Results Visualization

After the calculations, we can plot the pressure and velocity contours and obtain the drag and lift coefficient values.

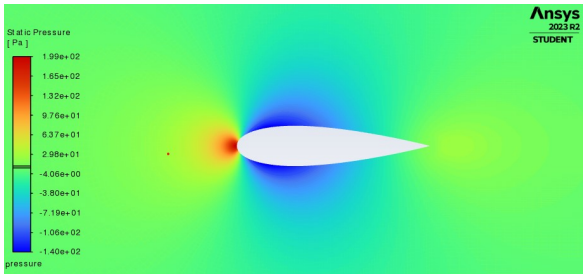

(a) Pressure Contour

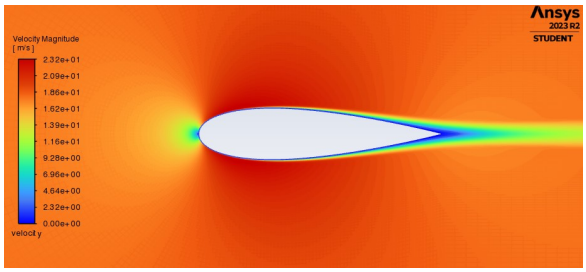

(b) Velocity Contour

	Cl
aifoil	0.00083039406
	Cd
aifoil	0.25260875

(c) Lift and Drag Coefficients

Figure 4.21: NACA0021 Simulation Results

4.3.2.9 Wall y^+

In computational fluid dynamics, y^+ is a dimensionless distance used to describe the position of the first cell center from the wall in a boundary layer.

Importance of $y^+ < 1$

When y^+ is less than 1, the first cell lies within the viscous sub-layer of the boundary layer. This is essential for:

1. **Accurate Turbulence Modeling:** For turbulence models that do not use wall functions (e.g., low Reynolds number models), resolving the viscous sub-layer directly is crucial for accurately capturing the near-wall behavior. $y^+ < 1$ ensures sufficient mesh resolution to resolve velocity and thermal gradients in the viscous sub-layer.
2. **Capturing Near-Wall Phenomena:** Many flow phenomena, such as separation, transition, and heat transfer, are strongly influenced by near-wall processes. A y^+ value less than 1 ensures high-fidelity capture of these effects.
3. **Improving Simulation Accuracy:** With $y^+ < 1$, wall shear stress and other near-wall quantities can be computed more accurately, leading to more reliable predictions of drag, lift, and heat transfer rates.

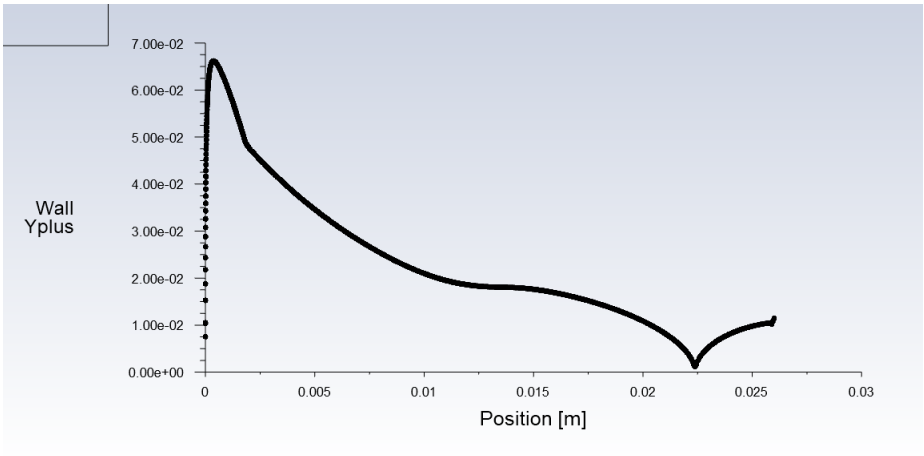

Figure 4.22: y^+ Plot Along the Wall

We can see that the y^+ value in our simulation is below 1. finally;

$$\boxed{C_d = 0.2526}$$

4.3.3 Rectangular cross-section simulation

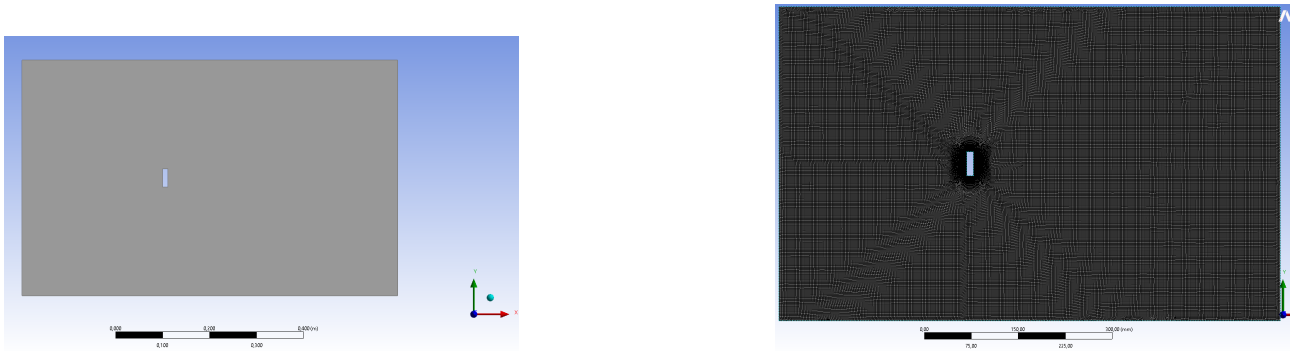

(a) Geometry in DesigModeler (b) Meshing

Figure 4.23: Pre-Processing

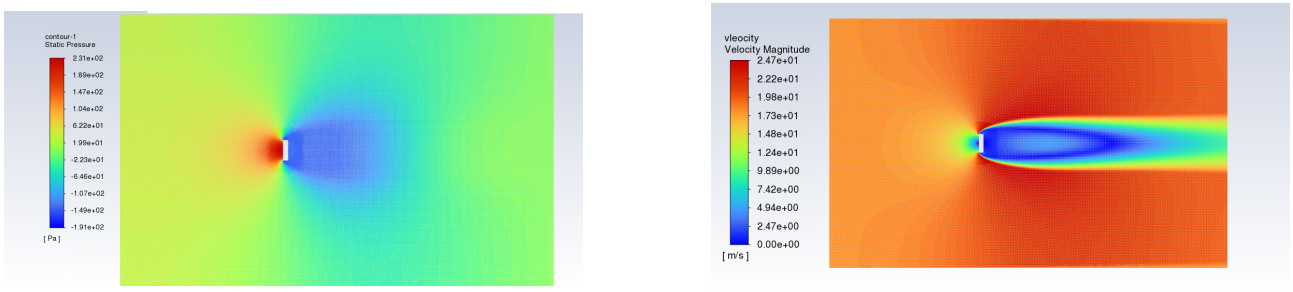

(a) Pressure Contour

(b) Velocity Contour

Figure 4.24: F450 Simulation Results

```
          lift_coef
--------------------
                            Cl
-------------------------------- --------------------
                        airfoil       -0.00040629362

          drag_coef
--------------------
                            Cd
-------------------------------- --------------------
                        airfoil            20.206017
```

Figure 4.25: Lift and Drag Coefficients

finally;

$$\boxed{C_d = 20.206}$$

4.3.4 Cylindrical cross-section simulation

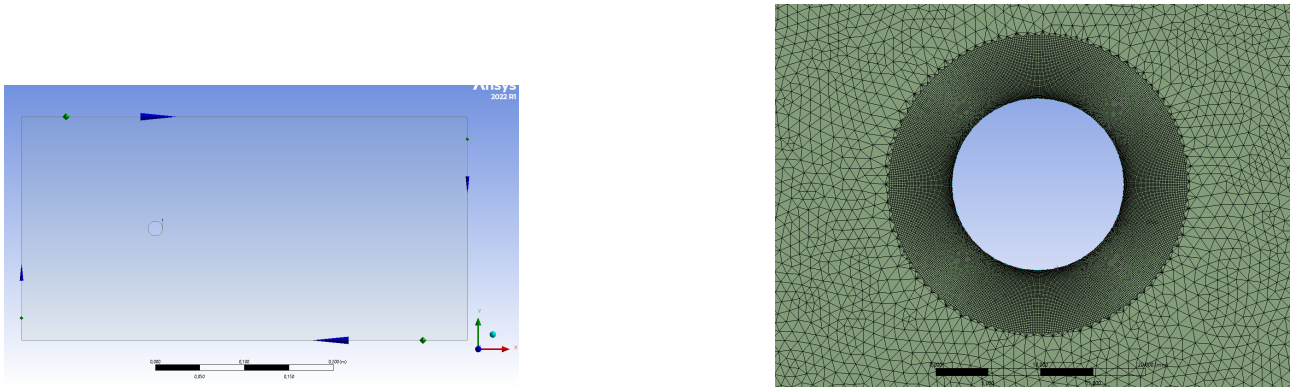

(a) Geometry in DesigModeler

(b) Meshing

Figure 4.26: Pre-Processing

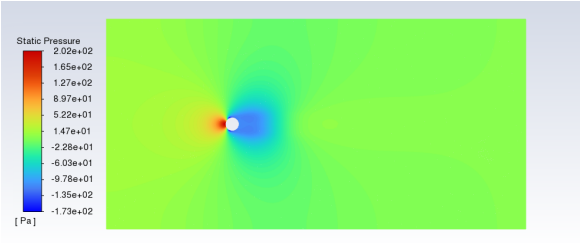

(a) Pressure Contour

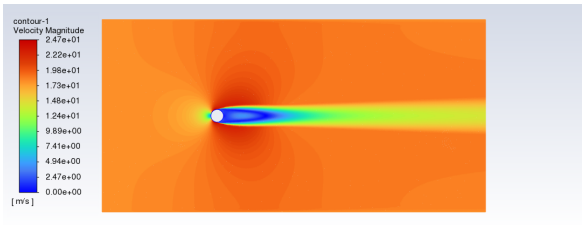

(b) Velocity Contour

	Cl
airfoil	0.002258376

	Cd
airfoil	3.9817756

(c) Lift and Drag Coefficients

Figure 4.27: Cylinder-Shape Simulation Results

finally;

$$\boxed{C_d = 3.982}$$

4.3.5 Comparing Results & Conclusion

The simulations reveal that the NACA0021 airfoil significantly outperforms both the cylindrical and rectangular cross-section shapes (like the F450 frame) when evaluated for drag reduction while maintaining the same moment of inertia.

- **Cylindrical Cross-Section:** The drag force generated by the cylindrical cross-section is significantly higher than that of the NACA0021 airfoil. Specifically, the NACA0021 airfoil produces 93.66% less drag force compared to the cylindrical shape. This is calculated as:

$$\text{Drag Reduction} = \frac{3.982 - 0.2526}{3.982} \times 100 = 93.66\%$$

- **Rectangular Cross-Section (F450):** The drag force generated by the rectangular cross-section is even higher. The NACA0021 airfoil results in a 98.75% reduction in drag force compared to the rectangular shape. This is calculated as:

$$\text{Drag Reduction} = \frac{20.21 - 0.2526}{20.21} \times 100 = 98.75\%$$

These findings indicate that the NACA0021 airfoil is optimal for our application, substantially reducing drag while maintaining structural integrity due to its low drag coefficient (C_d). This allows for using multiple airfoil-shaped arms to further reinforce the structure without significantly increasing drag, thus maintaining high performance.

Chapter 5

Structural Design and Analysis

After identifying the optimal aerodynamic shape to place beneath the propellers for drag reduction, we now need to design the remaining arm structure. This arm must have mounting holes for the motor and for attachment to the base. The structure should be lightweight, rigid, and high-performing.

To achieve this optimal shape, we will use a series of topology optimizations, redesigns, and static simulations. Before starting any simulations, we must choose and characterize the material to be used. Given the availability of 3D printers at our school and the cost-effectiveness of PLA, we will use PLA for both simulations and prototype fabrication.

5.1 PLA Characterization

5.1.1 What is PLA

Polylactic Acid (PLA) is a thermoplastic polymer derived from renewable sources like corn starch or sugar cane. Unlike traditional plastics made from fossil fuels, PLA is produced from biomass, making it more sustainable. It can be manufactured using the same equipment as conventional plastics, making production cost-efficient. PLA is the second most produced bioplastic, offering similar properties to polypropylene (PP), polyethylene (PE), and polystyrene (PS). Moreover, PLA is biodegradable.

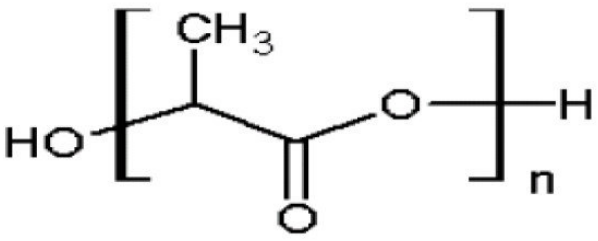

Figure 5.1: Chemical structure of polylactic acid (PLA) [18]

5.1.2 Isotropic or Orthotropic?

Characterizing PLA is essential not only due to limited mechanical property information from manufacturers but also because 3D-printed parts have different mechanical properties depend-

ing on the printing axis. Although PLA can be treated as a homogeneous, isotropic, and linear-elastic material, the printed parts are not.

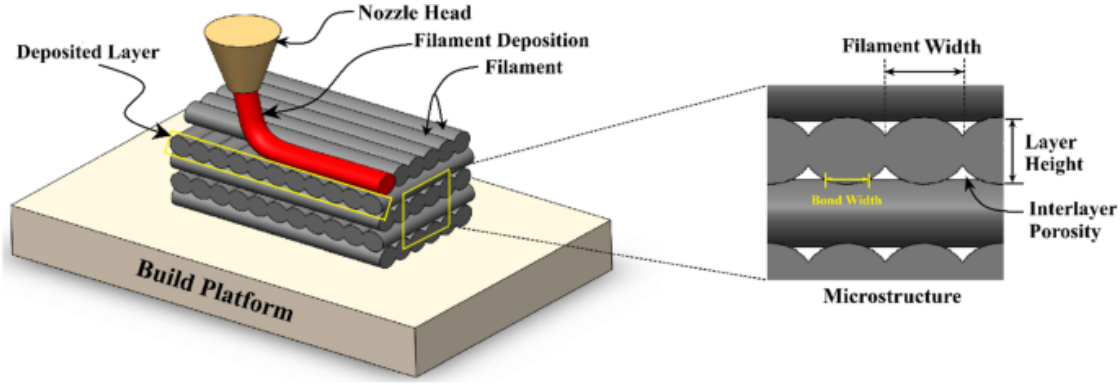

Figure 5.2: Process of 3D printing [19]

5.1.3 Tensile Test

Since we only have a longitudinal extensometer, we can extract Young's modulus, yield strength (elastic limit), and fracture point from this test. We will retrieve Poisson's ratio from the literature as it does not significantly change.

5.1.3.1 ASTM D638-03 Standard

This test method determines the tensile properties of unreinforced and reinforced plastics using standard dumbbell-shaped test specimens under defined conditions of pretreatment, temperature, humidity, and testing machine speed [35].

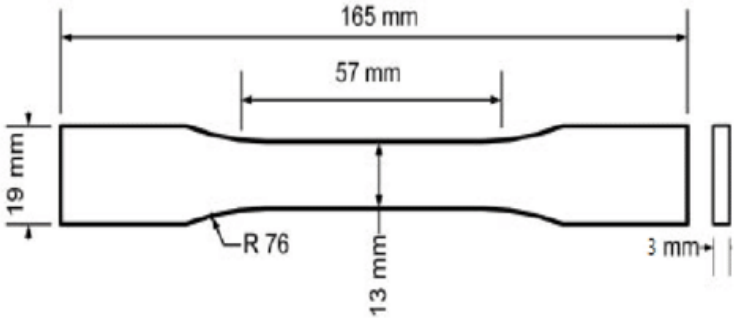

Figure 5.3: Specimen dimensions for tensile testing

5.1.3.2 Specimen Preparation

After designing the specimen, an STL file was generated and processed in the Ultimaker Cura slicer to create the paths. To achieve accurate results, we removed bottom layers and walls, generating lines in both 0° and 90° directions.

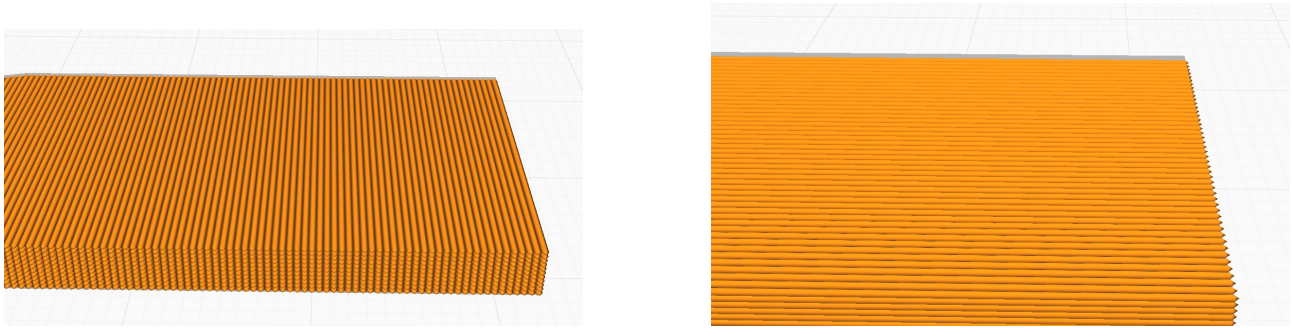

(a) 0° direction (b) 90° direction

Figure 5.4: Specimen slicing directions

The specimens were then printed under controlled environmental conditions, numbered, and labeled with the line direction:

(a) 3D printing using Creality Ender3

(b) Specimens after printing

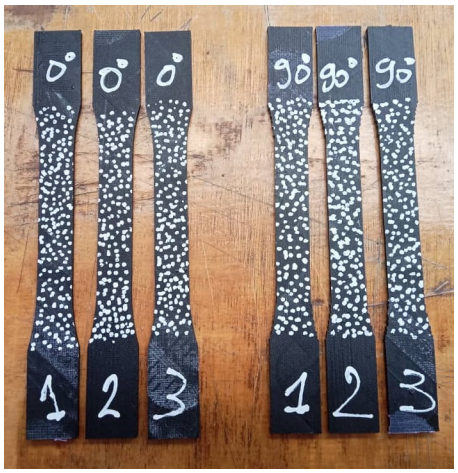

(c) Specimens after numbering and labeling

Figure 5.5: Specimen preparation

5.1.3.3 Conducting the Test

With the assistance of M. Belkacemi, each specimen was carefully installed. The plastic testing standard was selected in the tensile machine software, dimensions were input, a pre-tension was applied, and the extensometer was installed. Tests were conducted, with the extensometer being removed before it reached its limit to prevent breakage.

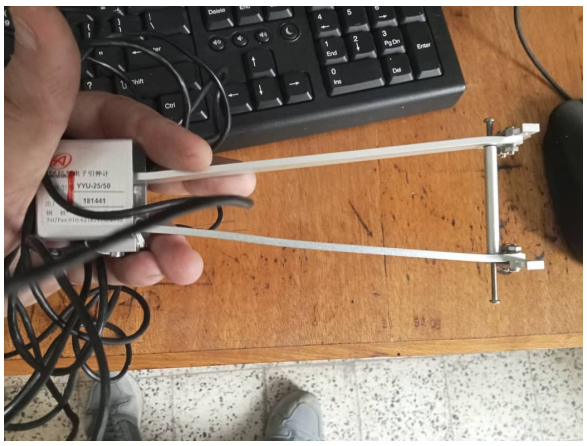

(a) Longitudinal extensometer used

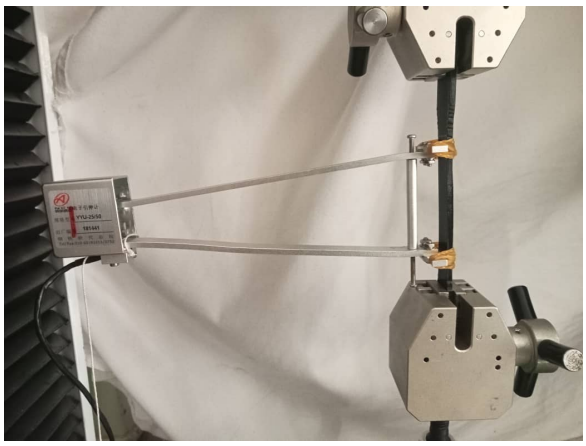

(b) Specimen installed with extensometer attached

(c) Specimen after fracture

Figure 5.6: Tensile test setup and results

5.1.3.4 Processing Data

The testing software provided the following load-displacement graphs:

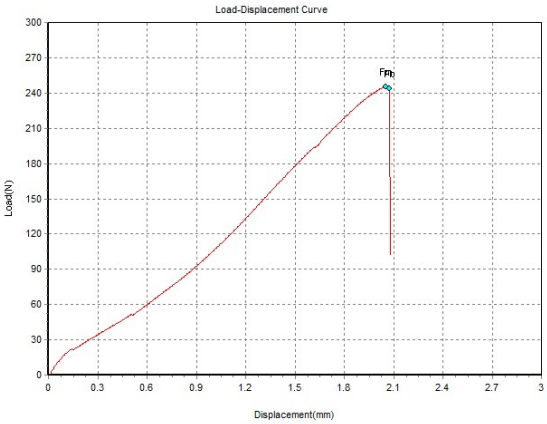

(a) Specimen 1, 0° direction

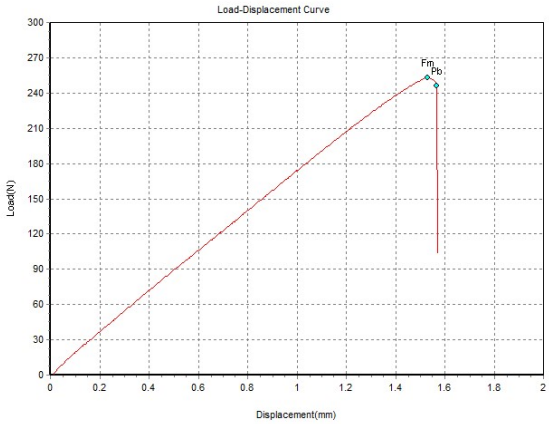

(b) Specimen 2, 0° direction

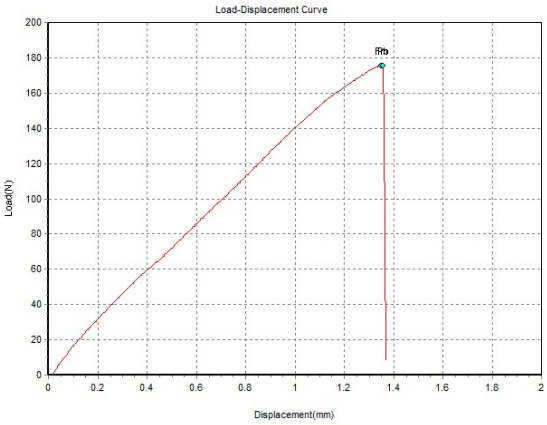

(a) Specimen 3, 0° direction

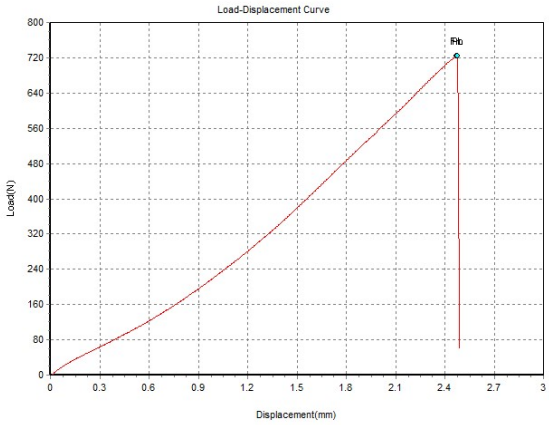

(b) Specimen 1, 90° direction

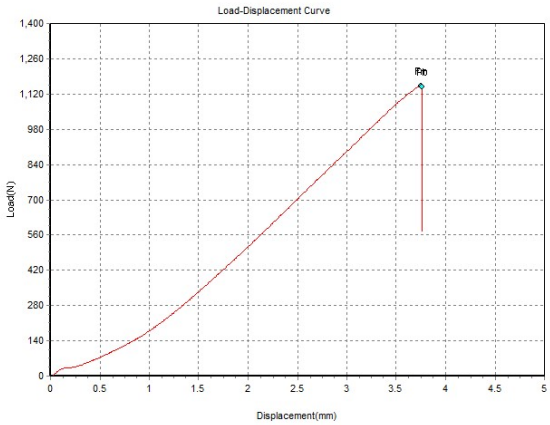

(c) Specimen 3, 90° direction

Figure 5.8: Load-displacement graphs

To calculate Young's modulus and the elastic limit, we will export the data to Excel and plot the stress-strain graphs. The graphs with the extensometer show a distinct change in slope when it is removed. We will use these for determining Young's modulus due to the extensometer's accuracy, and the other graphs for the elastic limit.

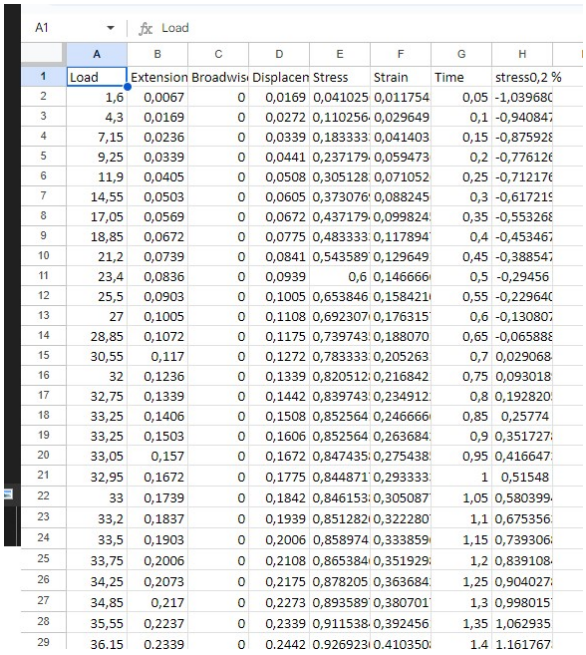

	A	B	C	D	E	F	G	H
1	Load	Extension	Broadwisi	Displacen	Stress	Strain	Time	stress0,2 %
2	1,6	0,0067	0	0,0169	0,041025	0,011754	0,05	-1,03968(
3	4,3	0,0169	0	0,0272	0,110256	0,029649	0,1	-0,940847
4	7,15	0,0236	0	0,0339	0,183333	0,041403	0,15	-0,875928
5	9,25	0,0339	0	0,0441	0,237179	0,059473	0,2	-0,77612(
6	11,9	0,0405	0	0,0508	0,305128	0,071052	0,25	-0,712176
7	14,55	0,0503	0	0,0605	0,373076	0,088245	0,3	-0,617215
8	17,05	0,0569	0	0,0672	0,437179	0,099824	0,35	-0,553268
9	18,85	0,0672	0	0,0775	0,483333	0,117894	0,4	-0,453467
10	21,2	0,0739	0	0,0841	0,543589	0,129649	0,45	-0,388547
11	23,4	0,0836	0	0,0939	0,6	0,146666	0,5	-0,29456
12	25,5	0,0903	0	0,1005	0,653846	0,158421	0,55	-0,22964(
13	27	0,1005	0	0,1108	0,692307	0,176315	0,6	-0,130807
14	28,85	0,1072	0	0,1175	0,739743	0,188070	0,65	-0,065888
15	30,55	0,117	0	0,1272	0,783333	0,205263	0,7	0,029068
16	32	0,1236	0	0,1339	0,820512	0,216842	0,75	0,093018
17	32,75	0,1339	0	0,1442	0,839743	0,234912	0,8	0,192820
18	33,25	0,1406	0	0,1508	0,852564	0,246666	0,85	0,25774
19	33,25	0,1503	0	0,1606	0,852564	0,263684	0,9	0,351727
20	33,05	0,157	0	0,1672	0,847435	0,275438	0,95	0,416647
21	32,95	0,1672	0	0,1775	0,844871	0,293333	1	0,51548
22	33	0,1739	0	0,1842	0,846153	0,305087	1,05	0,580399
23	33,2	0,1837	0	0,1939	0,851282	0,322280	1,1	0,675356
24	33,5	0,1903	0	0,2006	0,858974	0,333859	1,15	0,739306
25	33,75	0,2006	0	0,2108	0,865384	0,351929	1,2	0,839108
26	34,25	0,2073	0	0,2175	0,878205	0,363684	1,25	0,904027
27	34,85	0,217	0	0,2273	0,893589	0,380701	1,3	0,998015
28	35,55	0,2237	0	0,2339	0,911538	0,392456	1,35	1,062935
29	36,15	0,2339	0	0,2442	0,926923	0,410350	1,4	1,161767

(a) Example of processed data

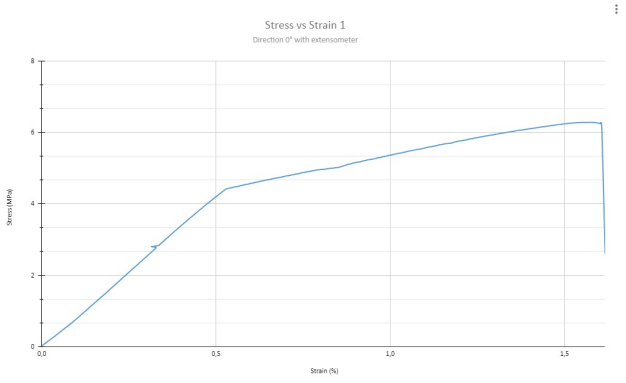

(b) Stress-Strain 1 with Extensometer Direction 0°

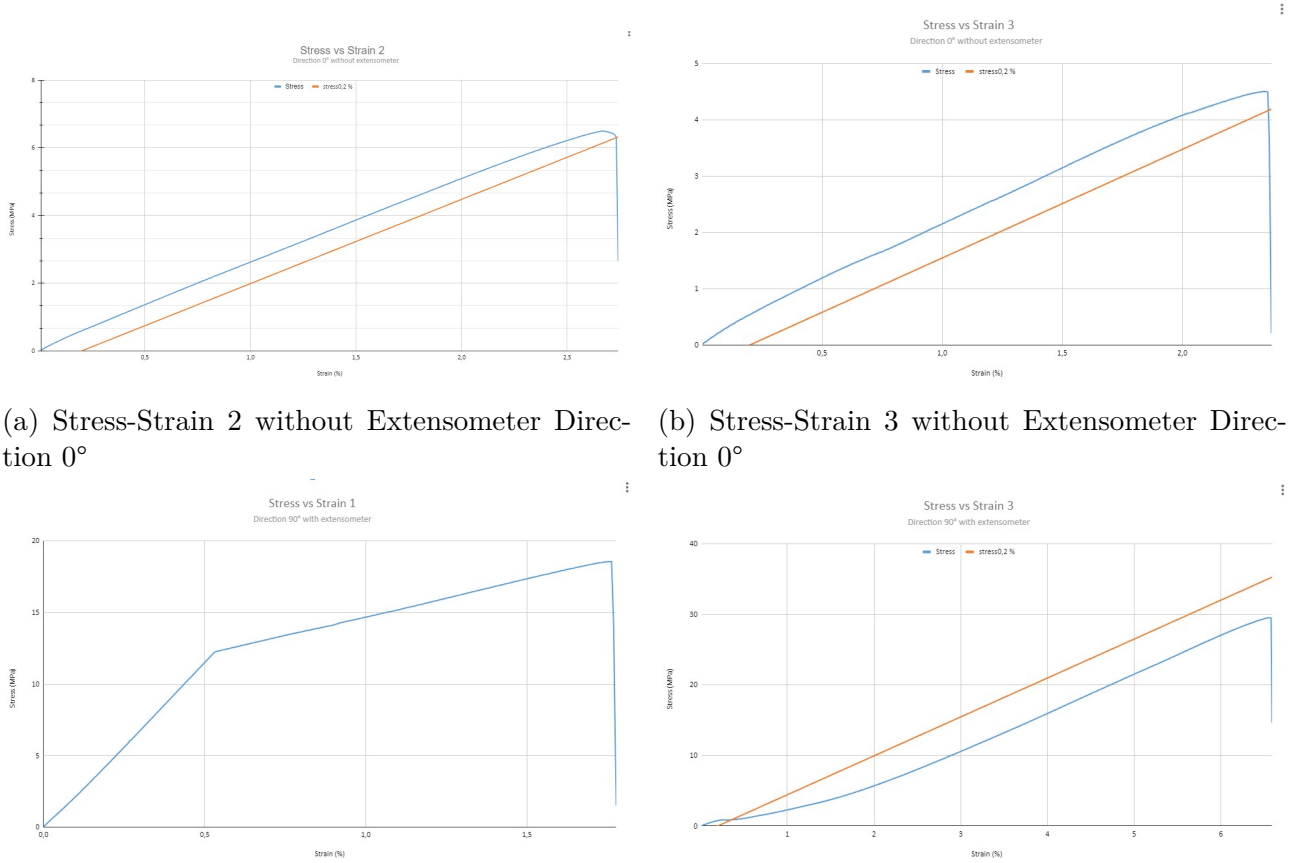

(a) Stress-Strain 2 without Extensometer Direction 0°

(b) Stress-Strain 3 without Extensometer Direction 0°

(c) Stress-Strain 1 with Extensometer Direction 90°

(d) Stress-Strain 3 with Extensometer Direction 90°

Figure 5.10: Stress-Strain Graphs

From the graphs obtained using the extensometer, we calculate the following Young's modulus:

$$E^{0^\circ} = \frac{4.35 - 3.06}{0.520 - 0.362} \times 100 = \boxed{816.45\text{MPa}}$$

$$E^{90^\circ} = \frac{10.798 - 4.478}{0.471 - 0.209} \times 100 = \boxed{2.36\text{GPa}}$$

To determine the elastic limit, the 0.2% offset method was attempted but was not applicable. However, since the material exhibits purely elastic behavior (no plastic region in the graph), the elastic limit can be considered the maximum stress before fracture. The values found are:

$$\boxed{\sigma_e^{0^\circ} = 6.32\text{MPa}}$$

$$\boxed{\sigma_e^{90^\circ} = 29.45\text{MPa}}$$

From the literature [36], the average Poisson's ratio for PLA is approximately $\mu = 0.34$.

5.2 Topology Optimization

5.2.1 What is Topology Optimization?

Topology Optimization (TO) is a computational technique used in engineering design to determine the most efficient material layout within a given design space, subject to specified loads, conditions, and constraints. The primary goal of TO is to maximize the performance and efficiency of a structure by strategically removing unnecessary material from areas that do not need to carry significant loads. This approach can reduce weight and solve design challenges such as minimizing resonance or thermal stress.[20]

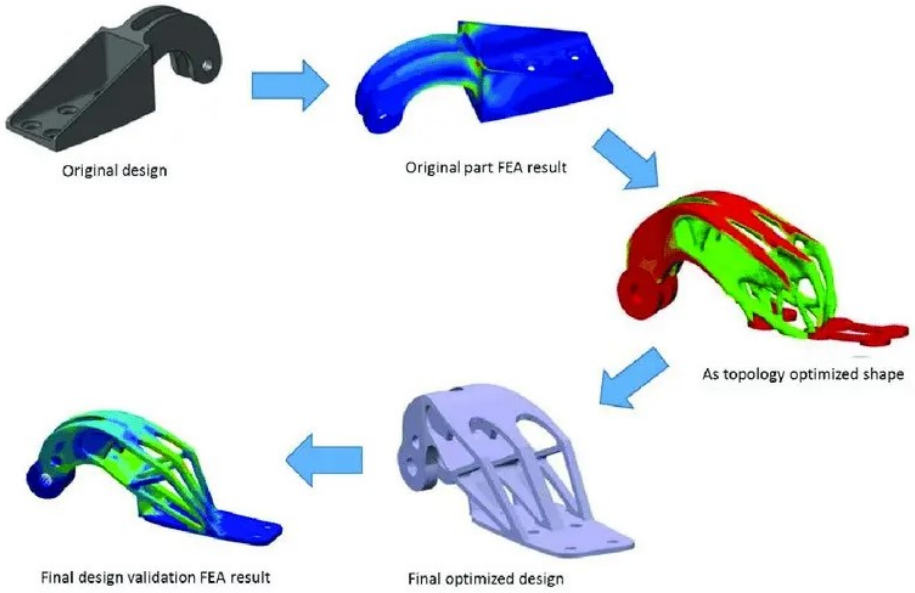

Figure 5.11: The topology optimization workflow [20]

5.2.2 How Topology Optimization Works

Topology optimization works through an iterative process involving the following steps:

1. **Initial Design Space:** The process begins with defining the design space, which is the volume or area within which the material can be distributed. This space is filled with an initial material distribution.

2. **Finite Element Analysis (FEA):** The design space is discretized into smaller elements using finite element analysis. This allows for the calculation of stress, strain, and other physical responses under the given loads and boundary conditions.

3. **Optimization Algorithm:** An optimization algorithm iteratively adjusts the material distribution. The algorithm evaluates the performance of the design in each iteration and modifies the material layout to improve the objective function (e.g., minimizing weight while maintaining structural integrity).

4. **Update Material Distribution:** Based on the optimization algorithm's feedback, the material is added or removed from the design space. Elements with low stress or strain

are identified as candidates for material removal, while elements with high stress or strain are retained.

5. **Convergence Check:** The process continues until a predefined convergence criterion is met. This criterion could be a specific number of iterations or a threshold for changes in the objective function.

6. **Final Design:** The resulting design typically features freeform and intricate shapes that are optimized for performance. These shapes may be challenging or impossible to manufacture using traditional methods but are well-suited for additive manufacturing techniques.

However, Topology Optimization designs are a perfect match for additive manufacturing processes, which have more flexible design rules and can easily reproduce complex shapes without additional costs.

5.3 Topology Optimization in SolidWorks

Topology Optimization in SolidWorks is a robust tool within the SolidWorks Simulation suite that enables engineers to optimize the material layout of their designs. This feature is instrumental in creating lightweight and efficient structures by removing unnecessary material while maintaining structural integrity.

5.3.1 Defining the Material

The first step is to create a new material and save it in the SolidWorks materials library, allowing for its use in this simulation and future ones.

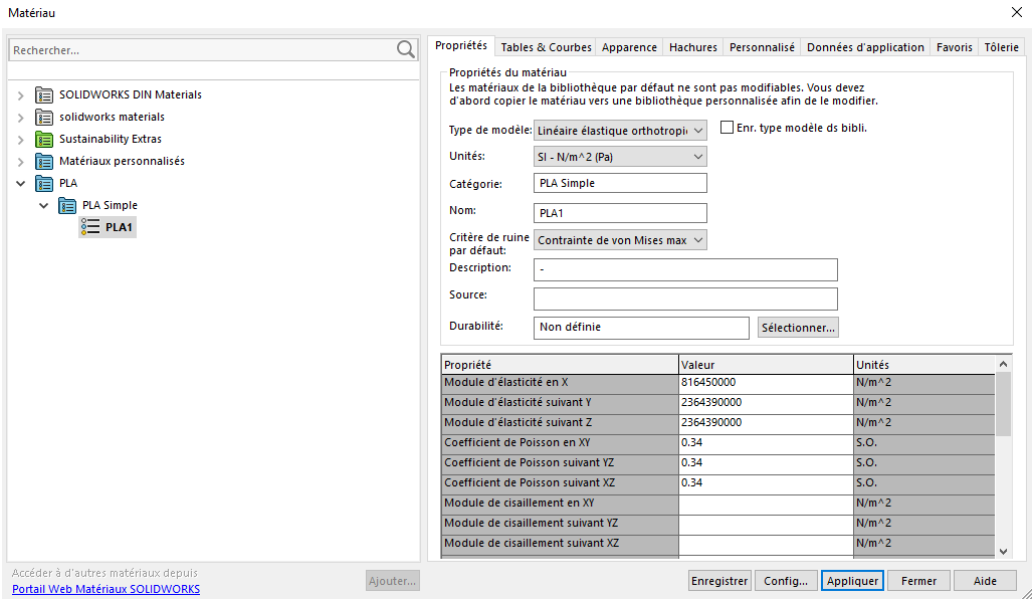

Figure 5.12: Creating PLA as a new orthotropic material

5.3.2 Designing the Raw Part

The raw part is designed based on the datasheet of the motor A2212. This includes dimensioning and placing the mounting holes for the motor and the base. Additional volume is provided to allow the algorithm to find the optimal material layout.

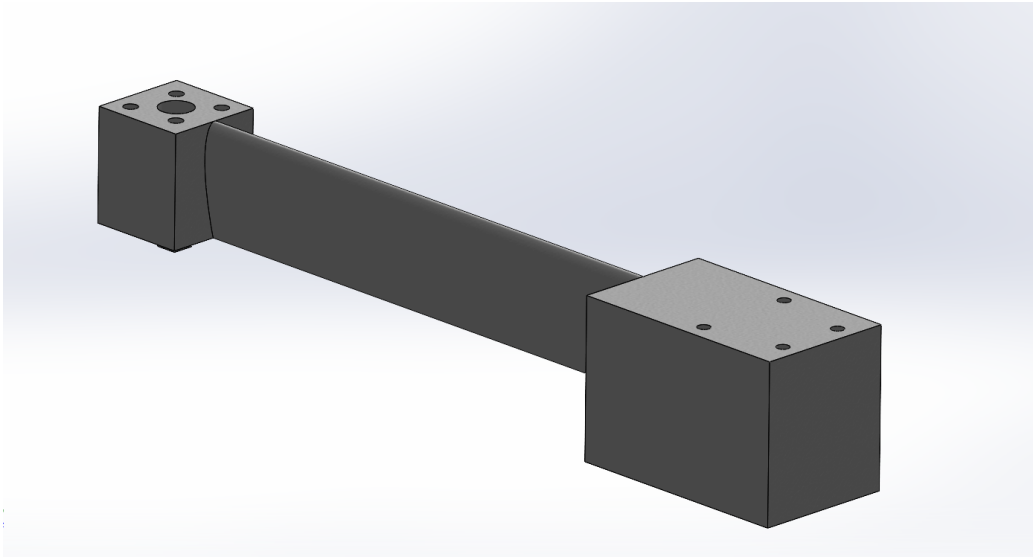

Figure 5.13: The raw part with a single airfoil

5.3.3 Adding Fixtures

Surfaces that will remain fixed during the optimization are defined.

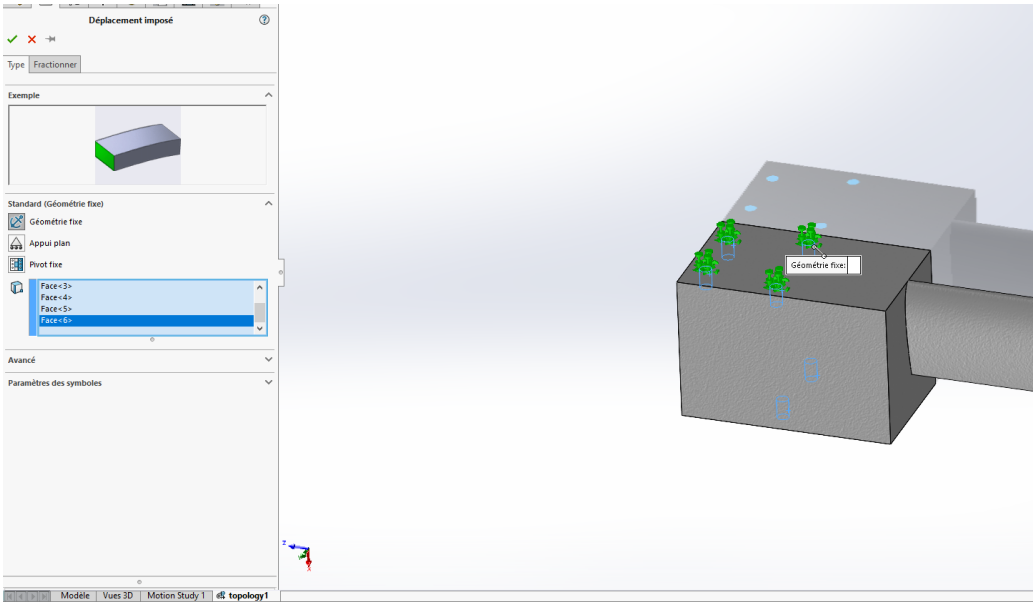

Figure 5.14: Adding fixtures at the mounting holes with the base

5.3.4 Adding Forces

Forces are applied at the mounting holes of the motor, with a maximum value of **10 N**, which is the maximum thrust that one propeller can generate.

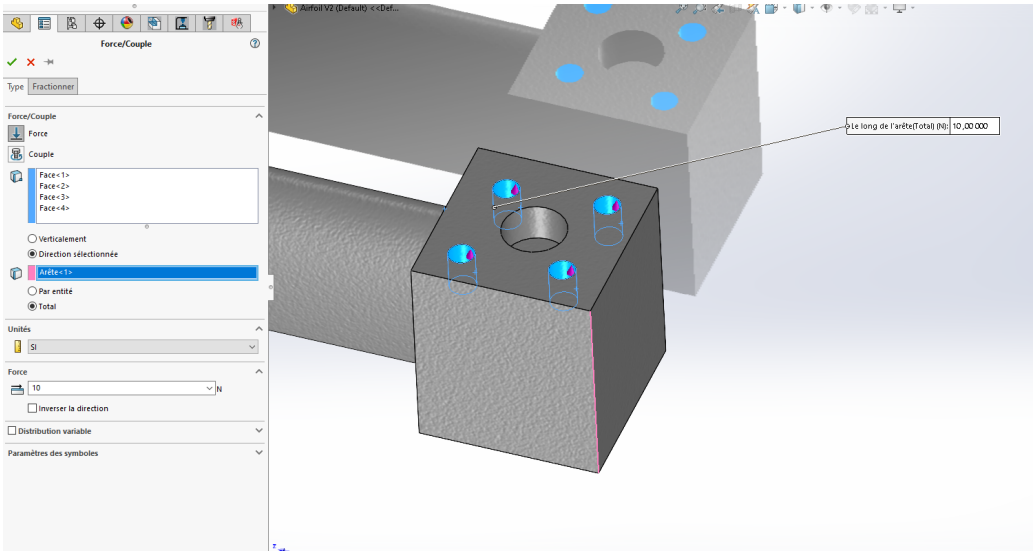

Figure 5.15: Applying forces

5.3.5 Adding Preserved Regions

Certain regions, such as the mounting holes for the motor and the arm with the base, are preserved to prevent the algorithm from removing them.

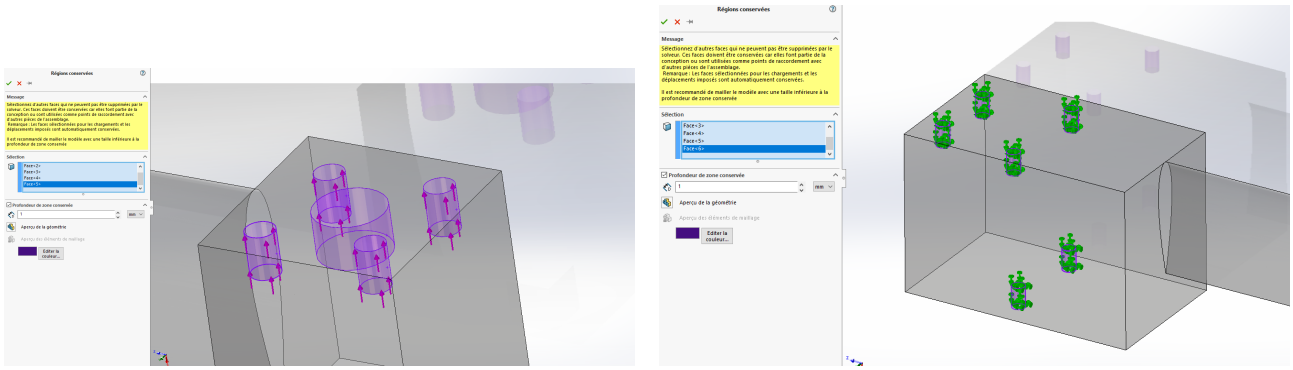

(a) Motor mounting holes (b) Arm with base mounting holes

Figure 5.16: Defining preserved regions

5.3.6 Meshing

A curvature-based mesh is created to ensure the mesher refines the mesh in regions with small details.

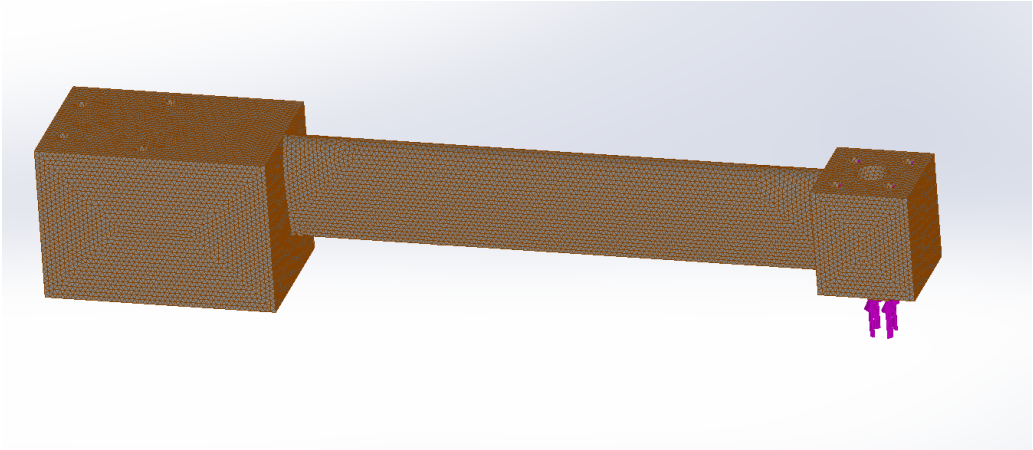

Figure 5.17: Meshing the part

5.3.7 Executing and Processing Results

Upon executing the topology optimization, the percentage of mass to be removed is chosen. The optimized model is then exported as a graphical body in a new configuration.

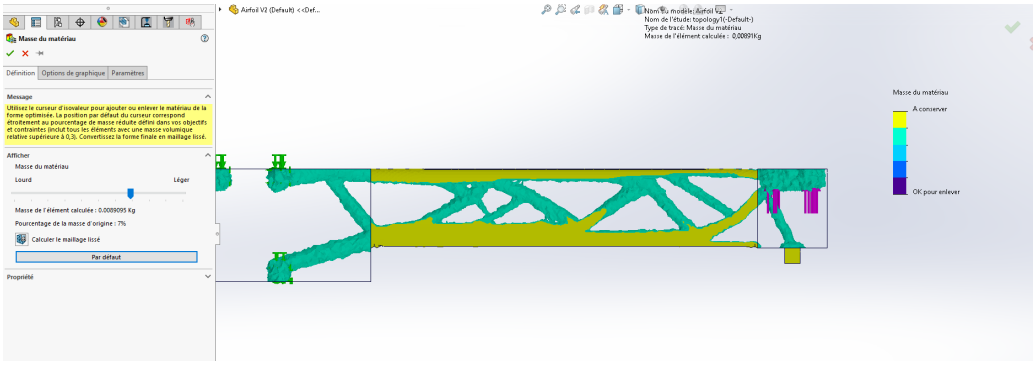

Figure 5.18: Topology optimization results

5.3.8 Post-Processing and Designing the New Part

A smoother sketch is drawn based on the exported graphical body from the previous step, and a new part is created.

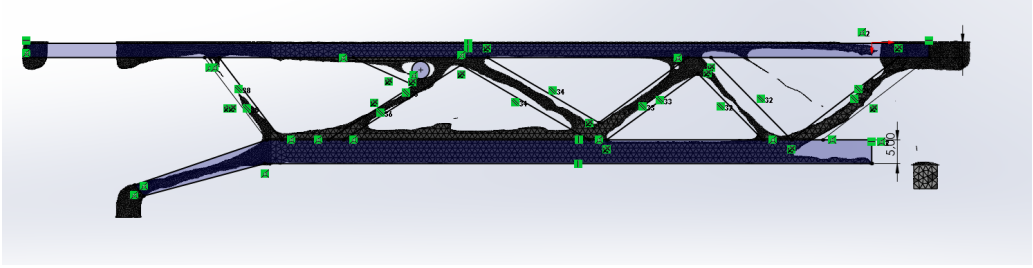

Figure 5.19: Sketching the new part

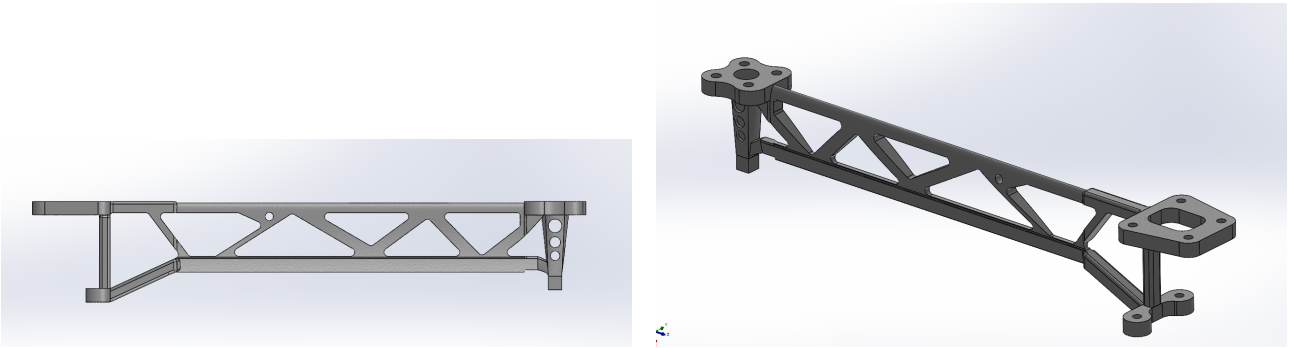

(a) Face view of the new optimized part (b) 3D view of the new optimized part

Figure 5.20: Optimized part

5.4 Performing Static Analysis in SolidWorks

After designing the new part based on topology optimization results, a static analysis is performed to ensure the part's performance under load conditions. The quadcopter is considered in extreme conditions, with an over-limit payload and motors providing a maximum thrust of **10 N**.

5.4.1 Adding Fixtures

Fixtures are added to the optimized part.

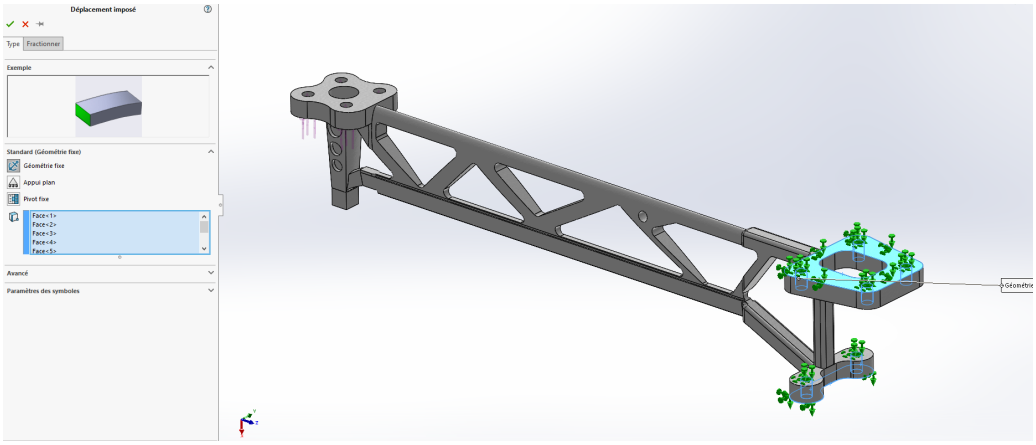

Figure 5.21: Adding fixtures to the optimized part

5.4.2 Adding Forces

Forces are applied to the optimized part.

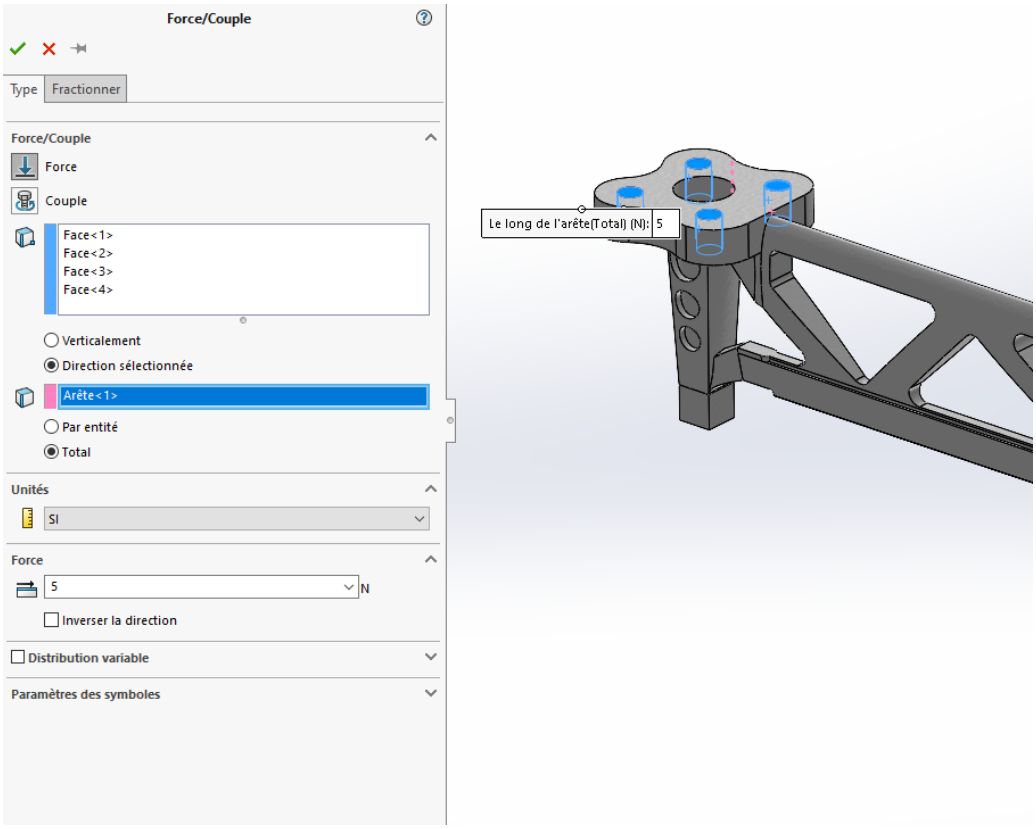

Figure 5.22: Applying forces to the optimized part

5.4.3 Meshing

The optimized part is meshed for analysis.

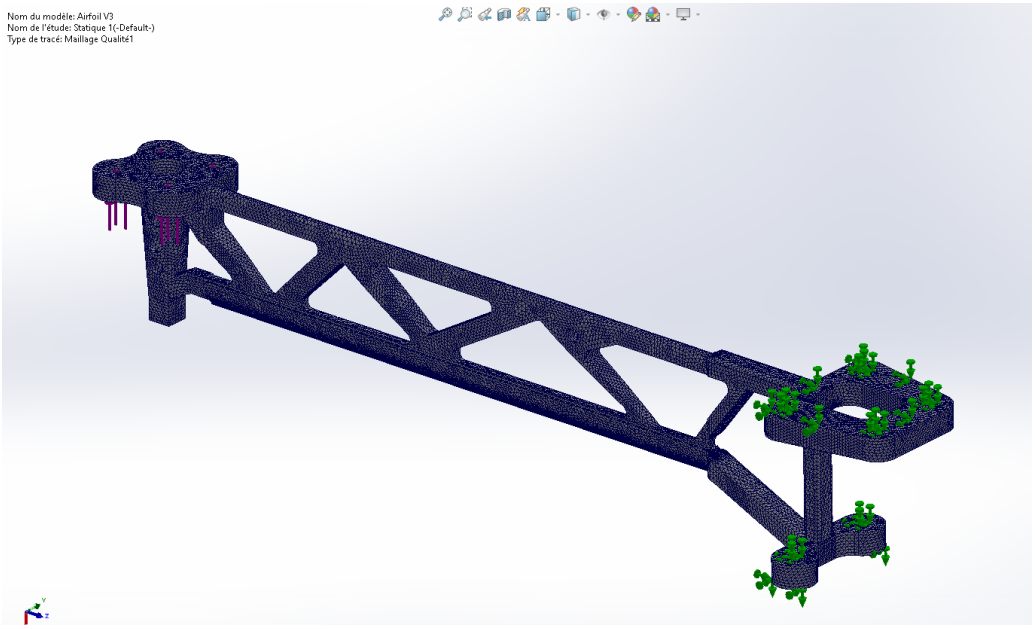

Figure 5.23: Meshing the optimized part

5.4.4 Executing and Processing Results

The results of the static analysis are processed to evaluate stress and displacement.

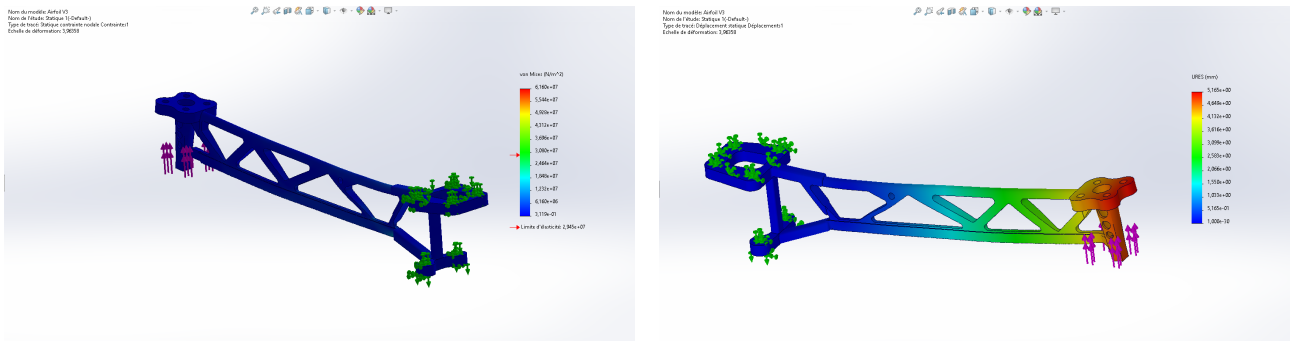

(a) Stress contours (b) Displacement

Figure 5.24: Static analysis results

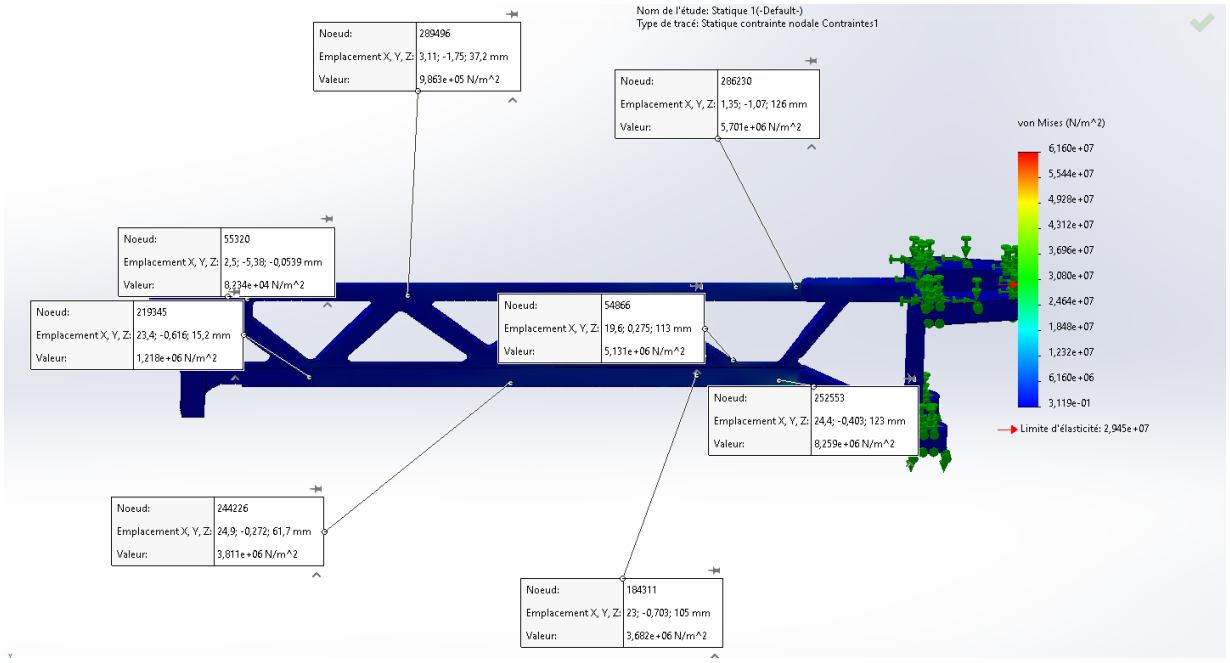

Figure 5.25: Probing stress values along the part

As observed, the stress values are within the elastic limit, ensuring the part's safety. However, displacements are relatively large, reaching **5.16 mm** at a **10 N** force, indicating a need for a more rigid model.

5.5 Adding the Airfoil

To enhance aerodynamic performance, an airfoil is added on top of the structure. This airfoil will be printed separately and added during assembly.

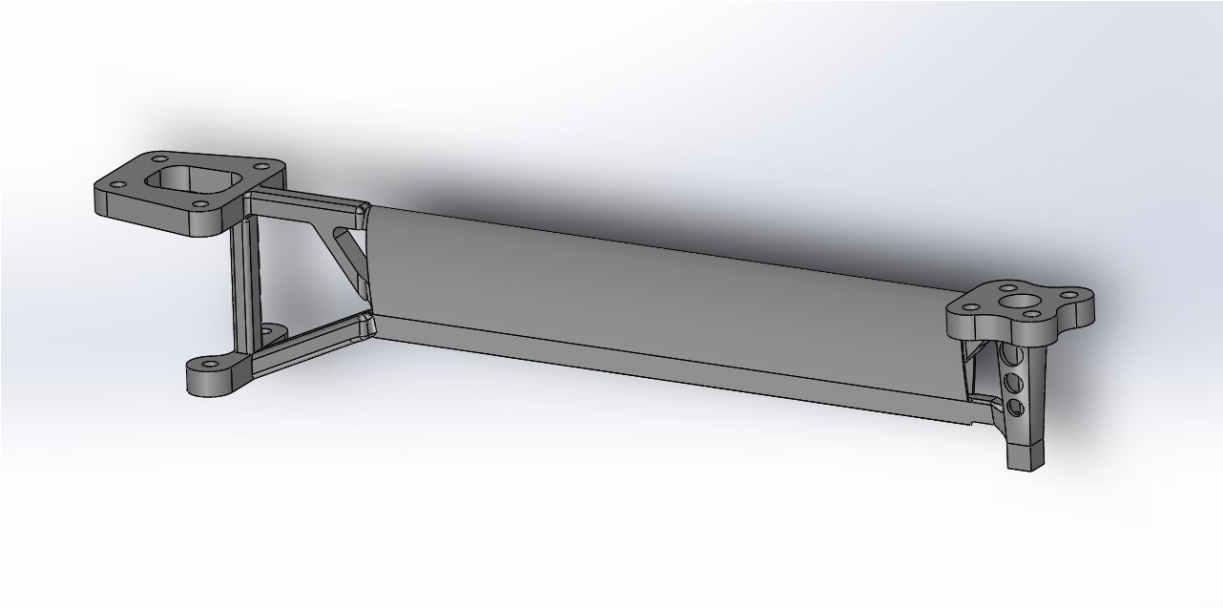

Figure 5.26: Optimized part after adding the airfoil

5.6 Designing Double-Airfoil Model

The design of our model leverages a lightweight and low-drag configuration. By incorporating a two-airfoil design, we aim to enhance the rigidity and resistance of the model. The process involves performing topology optimization followed by static analysis.

5.6.1 Designing the Raw Part

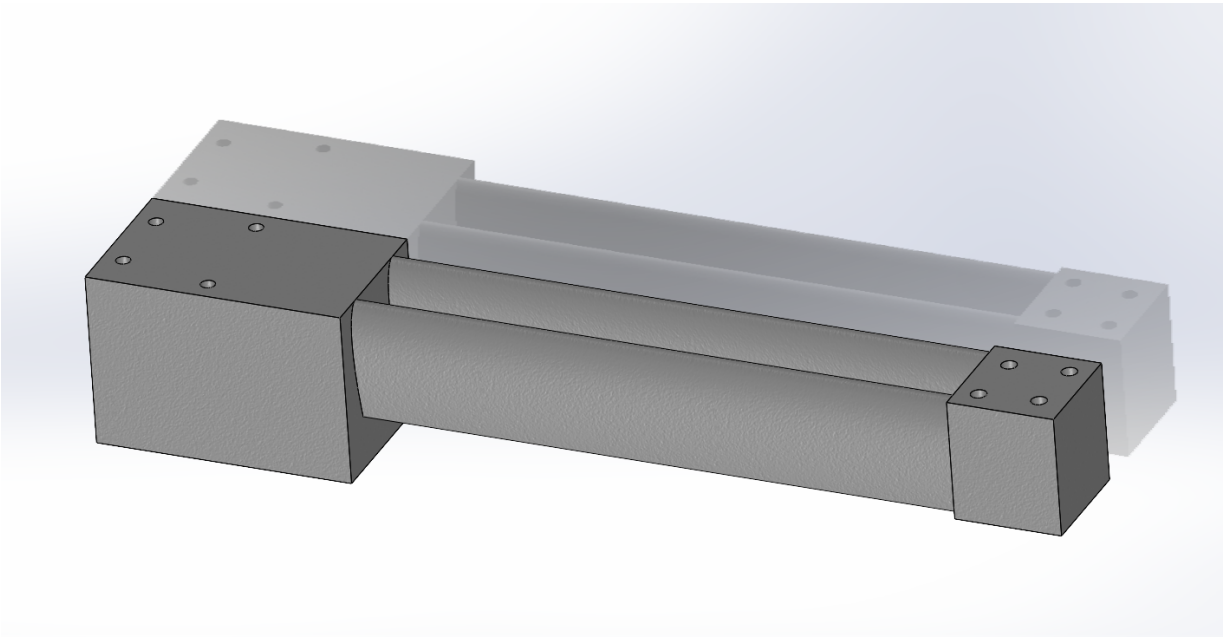

Figure 5.27: Initial design of the double-airfoil raw part

5.6.2 Performing Topology Optimization

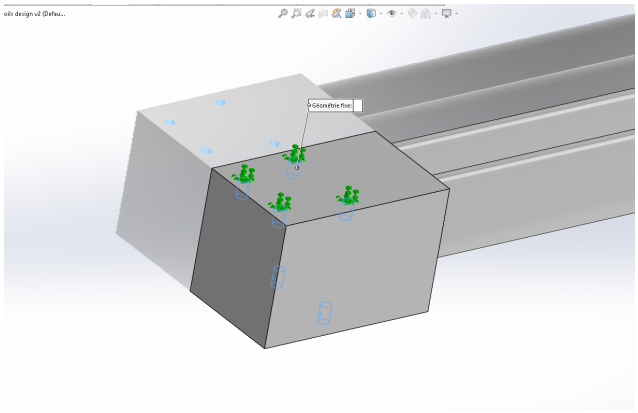

(a) Adding fixtures

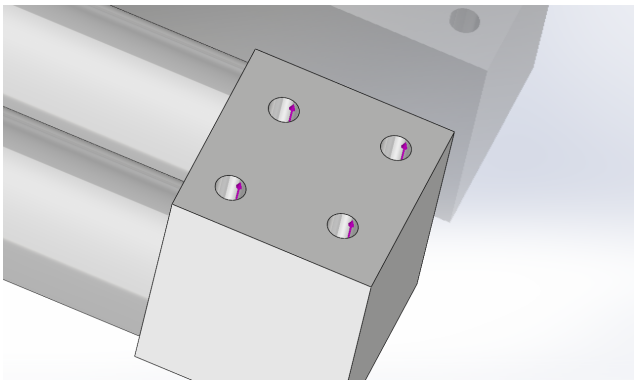

(b) Adding forces

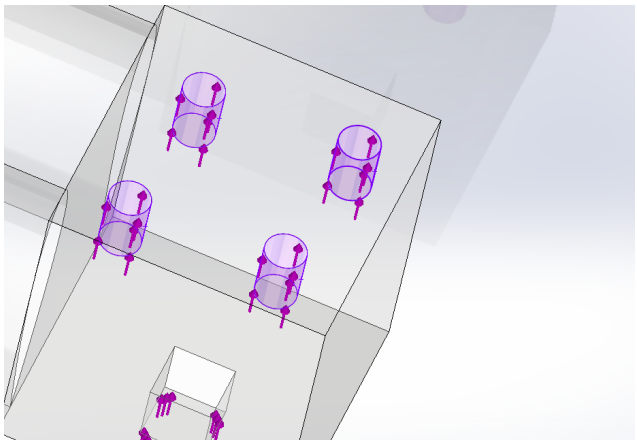

(c) Defining conserved regions

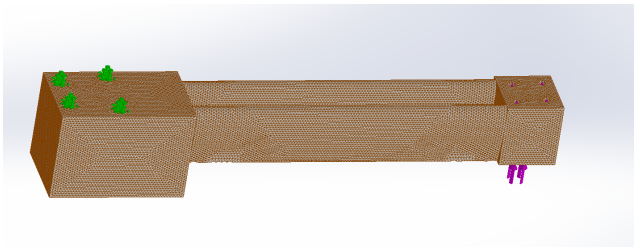

(d) Meshing

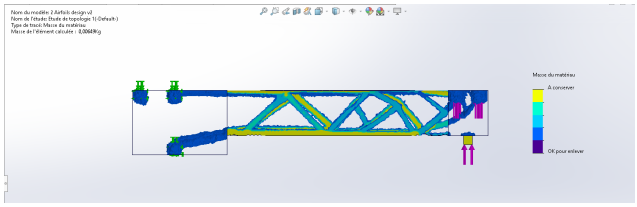

(e) Study result: side view

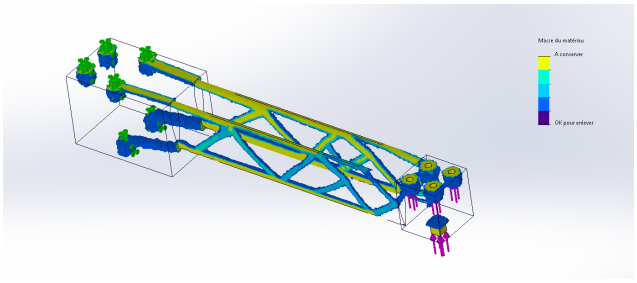

(f) Study result: 3D view

Figure 5.28: Topology optimization study for the double-airfoil part

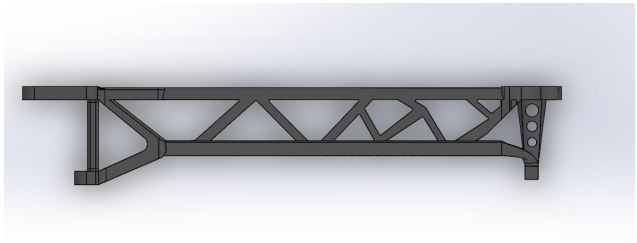

(a) Side view

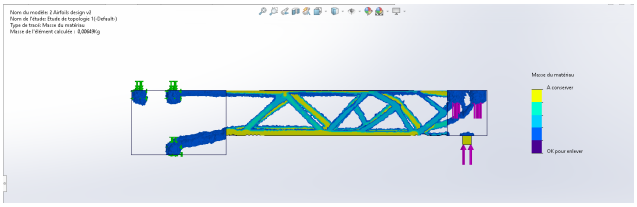

(b) 3D view

Figure 5.29: Redesigned double-airfoil part based on topology optimization results

5.6.3 Performing Static Analysis

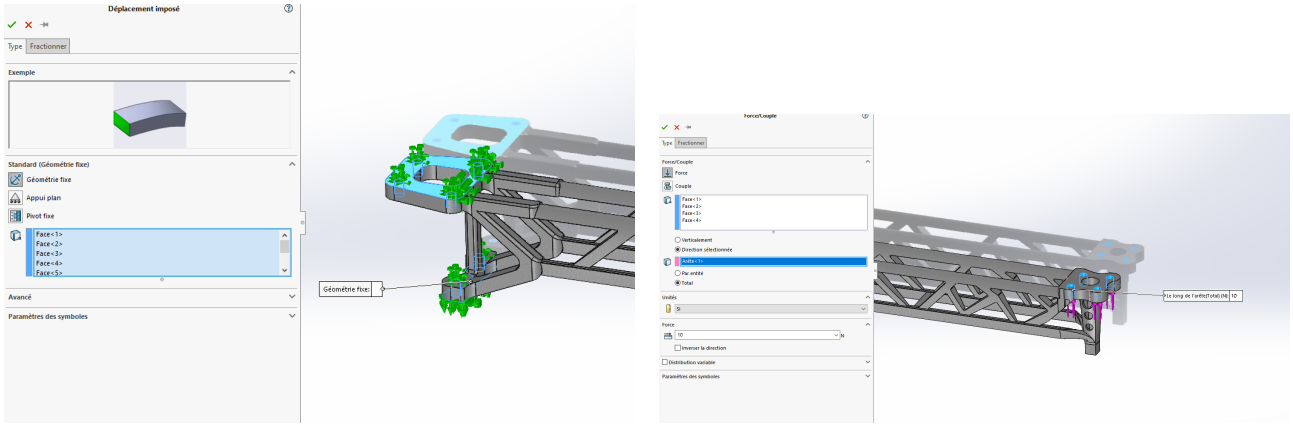

(a) Adding fixtures (b) Adding forces

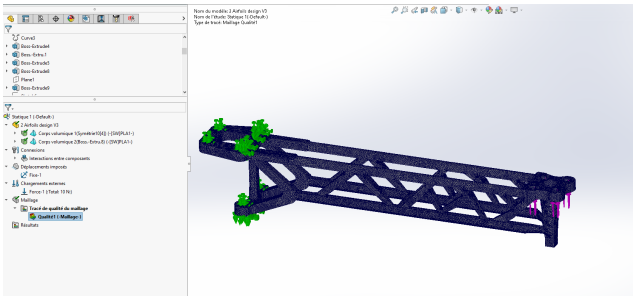

(c) Meshing

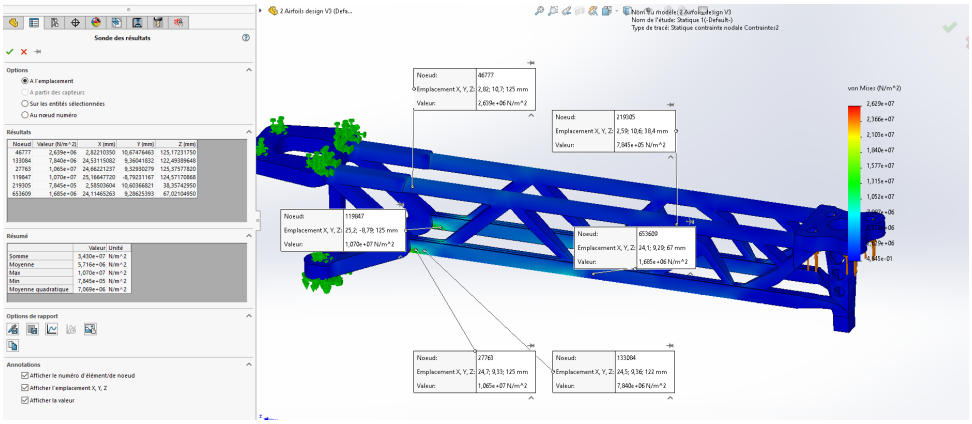

(d) Stress contours

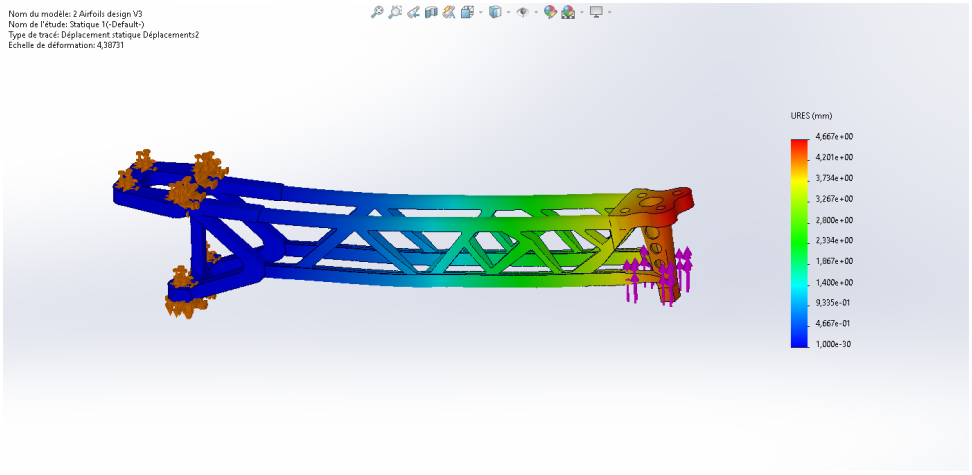

(e) Displacement

Figure 5.30: Static analysis study for the double-airfoil part

The static analysis reveals that the stress levels in the revised model are significantly lower compared to the initial design, resulting in a higher safety factor. Additionally, the displacement is reduced by 0.5 mm.

5.6.4 Adding the Airfoil

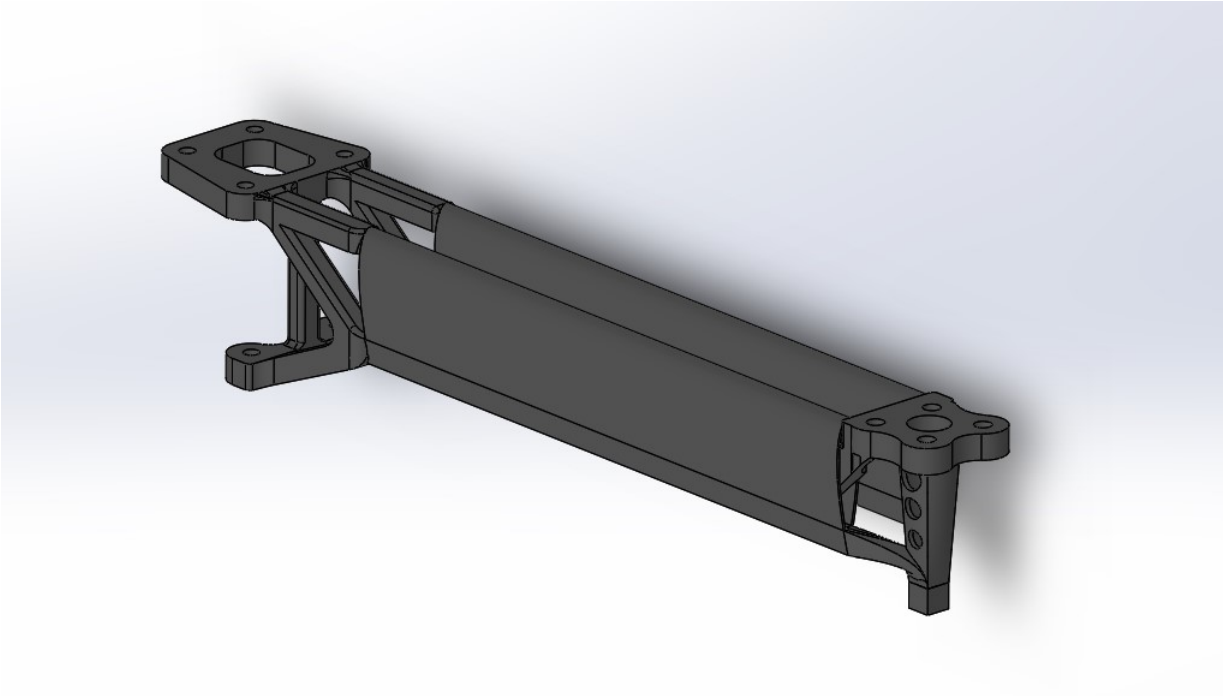

Figure 5.31: Optimized double-airfoil part with airfoils added

5.7 Mechanical Testing

Both models were subjected to mechanical testing under identical conditions to evaluate the maximum force each could withstand, simulating real-world application scenarios.

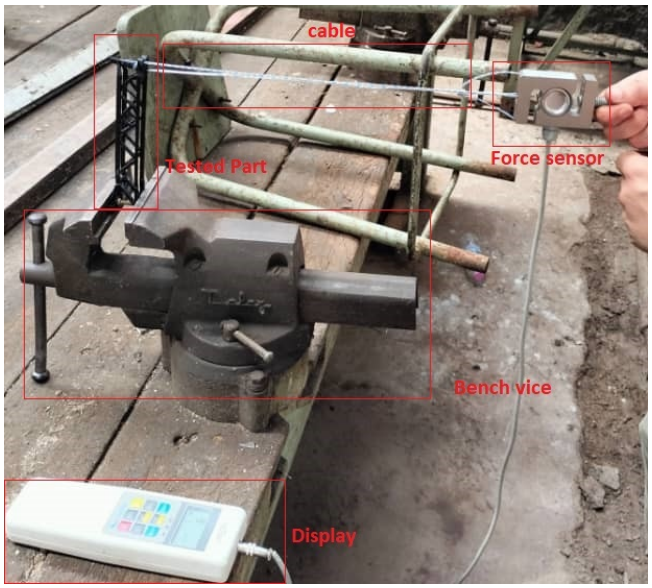

Figure 5.32: Explanation of the mechanical testing setup

(a) Testing the first model

(b) Peak force result for the first model

(c) Peak force result for the second model

Figure 5.33: Mechanical testing setup and results

5.8 Results Discussion & Conclusion

The testing indicates that the single-airfoil model can withstand a peak force of **14 N**, which is significantly higher than the thrust generated by a 1045 propeller (10 N). The double-airfoil model exhibits superior performance, withstanding up to **23 N** of force. The weights of the first and second models respectively are 30.9 g and 18.5g compared to 40.21 g of the commercial F450.

In conclusion, both models are viable for our application, but the double-airfoil model demonstrates higher strength and lower displacement compared to the single-airfoil model, making it the preferable choice.

Chapter 6

Vibration Analysis

Due to fabrication imperfections, every motor generates some degree of vibration. This occurs because the center of mass is offset from the rotational axis, resulting in a phenomenon known as rotating unbalance. The vibration produced has the same frequency as the motor's rotational frequency and can cause structural issues, particularly if it coincides with one of the natural frequencies of the structure to which the motor is attached.

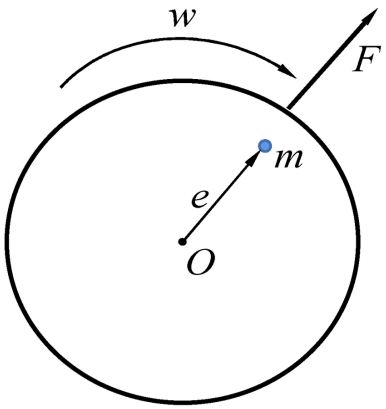

Figure 6.1: Illustration of rotating unbalance

The purpose of this analysis is to determine the natural frequencies of our structure. If necessary, we will modify the geometry of the models to ensure that the structure does not resonate with the soliciting frequency generated by the motors.

6.1 Motor Operating Frequencies

As calculated in the third chapter, our motor will need to operate at rotational speeds varying from $N_{\text{min}} = 3700\,\text{rpm}$ to $N_{\text{max}} = 4520\,\text{rpm}$, which corresponds to the following frequencies:

$$f_{\text{min}} = 61\,\text{Hz}$$
$$f_{\text{max}} = 75.33\,\text{Hz}$$

These values were confirmed through an experiment conducted at LGMD, using a contactless tachometer and one of the motors attached to the propeller. The rotational speed was varied until sufficient thrust was produced to achieve maximum thrust.

(a) Motor speed measurement setup

(b) Reflective tape added to one side of the propeller for measuring rotational speed

Figure 6.2: Measuring motor speed experiment

6.2 SolidWorks Frequency Analysis

Frequency analysis, also known as modal analysis, is a crucial aspect of structural analysis that helps in determining the natural frequencies and mode shapes of a structure. In SolidWorks, Frequency Analysis allows engineers to predict the vibrational characteristics of a model, which is essential in avoiding resonance and ensuring structural integrity.

6.2.1 How Frequency Analysis Works

Frequency analysis in SolidWorks operates by solving the eigenvalue problem associated with the structure's mass and stiffness matrices. The steps involved in conducting a frequency analysis are as follows:

1. **Pre-processing:** This involves defining the geometry of the model, material properties, and boundary conditions. Accurate modeling of these parameters is critical for obtaining reliable results.

2. **Meshing:** The geometry is discretized into finite elements. A finer mesh can provide more accurate results but at the cost of increased computational effort.

3. **Eigenvalue Problem:** SolidWorks solves the eigenvalue problem given by:

$$[K]\{\phi\} = \lambda[M]\{\phi\}$$

where $[K]$ is the stiffness matrix, $[M]$ is the mass matrix, $\{\phi\}$ are the mode shapes, and λ are the eigenvalues, which correspond to the squared natural frequencies.

4. **Post-processing:** The results, including the natural frequencies and corresponding mode shapes, are analyzed. The mode shapes show the deformation pattern of the structure at each natural frequency.

6.2.2 Analysis of the One-Airfoil Model

6.2.2.1 Pre-processing

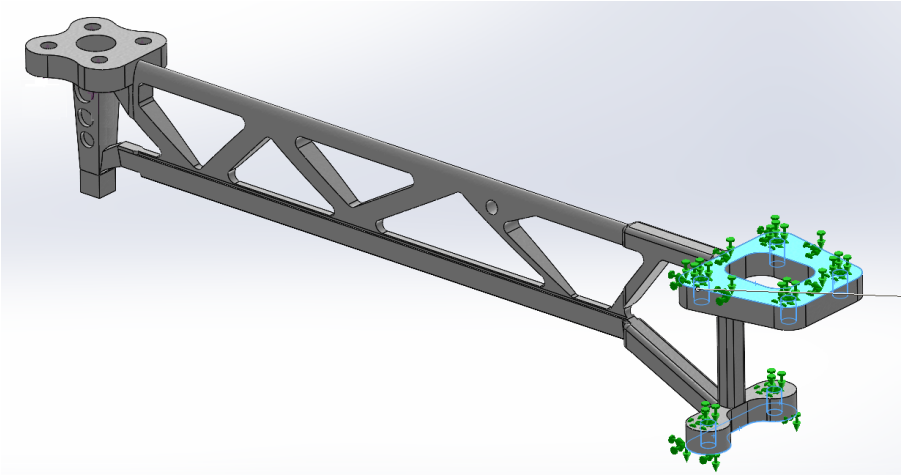

Figure 6.3: Importing the model and adding fixtures

6.2.2.2 Meshing

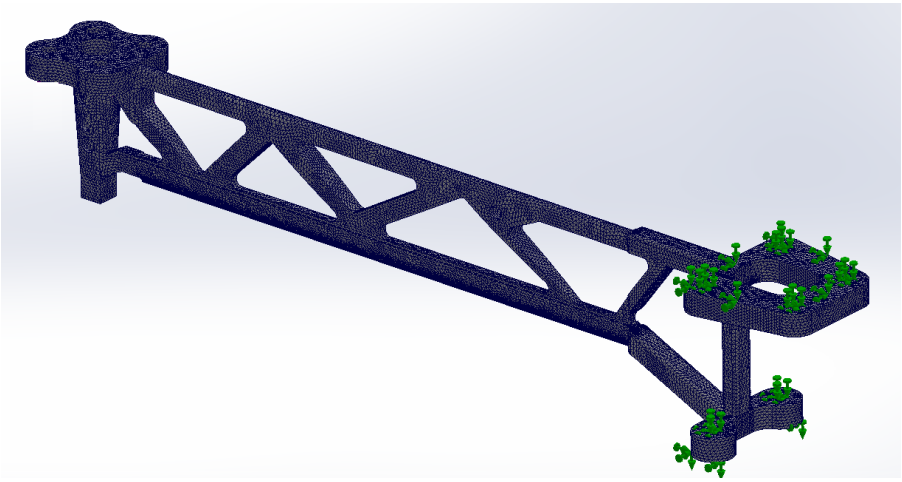

Figure 6.4: Meshing

6.2.2.3 Executing & Post-processing

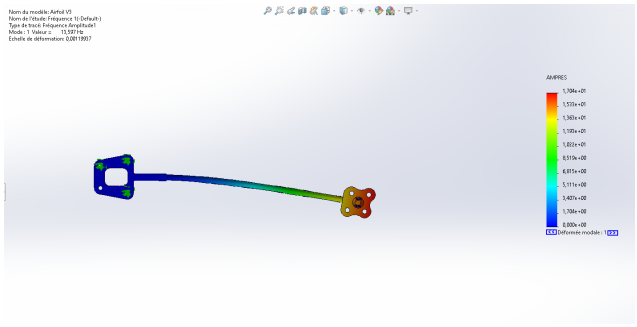

(a) Mode Shape 1

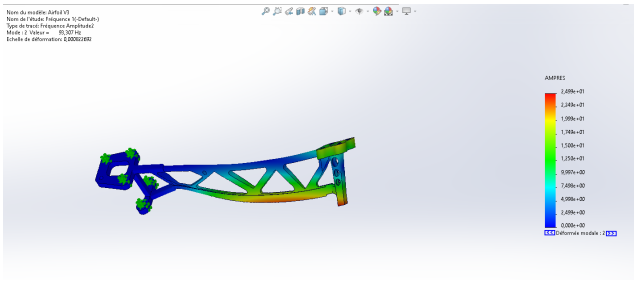

(b) Mode Shape 2

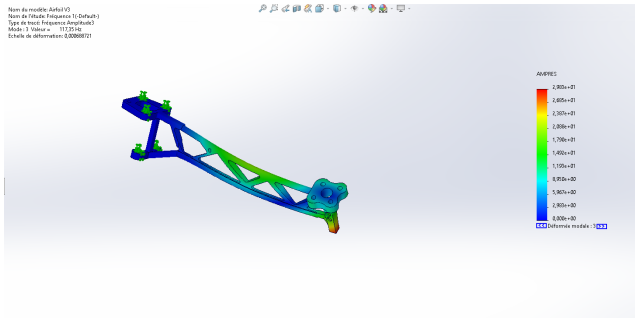

(c) Mode Shape 3

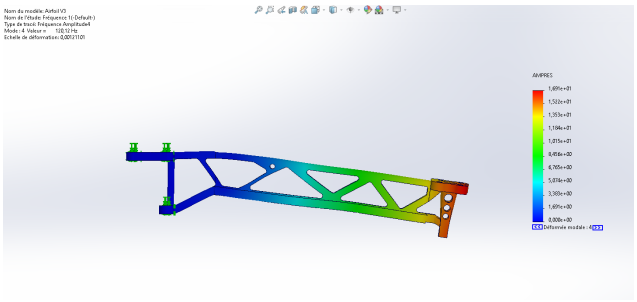

(d) Mode Shape 4

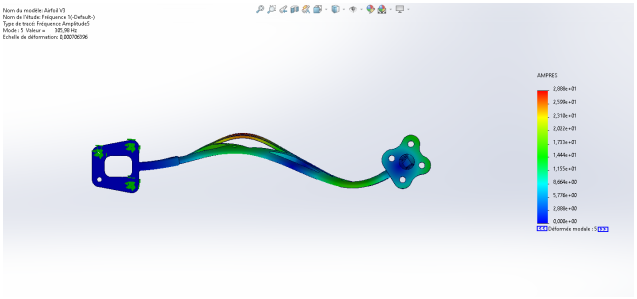

(e) Mode Shape 5

Figure 6.5: Modal shapes

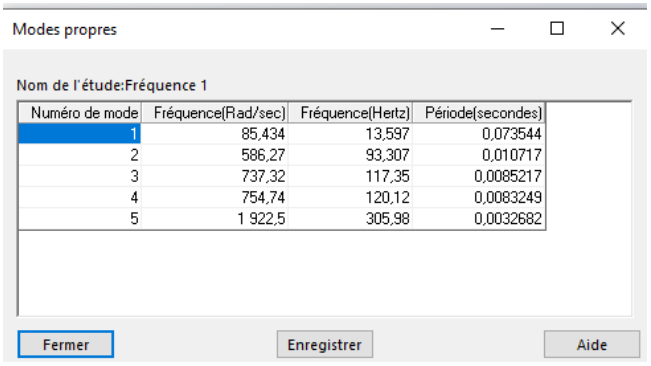

Figure 6.6: The first 5 natural frequencies

We observe that the minimum and maximum frequencies of the motor fall between the first and second natural frequencies of the structure and do not coincide with them. As a result, our structure will not resonate with these motor frequencies. However, during the initial startup and acceleration of the motor to its minimum frequency, it will pass through the first natural

frequency. This transient phase will not cause any significant issues as it is momentary and does not sustain resonance.

6.2.3 Analysis of the Double-Airfoil Model

6.2.3.1 Pre-processing

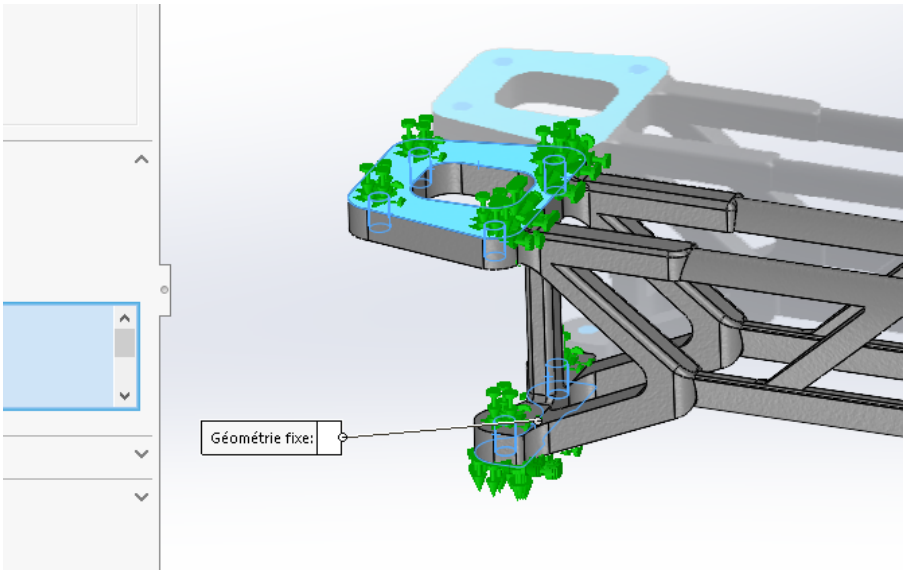

Figure 6.7: Importing the model and adding fixtures

6.2.3.2 Meshing

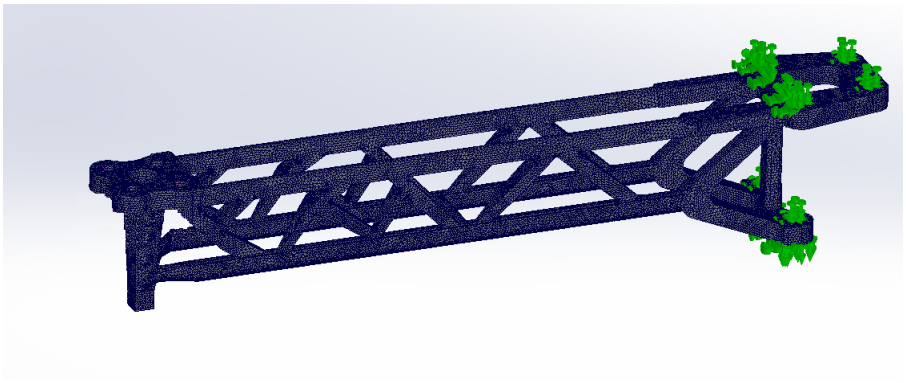

Figure 6.8: Meshing

6.2.3.3 Executing & Post-processing

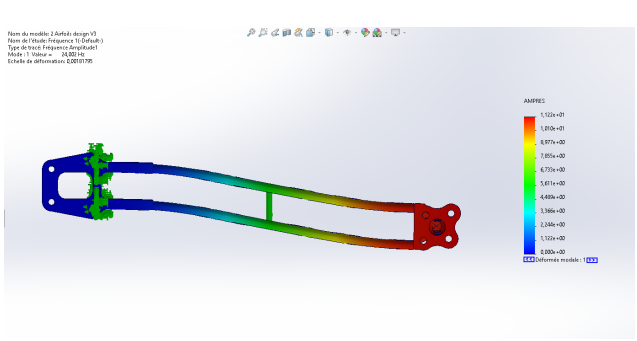

(a) Mode Shape 1

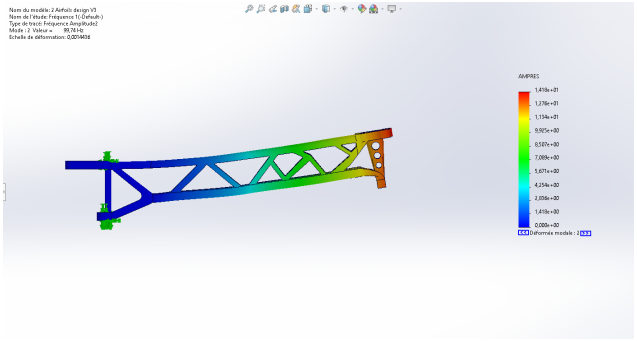

(b) Mode Shape 2

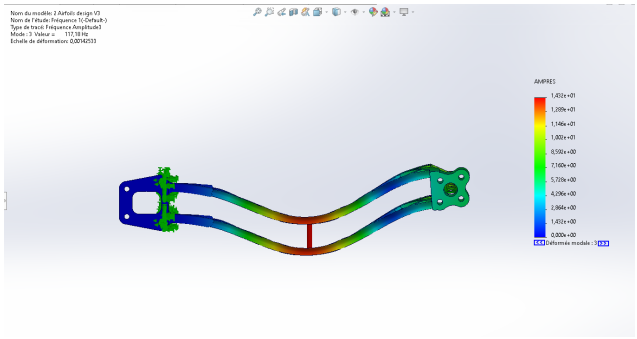

(c) Mode Shape 3

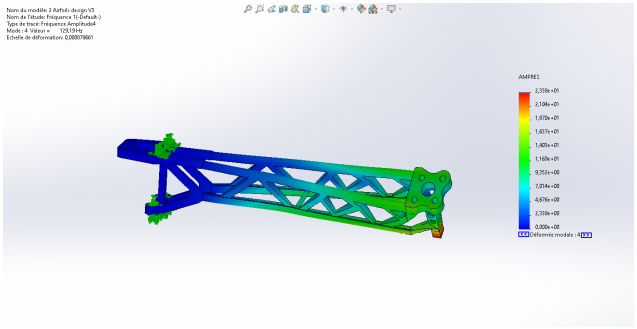

(d) Mode Shape 4

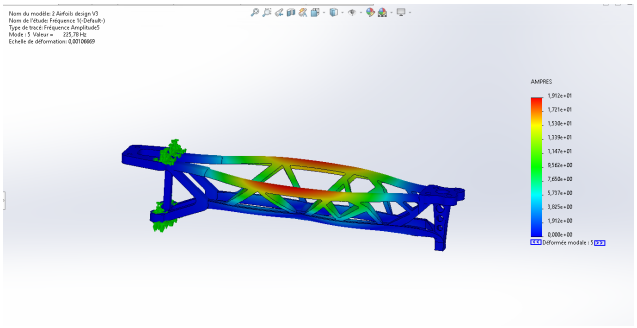

(e) Mode Shape 5

Figure 6.9: Modal shapes

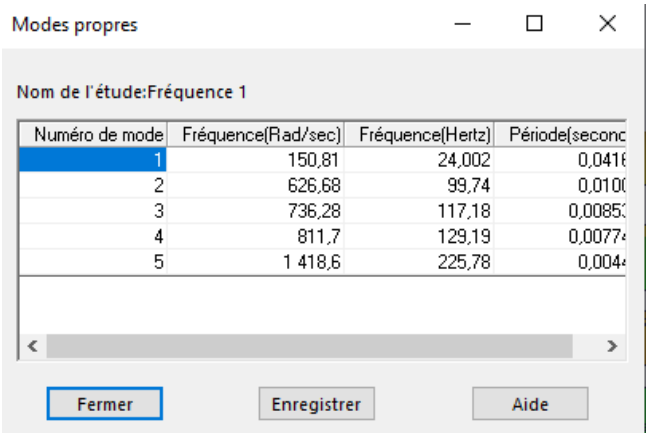

Figure 6.10: The first 5 natural frequencies

To minimize deformations in the region between the airfoils, a small cylinder was added to the structure. For this modified model, we also observe that the minimum and maximum

frequencies of the motor fall between the first and second natural frequencies of the structure. As these frequencies do not coincide with the natural frequencies, our structure will not resonate with the motor frequencies.

However, during the initial startup and acceleration phase, the motor will pass through the first natural frequency as it ramps up to its minimum operating frequency. This passage through the natural frequency is a transient event and will not cause any significant issues because it is brief and does not sustain resonance. Consequently, the structural integrity of the model is maintained during this phase, ensuring that no harmful vibrations are induced.

6.3 Conclusion

In this vibration analysis, we aimed to identify the natural frequencies of our structures and assess their potential for resonance with the motor's operating frequencies. Through detailed modal analysis using SolidWorks, we observed that the minimum and maximum operating frequencies of the motor (61 Hz to 75.33 Hz) fall between the first and second natural frequencies of both the single-airfoil and double-airfoil models. This ensures that the structures will not resonate with the motor frequencies, thereby preventing potential structural issues.

Chapter 7

Designing Auxiliary Mechanisms & Assembly

7.1 Designing the Latch-Detach Mechanism

To complete its delivery mission, our drone necessitates several essential components. Among these, a mechanism is vital for securely latching and detaching the payload as required. We designed a mechanism based on a Crank-piston mechanism and integrated it with a servo motor. This design was meticulously drawn and animated using Solidworks.

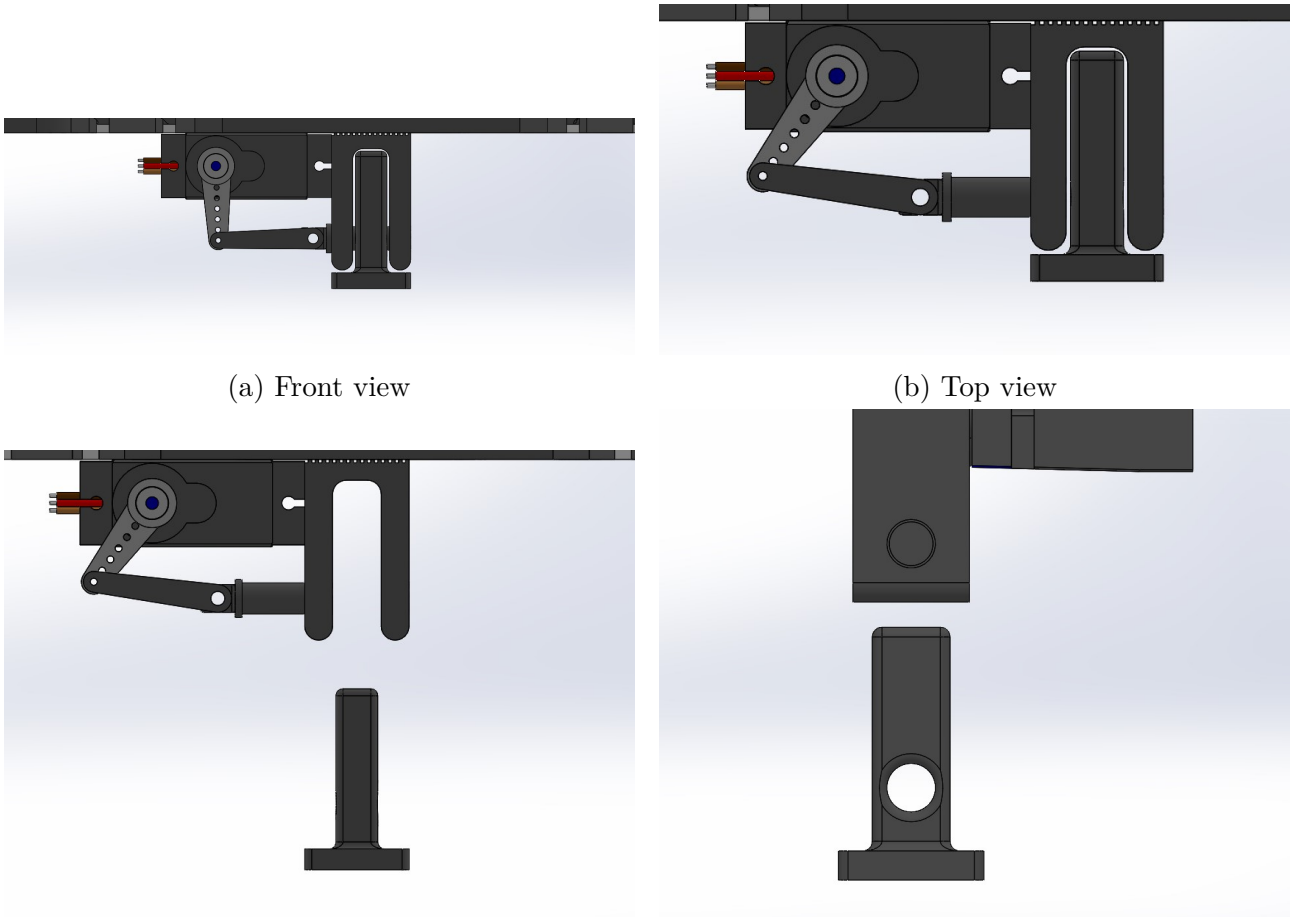

(a) Front view

(b) Top view

(c) Detailed view

(d) Side view

Figure 7.1: Working principle of the latch-detach mechanism

7.2 Designing the Landing Legs

The legs are designed to provide clearance for the payload beneath the drone's frame while supporting its weight. The design emphasizes lightweight construction to optimize flight efficiency.

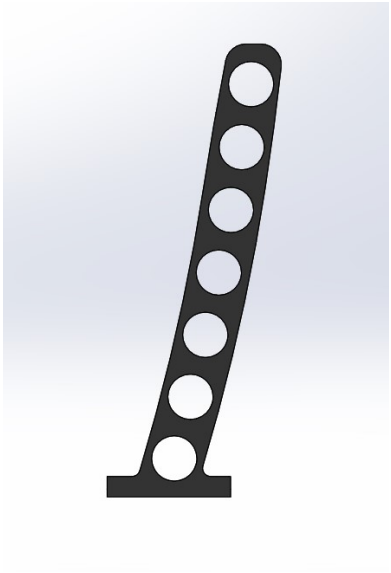

Figure 7.2: Landing leg design

7.3 Designing the Protective Shell

The protective shell safeguards the drone's sensitive electronic components from external elements such as water and dust.

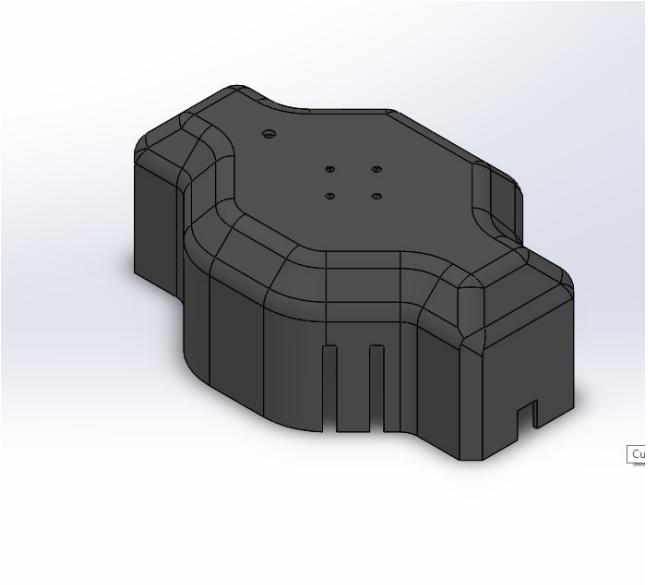

Figure 7.3: Protective shell design

Figure 7.4: Final assembly of the drone with shell

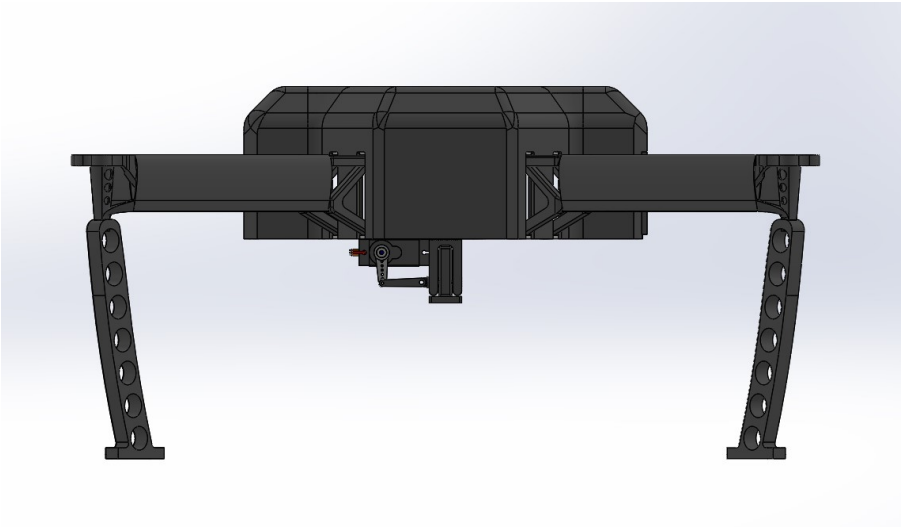

Figure 7.5: Side view of the final assembled drone

7.4 Assembling Phase

After 3D printing the parts and soldering electronic circuits, the assembly phase commences. Each component is carefully integrated to ensure functionality and durability.

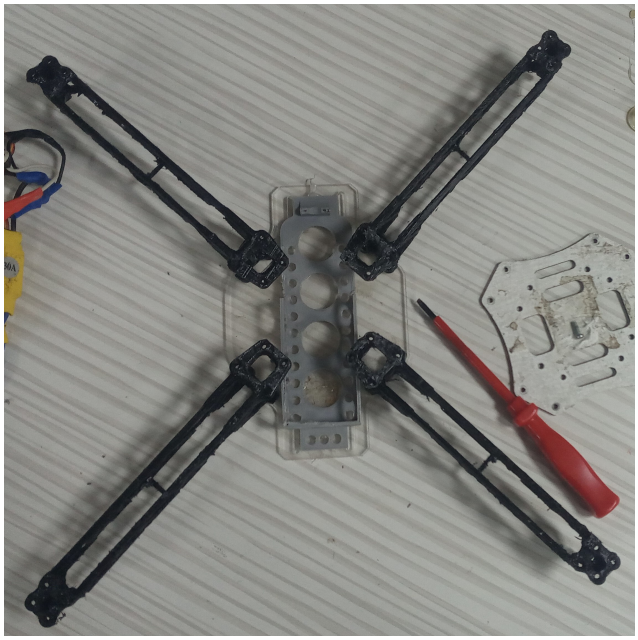

(a) Mounting the arms with lower base

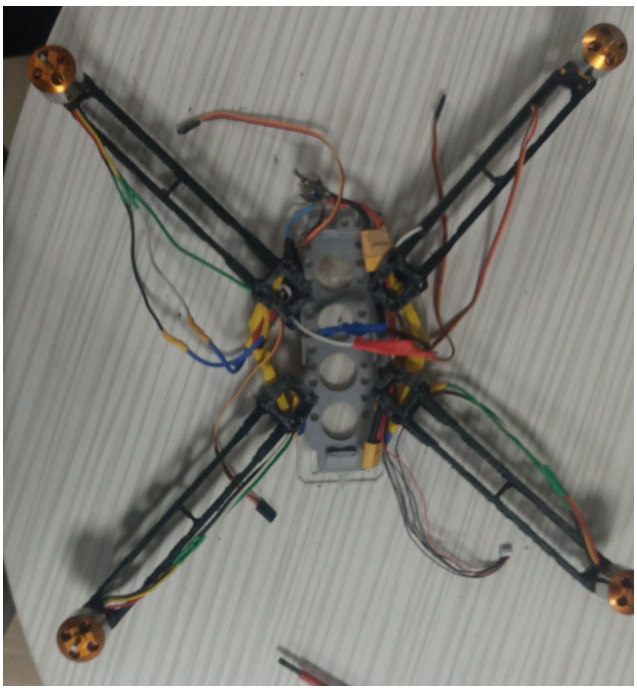

(b) Mounting the power distribution board with ESCs and BLDC

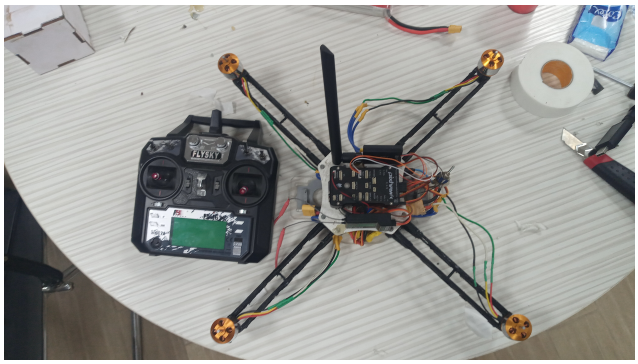

(c) Mounting the RC and Telemetry modules with flight controller

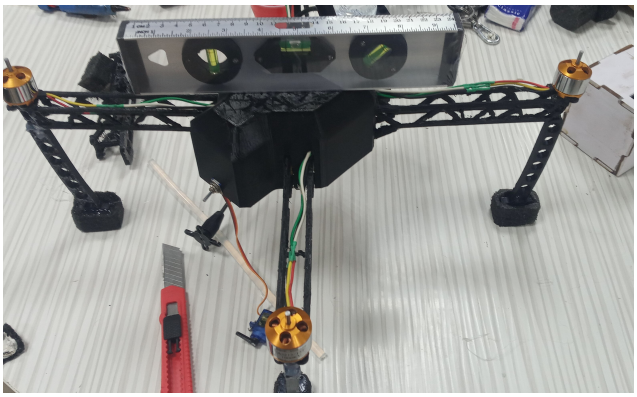

(d) Mounting the shell and legs

(e) Mounting the propellers

Figure 7.6: Assembly process

Figure 7.7: Fully assembled drone

7.5 Testing Phase

Following assembly, rigorous testing of the latch-detach mechanism ensures its reliability under operational conditions. The drone's propulsion systems are also tested for resilience and performance.

(a) Testing the latch-detach mechanism

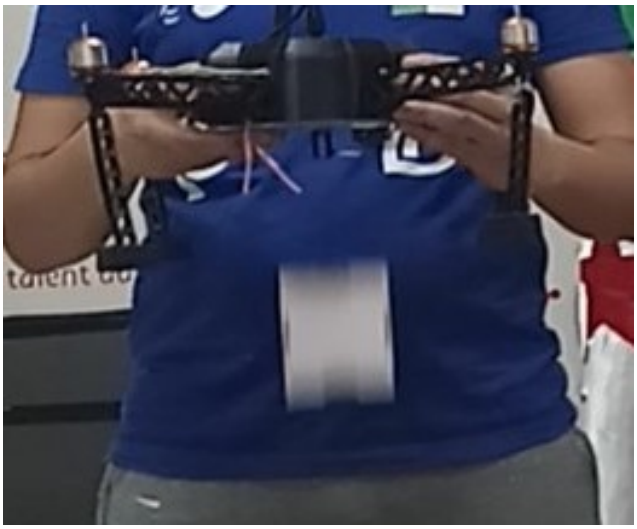

(b) Testing the motor resilience

Figure 7.8: Testing phase

Figure 7.9: First flight of the drone

Chapter 8

Conclusion and Future Perspectives

8.1 Conclusion

This graduation project addressed a multifaceted approach to designing a versatile delivery drone (quad-copter), covering various critical aspects from initial design considerations to advanced structural and performance analyses. The project commenced with meticulous design phases, including selecting propeller motors and optimizing the frame for minimal aerodynamic drag, crucial for efficient flight operations.

Most of the project focused on structural engineering, where two distinct drone models were developed using topology optimization techniques. These models underwent rigorous static and irrational analyses to ensure structural integrity and performance under varying operational conditions. Integrating advanced simulation tools and methodologies underscored the project's commitment to achieving optimal drone design through evidence-based engineering.

The fabrication phase was equally pivotal, involving the precise assembly of components and the design of auxiliary mechanisms essential for drone functionality. Emphasis was placed on lightweight materials and robust construction techniques to meet the demanding performance requirements of modern delivery drones.

Throughout the project, a strong emphasis was placed on the iterative refinement of design parameters and manufacturing techniques to achieve a balance between weight reduction and structural reliability. By leveraging computational tools and experimental validation, this project successfully demonstrated the feasibility of enhancing drone efficiency and performance in delivery applications.

8.2 Future Perspectives

Looking forward, several avenues for advancing the current research and its practical applications emerge:

- **Injection Molding for Frame Production:** Consider developing molds for plastic injection to eliminate the orthotropic effects associated with 3D printing. This would enhance structural uniformity and durability, crucial for scaling drone production.
- **Composite Material Integration:** Explore the use of composite materials such as

carbon and glass fibers in arm construction. This approach aims to fully exploit the benefits of lightweight structures, enhancing drone agility and endurance.

- **Diversified Drone Applications:** Test the quadcopter model in diverse operational scenarios beyond delivery services, including firefighting, seed planting, and pesticide spraying. This broadens the drone's utility and addresses various societal needs.

- **Collaborative Projects in Drone Development:** Foster interdisciplinary collaboration with the Department of Electrical and Control Engineering to enhance drone capabilities further. This joint effort can focus on integrating advanced control systems, sensor networks, and autonomous functionalities to create more capable and versatile Algerian drones.

In conclusion, this project not only provides a comprehensive exploration of delivery drone design and optimization but also sets the stage for future advancements in drone technology and its multifaceted applications. By pursuing these future perspectives, we aim to contribute significantly to the development of high-performance, locally manufactured drones tailored to Algerian needs and beyond.

Bibliography

[1] builtin.com. Article: 13 drone delivery companies to know. https://builtin.com/articles/drone-delivery-companies.

[2] www.grandviewresearch.com. Article: Delivery drones market size, share & growth report, 2030. https://www.grandviewresearch.com/industry-analysis/delivery-drones-market-report.

[3] droneanalyst.com. Article: Drone delivery by the numbers. https://droneanalyst.com/2014/10/02/drone-delivery-numbers.

[4] www.dropoff.com. Article: Drone delivery: Everything you need to know in 2024 - dropoff. https://www.dropoff.com/blog/drones-delivery/.

[5] www.thegpstime.com. Blog: What are the best drones for aerial photography in 2021. https://www.thegpstime.com/what-are-the-best-drones-for-aerial-photography-in-2021/.

[6] www.iwm.org.uk. Article: A brief history of drones | imperial war museums. https://www.iwm.org.uk/history/a-brief-history-of-drones.

[7] en.wikipedia.org. Image: Iai-scout-hatzerim-1 - iai scout. https://en.wikipedia.org/wiki/IAI_Scout#/media/File:IAI-Scout-hatzerim-1.jpg.

[8] afriqueeducation.com. Image. https://www.afriqueeducation.com/wp-content/uploads/2022/12/22dec1.jpg.

[9] Image. https://m.media-amazon.com/images/I/51KA0bQmPDL._AC_SL1500_.jpg.

[10] www.space.com. Article: How nasa's ingenuity helicopter opened the mars skies to exploration | space. https://www.space.com/mars-helicopter-ingenuity-opened-red-planet-skies-exploration.

[11] www.campaignlive.co.uk. Blog: Amazon plans 30-minute delivery by drones with prime air service. https://www.campaignlive.co.uk/article/amazon-plans-30-minute-delivery-drones-prime-air-service/1223302.

[12] www.makeuseof.com. Article: Which frame should you choose for your diy quadcopter? https://www.makeuseof.com/which-frame-should-you-choose-for-your-diy-quadcopter/.

[13] www.researchgate.net. Image: F450-frame-dimensions. https://www.researchgate.net/profile/Muneeb-Ullah-5/publication/355023499/figure/fig2/AS:1075864976531457@1633517607985/F450-Frame-dimensions.jpg.

[14] www.mdpi.com. Drones | free full-text | experimental and numerical considerations for the motor-propeller assembly’s air flow field over a quadcopter’s arm. https://www.mdpi.com/2504-446X/7/3/199.

[15] www.simscale.com. Blog: Drone flight simulation | simscale. https://www.simscale.com/blog/drone-flight-simulation/.

[16] www1.grc.nasa.gov. Blog: Shape effects on drag | glenn research center | nasa. https://www1.grc.nasa.gov/beginners-guide-to-aeronautics/shape-effects-on-drag-2/#:~:text=The%20Effect%20of%20Shape%20on%20Drag&text=A%20quick%20comparison%20shows%20that,a%20factor%20of%20almost%2030!

[17] Hoerner. Book: Fluid-dynamic drag. https://ia600707.us.archive.org/13/items/FluidDynamicDragHoerner1965/Fluid-dynamic_drag___Hoerner___1965_text.pdf.

[18] www.researchgate.net. Article: Chemical structure of poly lactic acid (pla). | download scientific diagram. https://www.researchgate.net/figure/Chemical-structure-of-poly-lactic-acid-PLA_fig4_51832364.

[19] springer.com. Article: Numerical prediction of orthotropic elastic properties of 3d-printed materials using micro-ct and representative volume element | acta mechanica. https://link.springer.com/article/10.1007/s00707-019-02544-2.

[20] formlabs.com. Blog: Topology optimization 101: How to use algorithmic models to create lightweight design | formlabs. https://formlabs.com/blog/topology-optimization/.

[21] Article: 237 ways drone applications revolutionize business | droneii. https://droneii.com/237-ways-drone-applications-revolutionize-business.

[22] Justin D. Murphy. Book: Military aircraft, origins to 1918: An illustrated history of their impact.

[23] Lennart Andersson. Book: Soviet aircraft and aviation, 1917-1941.

[24] H. R. Everett. Book: Unmanned systems of world wars i and ii. https://books.google.dz/books?id=fNjgCgAAQBAJ&pg=PA318&redir_esc=y#v=onepage&q&f=false.

[25] William Wagner. Book: Lightning bugs and other reconnaissance drones -.

[26] science.howstuffworks.com. Article: How the mq-9 reaper works | howstuffworks. https://science.howstuffworks.com/reaper.htm.

[27] Nagorno-Karabakh. Article: Nagorno-karabakh: New weapons for an old conflict spell danger | features | al jazeera. https://www.aljazeera.com/features/2020/10/13/nagorno-karabakh-new-weapons-for-an-old-conflict-spell-danger.

[28] bignet.in. Blog: A brief history of drones and their development! https://bignet.in/blog/282/a-brief-history-of-drones-and-their-development-in-english.

[29] science.nasa.gov. Article: Ingenuity mars helicopter - nasa science. https://science.nasa.gov/mission/mars-2020-perseverance/ingenuity-mars-helicopter/.

[30] www.army technology.com. Article: In data: Uas market projected to nearly double in ten years - army technology. https://www.army-technology.com/news/in-data-uas-market-projected-to-nearly-double-in-ten-years/.

[31] database.tytorobotics.com. Data base: 1045prop tmotor 900kv 3s test1b test data. https://database.tytorobotics.com/tests/7mn/1045prop-tmotor-900kv-3s-test1b.

[32] www.rhydolabz.com. Datasheet: Bldc_a2212_13t. https://www.rhydolabz.com/documents/26/BLDC_A2212_13T.pdf.

[33] www.optimusdigital.ro. Datasheet: 30a bldc esc product manual 2012-06-08.doc. https://www.optimusdigital.ro/ro/index.php?controller=attachment&id_attachment=451.

[34] genstattu.com. Article: How to choose quadcopter frame - genstattu. https://genstattu.com/blog/how-to-choose-quadcopter-frame.

[35] www.astm.org. Standard: D638 standard test method for tensile properties of plastics. https://www.astm.org/d0638-03.html.

[36] researchgate.net. Article: Pla and pla+cf poisson coefficients. | download table. https://www.researchgate.net/figure/PLA-and-PLA-CF-Poisson-coefficients_tbl3_316897831.